AN EXPERIMENTAL STUDY OF A PLANE TURBULENT WALL JET ON SMOOTH AND ROUGH SURFACES

A Thesis Submitted to the College of

Graduate Studies and Research

In Partial Fulfillment of the Requirements

For the Degree of Master of Science

In the Department of Mechanical Engineering

University of Saskatchewan

Saskatoon

By

Zhujun Tang

PERMISSION TO USE

In presenting this thesis in partial fulfilment of the requirements for a Postgraduate degree from the University of Saskatchewan, I agree that the Libraries of this University may make it freely available for inspection. I further agree that permission for copying of this thesis in any manner, in whole or in part, for scholarly purposes may be granted by the professors who supervised my thesis work or, in their absence, by the Head of the Department or the Dean of the College in which my thesis work was done. It is understood that any copying or publication or use of this thesis or parts thereof for financial gain shall not be allowed without my written permission. It is also understood that due recognition shall be given to me and to the University of Saskatchewan in any scholarly use which may be made of any material in my thesis.

Requests for permission to copy or to make other use of material in this thesis in whole or part should be addressed to:

Head of the Department of Mechanical Engineering

57 Campus Drive

University of Saskatchewan

Saskatoon, Saskatchewan S7N 5A9

Canada

ABSTRACT

This study presents an experimental investigation of incomplete similarity and the effect of surface roughness on a plane turbulent wall jet on a hydraulically smooth, transitionally rough and fully rough surface based on a new set of particle image velocimetry (PIV) measurements. The focus is on examining the changes in the characteristics of the mean velocity field. Velocity measurements were taken along the centerline of the ground plane with seven fields of view (FOV) covering the entire streamwise extent, i.e. the inflow, developing and fully developed regions. In each FOV, 2,000 and 4,000 pairs of instantaneous PIV raw images were captured at a sampling frequency of 4 Hz for the smooth and rough surface cases, respectively. Four series of measurements were conducted: two series of measurements were taken on the smooth surface at two inlet flow rates corresponding to slot Reynolds numbers of 7,190 and 14,300, respectively; then the rough surface was installed and two series of measurements were taken at the same two inlet flow rates corresponding to slot Reynolds numbers of 6,660 and 13,400, which resulted in a transitionally rough and a fully rough flow condition, respectively. In-house PIV software was used to complete the cross-correlation analysis of the PIV images and the post-correlation rejection of outlier velocity vectors with a dynamic threshold neural network technique to obtain the mean and fluctuating velocity data.

The results show that at the inlet boundary, the surface roughness decreases the mass flux near the wall due to the enhanced wall shear stress. In the initial developing region, which covers the first ten slot heights of streamwise distance, the enhanced wall friction associated with the rough surface shortens the potential core.

The surface roughness causes the onset of the fully developed region to appear farther downstream on the rough surface than on the smooth surface. For the low flow rate (LFR) case

on the rough surface, the roughness shift decreases monotonically with distance from the slot, which indicates that the effect of surface roughness on the mean velocity profile is decreasing. The profile fitting result for the fully rough case suggests that the value of von Karman's constant κ in the logarithmic law may depend on the surface roughness.

In the fully developed region, for the LFR case, the surface roughness enlarges the thicknesses of both the outer and inner layers, though this effect is much more significant for the inner layer than for the outer layer. This is also observed for the high flow rate (HFR) case, but with a much more noticeable effect of surface roughness. The surface roughness increases the spread rate of the inner layer significantly and penetrates into the outer layer, although the impact is much less for the outer layer. For the LFR case, while in general the surface roughness tends to increase the streamwise growth rate of the inner and outer half-widths, the magnitude of this effect becomes stronger as the wall-normal distance to the surface decreases. A significant increase in the skin friction coefficient due to the surface roughness, as large as 58% - 78% for the LFR case and 72% - 75% for the HFR case, is observed.

Incomplete similarity of the plane turbulent wall jet in terms of the slot height H is confirmed for all the flow conditions considered in this study, i.e., the hydraulically smooth, transitionally rough and fully rough flow cases. The outer scaling is observed to extend into the inner layer with varied extent for different flow cases, which indicates that the upper region of the inner layer in a plane wall jet is essentially part of the outer layer in a canonical zero-pressure-gradient turbulent boundary layer. In general the velocity profiles tend to collapse better when the rough surface is present compared to the smooth surface, which implies that the surface roughness strengthens the coupling between the inner and outer layers.

ACKNOWLEDGMENTS

First I would like to thank Professor Donald J. Bergstrom and Professor James D. Bugg for your advice, guidance and financial support during the course of my research program.

I would like to thank Professor David Sumner and Professor Scott D. Noble for being my advisory committee members. Your suggestions and insights helped improve the overall quality of this study.

I would also like to thank Dave Deutscher, Rob Peace and Melanie Fauchoux for your technical expertise in supporting the present study.

I gratefully acknowledge the financial support from the University of Saskatchewan Graduate Research Fellowship.

Last but not least, I would like to thank my family and friends for your continuous support.

DEDICATION

To my parents, Leilei Tang and Linxia Hu.

TABLE OF CONTENTS

LIST OF TABLES

LIST OF FIGURES

NOMENCLATURE

Roman

C_f	Skin fiction coefficient
DNS	Direct numerical simulation
FOV	Field of View
H	Slot exit height [m]
HFR	High flow rate
HWA	Hot-wire anemometry
IA	Interrogation area (side length) [pixel]
k	Average height of the roughness elements [m]
k_s	Equivalent sand grain roughness [m]
k_s^+	Equivalent sand grain roughness Reynolds number
LDA	Laser Doppler anemometry
LES	Large-eddy simulation
LFR	Low flow rate
PIV	Particle image velocimetry
Re_{m}	Local Reynolds number based on the maximum velocity, $Re_{\mathrm{m}} = U_{\mathrm{m}} y_{\mathrm{m}} / \upsilon$
Re_{o}	Slot Reynolds number based on the inlet bulk velocity and the slot height
$\widetilde{U}$	Instantaneous streamwise velocity [m/s]
U	Mean streamwise velocity [m/s]
U_{m}	Local maximum mean streamwise velocity [m/s]
U_{o}	Inlet bulk velocity [m/s]

$U_{m,o}$	Initial maximum mean streamwise velocity [m/s]
U_τ	Friction velocity [m/s]
u	Streamwise instantaneous fluctuating velocity [m/s]
$u'\left(=\langle u^2\rangle^{\frac{1}{2}}\right)$	Streamwise time-averaged (root-mean-square) fluctuating velocity [m/s]
$\langle u^2\rangle$	Streamwise normal Reynolds stress [m^2/s^2]
$\langle uv\rangle$	Reynolds shear stress [m^2/s^2]
v	Transverse instantaneous fluctuating velocity [m/s]
$v'\left(=\langle v^2\rangle^{\frac{1}{2}}\right)$	Transverse time-averaged (root-mean-square) fluctuating velocity [m/s]
$\langle v^2\rangle$	Transverse normal Reynolds stress [m^2/s^2]
W	Slot exit width [m]
x, y, z	Cartesian coordinate system [m]
x_p	Potential core length [m]
$(y_{1/2})_{in}$	Inner half-width [m]
y_m	The wall-normal height of the location where U_m occurs [m]
$(y_{1/2})_{out}$	Outer half-width [m]
$(y_{1/2})^+_{out}$	Local Reynolds number based on the outer half-width, $(y_{1/2})^+_{out}=(y_{1/2})_{out}U_\tau/\upsilon$

Greek

ε_y	fluctuating tion of the wall-normal coordinate in the velocity profile [m]

υ	Kinematic viscosity of the fluid [m^2/s]
ρ	Fluid density [kg/m^3]
τ_w	Wall shear stress [Pa]
Π	Dimensionless similarity parameter

CHAPTER 1

INTRODUCTION

1.1 Motivation

A plane turbulent wall jet is a shear flow created by directing the fluid discharged from a slot along a surface. The surface can be either smooth or rough. The flow is characterized by a peak value of the momentum flux close to the wall. At the surface, momentum is continually extracted from the flow by the wall shear stress, while at the outer edge of the wall jet there is turbulent mixing with the ambient fluid.

The plane turbulent wall jet is a flow of special interest to fluids researchers because of its significant theoretical importance and wide industrial application. From a theoretical viewpoint, the turbulent wall jet is a prototypical near-wall flow which is comparable to, but more complex than, a canonical turbulent boundary layer. It consists of an inner layer which resembles a turbulent boundary layer and an outer layer which exhibits the mixing characteristics of a free jet. In this regard, a critical research issue is the interaction of the inner and outer layers, and their equilibrium with each other, together with relevant scaling issues. In addition, the effects of different surface roughness on the dynamics of the plane wall jet remains to be fully understood. On the practical side, plane wall jets are used in a variety of industrial applications. For instance, the flow over the external cowl of a turbo-fan engine resembles a plane wall jet, as does the flow over the extended slotted flap of an airfoil (Rostamy *et al*., 2011a). This type of flow is also relevant to the design of film cooling applied in modern aero-engines (Hammond, 1982). Knowledge of the velocity distribution and the skin friction coefficient can facilitate the

calculation of parameters of industrial significance, such as the friction force and the wall heat and mass transfer rates (Rostamy *et al*., 2011b).

1.2 Plane Turbulent Wall Jet

1.2.1 Flow Geometry

Figure 1.1 shows a schematic of a two-dimensional plane wall jet, where H is the slot exit height, and x, U, u' and y, V, v' are the coordinate distance, mean velocity and fluctuating velocity components in the streamwise and wall-normal directions, respectively. The x direction and y direction will hereafter be referred to as the streamwise and wall-normal directions, respectively. U_{m} is the local maximum mean streamwise velocity and y_{m} is its wall-normal location. As shown, a wall jet is generally characterized by an inner layer extending from the wall up to y_{m} that closely resembles a boundary layer, and an outer layer stretching from y_{m} to the outer edge of the jet that is similar to a free jet. The velocity is zero at the wall due to the no-slip condition of the viscous flow, and is approximately zero at a certain wall-normal distance above the surface where the outer edge of the wall jet merges with the ambient fluid. Typically, the ambient fluid will have approximately zero streamwise velocity with a finite wall-normal velocity due to the effect of entrainment. The outer half-width $(y_{1/2})_{\mathrm{out}}$ and the inner half-width $(y_{1/2})_{\mathrm{in}}$ (not shown) denote the wall-normal location where $U = U_{\mathrm{m}}/2$ occurs in the outer and inner layers, respectively.

For the convenience of discussion, the stratification of a plane wall jet presented by George *et al*. (2000) which is based on the inner scales is adopted in this thesis unless stated otherwise. A dimensionless wall-normal distance y^+ is defined as $y^+ = yU_\tau/\upsilon$, where U_τ is the

friction velocity which can be expressed as $U_\tau = \sqrt{\tau_w/\rho}$ and υ is the fluid kinematic viscosity. Accordingly a plane wall jet is comprised of the following layers (regions): the region of $0 < y^+ < 3$ is called the "linear sublayer"; the region of $3 < y^+ < 30$ is called the "buffer layer"; the linear sublayer and the buffer layer constitute the "viscous sublayer"; the region of $30 < y^+ < 300$ is called the "mesolayer"; the region of $300 < y^+ < 0.1\left(y_{1/2}\right)^+_{\text{out}}$ is called the "inertial sublayer", where $\left(y_{1/2}\right)^+_{\text{out}} = \left(y_{1/2}\right)_{\text{out}} U_\tau/\upsilon$; the mesolayer and the inertial sublayer constitute the "overlap region"; the region of $y^+ > 0.1\left(y_{1/2}\right)^+_{\text{out}}$ is called the "outer wall jet region"; the viscous sublayer and the overlap region constitute the "inner layer", while the overlap region and the outer wall jet region constitute the "outer layer". Previous studies usually showed $0.1\left(y_{1/2}\right)^+_{\text{out}} < 300$ for a plane turbulent wall jet, which means the inertial sublayer was seldom observed.

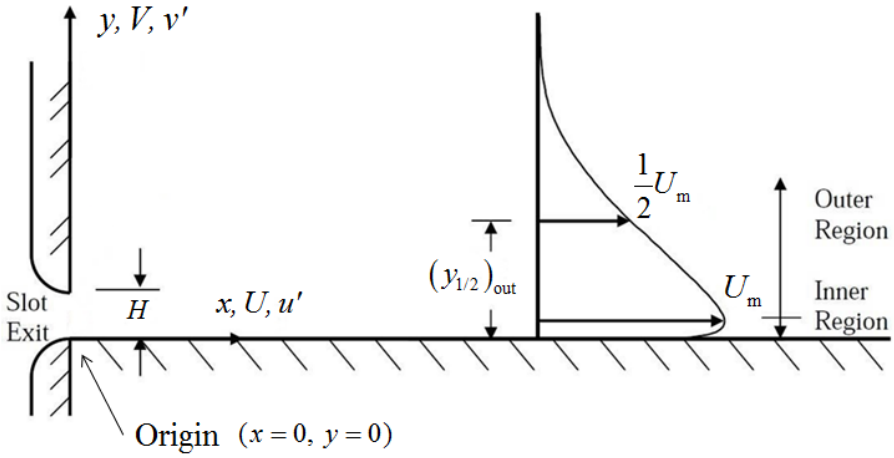

Figure 1.1: A schematic representation of a plane wall jet

From a theoretical perspective, an ideal two-dimensional plane wall jet would be discharged from a slot exit with a finite height and an infinite width into a body of fluid that has

no far-field boundaries in all three coordinate directions, i.e. streamwise, wall-normal and spanwise directions. As an infinite slot width cannot be achieved in practice, the slot exit is usually made to have a large width-to-height ratio (normally larger than 70) in order to produce a two-dimensional initial flow as documented by Eriksson *et al*. (1998) and Tachie *et al*. (2004). The boundary condition above the slot exit can be either a thin lip or a vertical wall; the latter geometry can be better implemented in computational simulations (Eriksson *et al*., 1998). Typically, to evaluate the effect of finite streamwise scale of the experimental facility, the data for the farthest downstream location are checked in comparison to data for other more upstream locations (Eriksson *et al*., 1998). In addition, measurements are typically taken along the centerline of the ground plane so as to minimize the effect of side walls (Eriksson *et al*., 1998). The entrainment in the wall-normal direction causes a reverse flow which will be introduced later in this chapter.

1.2.2 Governing Equations

Typically, two conservation equations are used to define the mathematical model for a turbulent wall jet: the continuity equation, and the Reynolds-Averaged Navier-Stokes (RANS) equation, i.e. the momentum equation.

The wall jet considered in this study is a steady, incompressible, two-dimensional, turbulent plane wall jet with constant properties. For such a flow, the continuity equation has the form

$$\frac{\partial U}{\partial x}+\frac{\partial V}{\partial y}=0 \tag{1.1}$$

and the Reynolds-Averaged Navier-Stokes equation for the streamwise direction has the form

$$U\frac{\partial U}{\partial x}+\frac{\partial}{\partial x}\left(\left\langle u^2\right\rangle\right)+V\frac{\partial U}{\partial y}+\frac{\partial}{\partial y}\left(\left\langle uv\right\rangle\right)=-\frac{1}{\rho}\frac{\partial P}{\partial x}+\frac{\partial}{\partial y}\left(\upsilon\frac{\partial U}{\partial y}\right), \tag{1.2}$$

where P is the pressure and ρ is the fluid density. By integrating the RANS equation for the wall-normal direction across the wall jet and applying the Thin Shear Layer Approximation which is valid for a plane wall jet, i.e. retaining only the gradient in the wall-normal direction for the diffusion terms, Equation (1.2) can be transformed to

$$U\frac{\partial U}{\partial x}+V\frac{\partial U}{\partial y}=\frac{\partial}{\partial x}\left[\left\langle v^2\right\rangle-\left\langle u^2\right\rangle\right]+\frac{\partial}{\partial y}\left[\upsilon\frac{\partial U}{\partial y}-\left\langle uv\right\rangle\right] \tag{1.3}$$

with the boundary conditions that $U\to 0$ as $y\to\infty$ (for the ambient stagnant fluid) and $U = 0$ at $y = 0$ (for the no-slip condition at the wall) according to George *et al*. (2000). Here $\left\langle u^2\right\rangle$ and $\left\langle v^2\right\rangle$ denote the streamwise and wall-normal Reynolds stress components, respectively, while $\left\langle uv\right\rangle$ represents the Reynolds shear stress; the term $\upsilon\frac{\partial U}{\partial y}$ is the laminar shear stress, where υ is the kinematic viscosity of the fluid.

Equation (1.1) gives a mathematical relation between the mean streamwise and wall-normal velocity components in a two-dimensional incompressible flow. Equation (1.3) shows that in the streamwise direction the convection terms on the left-hand side are balanced by the gradients of the turbulent stresses and the viscous diffusion on the right-hand side.

1.2.3 Self-similarity and Scaling Laws

As introduced by George (1989), the concepts of self-preservation or self-similarity can be traced back as early as the 1900's when such ideas were proposed in the context of laminar boundary layer theory. They were first applied to turbulence in 1937 and ever since have been one of the backbones of turbulent flow theory (George, 1989). Stewart and Townsend (1951) were among the first to clearly discuss the closely related yet different concepts of self-preservation and self-similarity. They distinguished between these two concepts by noting that the case of self-preservation is a subset of the case of self-similarity, i.e. if a flow is self-preserved it is not necessarily self-similar, but if a flow is self-similar it is certainly self-preserved. They referred to self-preservation as a state when the structure of a particular variable (e.g. the distribution of mean or fluctuating velocity) within a turbulent flow remains self-similar during its development, and such a structure can be expressed in terms of a single length scale and a single velocity scale. In contrast, self-similarity was defined as a state in which a single length scale and a single velocity scale alone are sufficient to describe the self-similar structure of any variable within a turbulent flow.

To avoid confusion and ambiguity, as well as to follow the customary terminology of the turbulence research community, in this thesis "self-preservation" and "self-similarity" both refer to the concept of self-preservation as defined by Stewart and Townsend (1951) except when explicitly stated otherwise, and the terms "self-similarity" and "self-similar" will be used to describe such a state.

A more understandable and detailed definition of self-similarity was given by George (1989). From the perspective of the dynamical significance of self-similarity, he indicated that a flow can be claimed to exhibit self-similarity if there exist solutions, e.g. an equation for the

mean velocity distribution, to its governing equations and boundary conditions for which all terms of dynamical significance have the same relative value at the same relative location. Alternatively, as described by Dunn (2010), a flow is said to be self-similar when the velocity profiles can be non-dimensionalized by certain scale factors, e.g. the local maximum mean streamwise velocity U_{m} and the outer half-width $\left(y_{1/2}\right)_{\mathrm{out}}$, to converge to a single common profile. Such a non-dimensionalized profile and its corresponding mathematical equation are called the similarity-solution, and the specific choice of the scale factors is referred to as the scaling law (Barenblatt, 2003). The flow region where the mean velocity field has become self-similar is conventionally called the fully developed region (Dunn, 2010).

The state of self-similarity in turbulent flows has been one of the major research topics among the fluid dynamics community for the past decades because one direct consequence of such a state is that the governing equations and boundary conditions for the flow will become independent of the particular variable(s) on which the scale factors depend and the resultant similarity-solution is thereby reduced by one (or more) variable(s) in its functional dependence (George, 1989). For instance, it is widely observed that in the fully developed region the mean streamwise velocity profiles in the outer layer of the wall jet on a smooth surface collapse to a single curve when non-dimensionalized using the local maximum mean streamwise velocity U_{m} as the velocity scale and the outer half-width $\left(y_{1/2}\right)_{\mathrm{out}}$ as the length scale (George *et al*., 2000), which implies self-similarity. These two scale factors, U_{m} and $\left(y_{1/2}\right)_{\mathrm{out}}$, depend on the streamwise distance from the slot exit, *x*, therefore in the corresponding similarity-solution the variable *x* is no longer relevant since the non-dimensionalized local streamwise mean velocity U/U_{m} is independent of *x*.

In addition to simplifying the mathematical model, self-similarity also indicates that the flow has reached a balance where the internal dynamical adjustment is complete (George, 1989), which marks the onset of the fully developed region.

1.2.4 Complete Similarity and Incomplete Similarity

As pointed out by George (1989), until the 1970's it was still widely accepted by the turbulence research community that a self-similar flow achieves the state of self-similarity by becoming asymptotically independent of the inlet boundary conditions. This follows the belief that a turbulent flow will gradually become uncorrelated with its initial conditions and consequently the fully developed flow can be modeled based solely on local properties. This concept is usually referred to as "asymptotic independence" and even today it still dominates most texts on turbulent flow (George, 2012). Based on his review of some canonical turbulent flows, e.g. wakes, jets, and homogeneous decaying turbulence, George (2012) rejected the concept of "asymptotic independence"; instead he concluded that for many types of flows the initial conditions play an essential role in the spatial evolution of the flow (George, 1989). George (2012) also noted the potential for implementing turbulence control by adjusting the initial flow conditions. Finally, George (2012) indicated that it was not clear whether a dependence on initial conditions is a general feature of most turbulent flows.

Barenblatt (2003) studied the roles of both small and large parameters in the mathematical description of certain physical phenomenon, e.g. a turbulent boundary layer flow or a plane turbulent wall jet. "Small or large" here means the relative magnitude in comparison to the characteristic scales of the physical phenomenon under consideration. He proposed the concepts of complete similarity and incomplete similarity to describe two mutually exclusive

outcomes from such an examination of a self-similar phenomenon: if all parameters of small (or large) value can be excluded from the final similarity-solution of a physical phenomenon, the phenomenon is said to exhibit complete similarity; on the contrary, if any parameters of small (or large) value are still retained in the final similarity-solution of a physical phenomenon no matter how small (or large) that parameter is, the phenomenon is said to exhibit incomplete similarity. By applying this theory to the experimental data of Karlsson *et al*. (1991), Barenblatt *et al*. (2005) focused specifically on the role of the slot height H in the evolution of the plane turbulent wall jet on a smooth surface. They concluded that this special type of turbulent flow exhibits incomplete similarity, which means that the slot height H, no matter how small, remains a significant parameter. Although the analytical method they used is logical and coherent, they emphasized their conclusions were not established fact due to the restricted amount of experimental data available for validation. More specifically, the experimental data they used were for a single slot Reynolds number and a single type of surface, i.e. a smooth surface, which leaves the validity of their conclusions for flows at different Reynolds numbers and for other types of surface, e.g. a rough surface, subject to future verification. In addition, they indicated that the slot Reynolds number dependence of the power coefficients involved in their scaling laws was inconclusive. These issues warrant further investigation.

1.2.5 Slot Boundary Conditions

As mentioned by Dunn (2010) and other studies, it is important to document the boundary conditions, i.e. the mean and fluctuating velocity fields at the slot exit, to facilitate a comprehensive analysis of the experimental results as well as possible future numerical studies. More specifically, from an experimental viewpoint, measurement of the flow field at or near the

slot exit can provide direct information of the initial streamwise bulk velocity U_o. Ideally the profile for U_o is uniform with a low turbulence intensity, preferably less than 1% (Rostamy *et al*., 2011a) and normally not larger than 5% (Tachie *et al*., 2004).

1.2.6 Initial Development

As discussed by George (1989), in terms of spatial development, no flow will begin in a self-similar state (unless particular care was taken in its initiation) since inner and outer dynamical readjustments are always needed for the flow to smooth out the details of the initial conditions, e.g. infinite or very large gradients in velocity profiles, so as to finally achieve the self-similar state. The region next to the inflow is often referred to as the initial development region. For a plane turbulent wall jet, in this region the flow will experience a transition in which the initial uniform mean velocity profile gradually loses uniformity.

A criterion to quantitatively determine the length of this region is to check the maximum streamwise distance over which the potential core is preserved. According to Rajaratnam (1976), at a downstream location where the boundary layer in the inner region of the wall jet meets the shear layer in the outer region, U_m will drop below the initial maximum mean streamwise velocity $U_{m,o}$ and hence the potential core is considered depleted. The streamwise distance over which $U_{m,o}$ is sustained is called the potential core length x_p.

1.2.7 Fully Developed Region

As defined above, the fully developed region is a portion of the flow domain over which a self-similar state exists. Since the flow in this region is stable in terms of the flow-specific features, it is customary to study the major characteristics of the flow in this region. These major

characteristics usually include such mean velocity field features as the non-dimensional streamwise mean velocity profile, the streamwise development of the outer half-width $(y_{1/2})_{\text{out}}$ and the inner half-width $(y_{1/2})_{\text{in}}$, the change in the local maximum mean streamwise velocity U_{m} and its wall-normal location y_{m}, and the variation of the skin friction coefficient C_f in the streamwise direction. The fluctuating velocity field features, including the Reynolds stress profiles, also constitute major characteristics of the flow. These results will provide detailed information about the structure of the flow under study.

1.2.8 Effects of Surface Roughness

The plane turbulent wall jet on a smooth surface is not as well studied as the canonical turbulent boundary layer (Rostamy, 2011a). The plane turbulent wall jet on a rough surface has received even less attention even though many industrial surfaces are rough. All previous studies indicated that the surface roughness will change the characteristics of the plane wall jet, especially in the inner layer. However, it is not yet clear to what extent the surface roughness will influence the structure of the plane wall jet in the outer layer.

Figure 1.2 shows a schematic of a plane wall jet on a rough surface. Compared to Figure 1.1, the only new parameter here is k which denotes the average thickness of the rough surface.

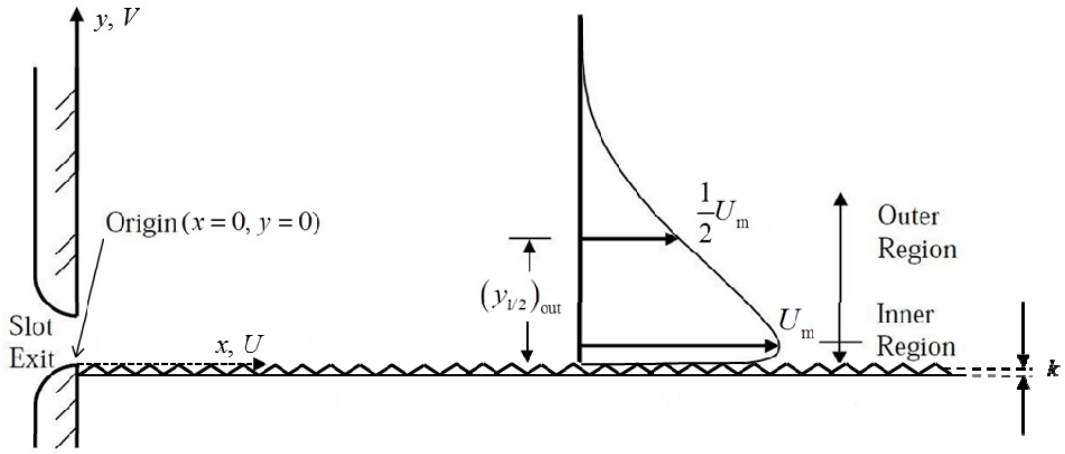

Figure 1.2: A schematic representation of a plane wall jet on a rough surface

1.2.9 Reverse Flow

As mentioned above, the ambient fluid into which an ideal two-dimensional plane turbulent wall jet is discharged should extend to infinity in all three coordinate directions. This cannot be fully satisfied in actual experiments. Instead, the finite dimensions of the experimental facility (a water tank in the present case) will always exert an influence on the development and characteristics of the plane wall jet and cause it to deviate from the theoretical predictions based on the assumption of an infinite ambient fluid. One of the features associated with the finite wall-normal domain is the reverse flow or recirculating flow. To reduce the influence of such a flow, the fluid depth in the experimental facility is usually kept at a consistent level throughout the measurements (Eriksson *et al*., 1998). The vertical wall above the slot exit will also contribute to the formation of this reverse flow (Eriksson *et al*., 1998). The precise effect of the reverse flow is inconclusive from previous studies.

1.3 Objectives

As described above, there are several unresolved questions on the characteristics of the plane turbulent wall jet that warrant further investigation. With the intention to clarify some of these issues, this thesis reports on a series of measurements of a plane turbulent wall jet using particle image velocimetry (PIV). The specific objectives of this research project are as follows:

1. Conduct velocity measurements in a plane turbulent wall jet for different inflow conditions and surface roughness, which include the fully rough regime.
2. Based on the experimental results, assess whether the flow characteristics are self-similar, and, more specifically, whether the mean velocity field shows incomplete similarity. This issue will be investigated for both smooth and rough surfaces. In addition, whether such similarity is affected by the surface roughness will also be studied.

1.4 Scope

The present study experimentally investigated the plane turbulent wall jet for three flow conditions: smooth, transitionally rough and fully rough flow. The measurements were conducted in a water tank facility at the University of Saskatchewan. A 3.7-kW/5hp pump together with a piping system were used to recirculate the water through the tank. PIV was used to measure the flow along the centerline of the ground plane. Two inlet flow rates were considered, i.e. a low flow rate which will hereafter be referred to as LFR, and a high flow rate which will hereafter be referred to as HFR, for each type of surface, i.e. a smooth surface and rough surface.

The scope can be described as follows:

- The slot Reynolds number, defined as $Re_o = U_o H/\upsilon$ which is based on the jet exit velocity and the slot height, was Re_o = 6,930 ± 6% for the LFR and Re_o = 13,900 ± 4% for the HFR cases, respectively.
- Four series of measurements were conducted: LFR on the smooth surface, HFR on the smooth surface, LFR on the rough surface, HFR on the rough surface. The first two series considered a wall jet on a smooth surface; the third and fourth series considered a transitionally rough and fully rough plane wall jet, respectively. Seven fields of view (FOV) were acquired from x = 0 to x = 110H for all four series of measurements. Two thousand and four thousand PIV images were captured for each field of view on the smooth and rough surface, respectively. Previous studies have shown that mean quantities converge with 2000 images (Shinneeb, 2006, and Dunn, 2010). In-house PIV control and processing software was used.
- The mean velocity fields for all four series of measurements were analyzed. The slot height H was chosen as the key parameter of interest in terms of the incomplete similarity in the present study.

1.5 Chapter Summary

This chapter gives an overview of a plane turbulent wall jet, including the theoretical and industrial motivation for the research, the fundamental concepts and relevant theory, and the unresolved questions left to be investigated. A focus of this chapter is the recently proposed theories of similarity, complete similarity and incomplete similarity, as well as the methodology to evaluate them. The effect of surface roughness is also given same attention. These two topics constitute the core of the analyses and discussions presented in this thesis.

Next, a literature review will be presented in Chapter 2. The description of the experimental facility and apparatus will be given in Chapter 3. Then the measured results will be analyzed in Chapters 4 through 6 discussing the initial development and the fully developed region of the plane wall jet, covering incomplete similarity as well as effects of the surface roughness and the reverse flow. Finally, major conclusions will be presented together with recommendations for future work in Chapter 7.

CHAPTER 2

LITERATURE REVIEW

This chapter presents a review of previous studies pertaining to the topics introduced in Chapter 1. An extensive review on wall jet studies prior to 1981 was presented by Launder and Rodi (1981, 1983). More recently, Banyassady and Piomelli (2014) provided a comprehensive survey of plane wall jet studies, especially those related to the effects of roughness. Therefore, this chapter will only reference select papers directly relevant to the key topics of the present study and discuss their implications for the experimental approach adopted.

2.1 Incomplete Similarity

The concept of incomplete similarity and the criteria to assess it were first proposed by Barenblatt (2003). According to this theory, any physically important relation, i.e. a relation expressing a physical law valid for various observers whose units of measurement are different, can be presented as

$$s = f\left(a_1, a_2, ..., a_k, b_1, b_2, ..., b_m\right) , \tag{2.1}$$

where s is the property being determined, and its $n = k + m$ parameters a_1, a_2, …… , a_k, and b_1, b_2, …… , b_m, called governing parameters, are assumed to be known. These governing parameters can always be divided into two groups: a group of k parameters a_1, a_2, …… , a_k that have independent dimensions, and another group of m parameters b_1, b_2, …… , b_m which can be presented as products of powers of the dimensions of parameters a_1, a_2, …… , a_k, i.e.

$$\left[b_i\right] = \left[a_1\right]^{p_i} \cdots \left[a_k\right]^{r_i} , \; i = 1, 2, \ldots, m . \tag{2.2}$$

The square bracket indicates the dimension of the parameter. If the dimensions of all governing parameters are independent, $m = 0$; if all governing parameters are dimensionless, $k = 0$. More generally, these parameters satisfy $k > 0$, $m > 0$.

According to Barenblatt (2003), the dimension of the property to be determined can be expressed in terms of the dimensions of the first group of governing parameters a_1, a_2, …… , a_k as

$$[s] = [a_1]^p \cdots [a_k]^r , \tag{2.3}$$

where p and r denotes the exponents to make this expression valid. Now, a series of dimensionless parameters Π_i , called similarity parameters, can be introduced as

$$\Pi = \frac{s}{a_1^p \cdots a_k^r}, \Pi_i = \frac{b_i}{a_1^{p_i} \cdots a_k^{r_i}} \quad (i = 1, \ldots, m) . \tag{2.4}$$

Therefore, relation (2.1) can be represented in the following dimensionless form:

$$\Pi = \Phi(\Pi_1, \ldots, \Pi_i, \ldots \Pi_m) . \tag{2.5}$$

Once a relation in the form of Equation (2.5) is established for a physical phenomenon, the next step is to determine the importance of each governing parameter b_i with a corresponding similarity parameter Π_i , i.e. to determine whether it is necessary to retain such a parameter b_i in the similarity solution or not. In general, if Π_i has a magnitude outside the range of 1/10 to 10, Π_i is regarded as either too small or too large with respect to the physical scale of the phenomenon (Barenblatt, 2003). A nominal assessment would tend to disregard such a similarity parameter (Barenblatt, 2003; George, 1989). This analysis is crucial because one of the goals of similarity analysis is to formulate general scaling laws using as few governing parameters as possible (Barenblatt, 2003).

As explained by Barenblatt (2003), the result of such an analysis divides the self-similarity of a physical phenomenon into two categories. If a governing parameter b_i remains essential, i.e. is not negligible in the final universal solution, no matter how small or large the corresponding similarity parameter Π_i is, there exists incomplete similarity of the physical phenomenon. On the contrary, if all governing parameters b_i, whose corresponding similarity parameters Π_i fall outside the range of 1/10 to 10, can be discarded in the final form of the universal solution, there exists complete similarity of the physical phenomenon in all the relevant parameters.

In practice, when analyzing a physical phenomenon, the assumption of either incomplete or complete similarity and the similarity solution based on this assumption will be evaluated against existing experimental data and/or numerical simulations to estimate the validity of the assumption (Barenblatt, 2003).

Following the theory by Barenblatt (2003), Barenblatt *et al*. (2005) considered incomplete similarity of a plane turbulent wall jet in terms of the slot height H. They proposed two hypotheses: first, a plane turbulent wall jet consists of three layers, i.e. an outer layer, an inner layer and an intermediate layer between them; second, the flow has the property of incomplete similarity in the parameter H. Based on these hypotheses and the related dimensional analysis, they concluded that the dimensionless relation for the mean streamwise velocity distribution has a definite form as

$$\frac{U}{U_{\mathrm{o}}}=\left(\frac{x}{H}\right)^{\gamma_{\mathrm{m}}}\phi\left(\frac{\frac{y}{H}}{\left(\frac{x}{H}\right)^{\gamma}},Re_{\mathrm{o}}\right), \tag{2.6}$$

where Re_o is the slot Reynolds number and ϕ is a function not explicitly determined. The exponent γ is different for the outer and inner layers, i.e. $\gamma = \gamma_o$ for the outer layer and $\gamma = \gamma_i$ for the inner layer. The exponential coefficients γ_m and γ are defined in power law relations as follows:

$$\frac{U_m}{U_o} = A_m \left(\frac{x}{H} \right)^{\gamma_m} \tag{2.7}$$

and

$$\frac{\left(y_{1/2} \right)_{out}}{H} = A_o \left(\frac{x}{H} \right)^{\gamma_o} \tag{2.8}$$

$$\frac{\left(y_{1/2} \right)_{in}}{H} = A_i \left(\frac{x}{H} \right)^{\gamma_i} \tag{2.9}$$

for the outer and inner layer, respectively. The coefficients A_m, A_o and A_i are determined by fitting the experimental data or numerical results to these relations. The values of γ_m and γ can only be obtained from experimental or numerical data (Barenblatt, 2003; Barenblatt *et al*., 2005).

By using Equations (2.7) through (2.9), Equation (2.6) can be rewritten as

$$\frac{U}{U_m} = \left(A_m \right)^{-1} \phi \left(\frac{A_o y}{\left(y_{1/2} \right)_{out}}, Re_o \right) \tag{2.10}$$

and

$$\frac{U}{U_m} = \left(A_m \right)^{-1} \phi \left(\frac{A_i y}{\left(y_{1/2} \right)_{in}}, Re_o \right) \tag{2.11}$$

for the outer and the inner layer, respectively. These two equations indicate that the relation shown by Equation (2.6) can be represented as a specific scaling law such that the velocity scale

is U_m and the length scale is $\left(y_{1/2}\right)_{out}/A_o$ or $\left(y_{1/2}\right)_{in}/A_i$. Note that $\left(y_{1/2}\right)_{out}$ and $\left(y_{1/2}\right)_{in}$ are nonlinear functions of x/H here.

Furthermore, Barenblatt *et al*. (2005) concluded that Equation (2.6) can be represented in a dimensional form, which was considered to be a universal relation for the plane turbulent wall jet, as follows:

$$U = \left(\frac{J}{\rho H}\right)^{\frac{1}{2}} \left(\frac{x}{H}\right)^{\gamma_m} \phi\left(\frac{\frac{y}{H}}{\left(\frac{x}{H}\right)^{\gamma}}, Re_o\right) , \tag{2.12}$$

where J is the inlet momentum flux (per unit spanwise width of the slot) defined as $J = U_o^2 \rho H$.

Recalling the definitions of incomplete and complete similarity introduced above, Equation (2.12) shows that if the hypothesis of incomplete similarity of a plane wall jet in terms of H is correct, then $\gamma \neq 1$ and/or $\gamma_m \neq$ -0.5, i.e. H remains essential in the final universal relation for the distribution of U even if the corresponding similarity parameter x/H has a magnitude clearly outside the range of 1/10 to 10.

Based on this criterion, Barenblatt *et al*. (2005) used the high-resolution LDA data of Karlsson *et al*. (1991) to investigate the hypothesis of incomplete similarity in a plane wall jet on a smooth surface. They confirmed that the scaling laws in the outer and inner layers are substantially different and each shows self-similarity. They obtained γ_o = 0.93, γ_i = 0.68 and γ_m = -0.6, which supports the hypothesis of incomplete similarity. However, they also emphasized that their hypotheses were not yet established due to the limited amount of available experimental data considered. In particular, the slot Reynolds number dependence of the exponents γ and γ_m was inconclusive since the LDA data they used were for only one slot Reynolds number.

Following the theory and methodology of Barenblatt *et al*. (2005), Rostamy *et al*. (2011c) conducted an experimental study based on a new set of LDA measurements for a plane wall jet on a smooth surface and found similar results, i.e. the presence of incomplete similarity was observed. By combining the rough surface data of Rostamy *et al*. (2011a) and Rostamy *et al*. (2011b), Bergstrom *et al*. (2013) and Tang *et al*. (2015) presented comprehensive analyses of the fully developed mean velocity field in a plane turbulent wall jet on both smooth and transitionally rough surfaces. They confirmed the validity of the incomplete similarity theory of Barenblatt *et al*. (2005) for a transitionally rough plane wall jet. The values of the power law relations obtained in these recent studies are presented in Table 2.1.

Table 2.1: Summary of recent studies on incomplete similarity of turbulent plane wall jet

Study	Surface	H (mm)	Re_o	γ_o	γ_i	γ_m
Barenblatt *et al*. (2005)	Smooth	9.6	9,600	0.93	0.68	-0.56
Rostamy *et al*. (2011c)	Smooth	6.0	7,500	0.78	0.50	-0.41
Tang *et al*. (2015)	Transitionally rough	6.0	7,500	0.82	0.40	-0.58

To summarize, this section provides a review of studies directly relevant to the topic of incomplete similarity of a plane wall jet in terms of the slot height H. While incomplete similarity for plane wall jets on smooth and transitionally rough surfaces has been previously studied, a fully rough plane wall jet has not yet been studied in detail. Such an investigation will be one of the core objectives of the present study. The next parts of this chapter will focus on previous studies of specific plane wall jet features in the initial development and fully developed region.

2.2 Inlet Flow Quality

In this section, previous experimental studies are reviewed to provide reference for the inlet flow features with a focus on the uniformity and the turbulence level of the inlet velocity profile.

As pointed out by Smith (2008), for a zero-pressure-gradient (ZPG) boundary layer, a plane free jet and a plane wall jet, the momentum equation is the same, but the boundary conditions for these prototypical flows are different. This illustrates that the boundary conditions play a critical role in the formation of the various flow conditions. In addition, the analysis of the experimental results will involve parameters such as the slot exit height H and the initial bulk velocity U_o. Therefore, it is worthwhile to first examine the slot boundary conditions before considering the fully developed region.

Eriksson *et al*. (1998) conducted high-resolution laser Doppler anemometry (LDA) measurements for the plane wall jet on a smooth surface. They set the slot height to H = 9.6 mm and the slot width-to-height ratio to 151. The inlet bulk velocity was U_o = 1.0 m/s, which resulted in a slot Reynolds number of Re_o = 9,600. Their facility produced a fairly uniform inlet velocity profile with a deviation of ± 0.25% in the mean streamwise velocity distribution at y = 4.5 mm along the spanwise direction. The streamwise turbulence intensity in the uniform part of the profile across the slot height was less than 1%.

Dunn (2010) studied a plane wall jet on a smooth surface using PIV with 2,000 pairs of images for each field of view captured at a sampling frequency of 4 Hz. In the experiment the slot height was H = 6.0 mm and the slot width was 756 mm, resulting in a width-to-height ratio of 126. For a velocity profile at x = 2/3H, which was representative of the inlet boundary

conditions, the maximum streamwise velocity was $U_{m,o}$ = 1.42 m/s and the average velocity across the height of the slot to be U_o = 1.29 m/s. The corresponding slot Reynolds number was Re_o = 7,860. The deviation of the mean streamwise velocity profile was less than 0.3% over 71% of the slot height. Within this uniform region the streamwise turbulence intensity was 1.45%. The mean wall-normal velocity along the slot height was close to zero. The fluctuating velocity had the same magnitude as the streamwise component, while the relative turbulence level normalized by the mean velocity was significantly higher than for the streamwise case.

Rostamy *et al*. (2011b) conducted LDA measurements in the same facility as used by Dunn (2010), but their experiments involved two surfaces: a smooth surface and a transitionally rough surface. The number of samples used to obtain the mean velocity component at each measurement point was 5,000. The slot height was kept as H = 6.0 mm. For both surfaces, the slot bulk velocity was set to U_o = 1.21 m/s, resulting in a slot Reynolds number of Re_o = 7,500. At $x = H$, the streamwise turbulence intensity in the uniform part of the mean velocity profile, which accounted for approximately 78% of the slot height H, was reported to be less than 1%.

2.3 Initial Development

As introduced in Chapter 1, the initial development region of a plane wall jet is the region where the inlet maximum mean streamwise velocity $U_{m,o}$ is sustained, and the streamwise range of this region is represented by the potential core length x_p. Rajaratnam (1976) provides a comprehensive analysis of previous studies on the initial development region of a plane wall jet on both smooth and rough surfaces. Based on select experimental observations, for the smooth surface case he proposed a theoretical relation for the potential core length x_p which depends

only on the slot Reynolds number Re_o and the slot height H, and found that x_p changes from 6.1H to 6.7H for $Re_o = 1\times10^4$ and 1×10^5. As for the rough surface case, he proposed a relation for the potential core length x_p, which is a function of the slot height H and the average height of the roughness elements k_e but is independent of Re_o. By examining his results for the rough surface cases over slot Reynolds numbers of $1.91\times10^4 \leq Re_o \leq 1.02\times10^5$, he concluded that the potential core length is appreciably influenced by the surface roughness, generally decreasing with the increasing relative roughness k_e /H.

More recently, Dunn (2010) performed an analysis on the initial development region based on measurements on a smooth surface. He reported a noticeable drop in the maximum velocity at $x/H = 7$ compared to the initial maximum velocity of the jet and estimated the length of the potential core as $x_p = 6H$. He also observed from the mean streamwise velocity profiles at $1 \leq x/H \leq 6$ that the wall jet grows in the wall-normal direction and the maximum velocity decreases with downstream distance, which was due to the combined effects of the shear force at wall and at the interface between the jet and the ambient fluid.

2.4 Fully Developed Region

This section presents the analysis methods and typical results for the fully developed region presented in select studies, which provided guidance and references for analyzing the data of the fully developed region in the present study.

2.4.1 Friction Velocity

As noted in many studies (e.g. George *et al.*, 2000), the friction velocity, defined as $U_\tau = \sqrt{\tau_w/\rho}$ where τ_w is the wall shear stress and ρ is the fluid density, is a key velocity scale in analyzing the similarity of the plane wall jet.

As concluded by Wygnanski *et al.* (1992), the most reliable method to determine U_τ is by measuring the slope of the mean velocity profile near the surface to calculate the wall shear stress through the definition $\tau_w = \mu\left(\partial U/\partial y\right)_{y\approx 0}$. However, this is usually challenging in experiments due to the resolution limit near the surface, especially for PIV which will be further discussed in the following chapters.

Rostamy *et al.* (2011b) provided a thorough examination of the several possible methods to determine U_τ for a plane wall jet on a smooth surface. The first method was by fitting the mean streamwise velocity data in the overlap region, i.e. $30 < y^+ < 0.1\left(y_{1/2}\right)^+_{out}$, of the wall jet to a composite profile proposed by George *et al.* (2000) which is valid across the viscous sublayer (i.e. $y^+ < 30$), mesolayer (i.e. $30 < y^+ < 300$) and inertial sublayer (i.e. $300 < y^+ < 0.1\left(y_{1/2}\right)^+_{out}$) for a wall-bounded flow on a smooth surface. It can be expressed in the following form:

$$\begin{aligned} U^+ = &\left[y^+ + c_4\left(y^+\right)^4 + c_5\left(y^+\right)^5 \right]\exp\left[-d\left(y^+\right)^5 \right] \\ &+ C_i\left(y^+\right)^\gamma \left[1 + \gamma a^+\left(y^+\right)^{-1} + \frac{1}{2}\gamma\left(\gamma-1\right)\left(a^+\right)^2\left(y^+\right)^{-2} \right] \\ &\times \left[1 - \exp\left(-d\left(y^+\right)^6 \right) \right], \end{aligned} \tag{2.13}$$

where $U^+ = U/U_\tau$, c_4 = -0.0003, c_5 = 1.35 × 10^{-5}, d = 8 × 10^{-8} and a^+ = -16 are constants given by George *et al.* (2000), and C_i and γ are each a specific function of the local Reynolds number based on the outer half-width, i.e. $\left(y_{1/2}\right)^+_{\text{out}} = \left(y_{1/2}\right)_{\text{out}} U_\tau/\upsilon$.

The second method was a theoretical relation derived by George *et al.* (2000) based on the power law, i.e.

$$\frac{U_\tau}{U_{\text{m}}} = \frac{C_{\text{o}}}{C_{\text{i}}}\left(D\left(y_{1/2}\right)^+_{\text{out}}\right)^{-\gamma}, \tag{2.14}$$

where $C_{\text{o}}/C_{\text{i}}$ and D are constants given by George *et al.* (2000), and γ has the same definition as in Equation (2.13) above. Solving the nonlinear equation for each downstream location with U_τ as the sole unknown value can give U_τ values.

A third method was a relation proposed by Wygnanski *et al.* (1992) based on the momentum integral analysis for the wall shear stress τ_{w}. It has the following form:

$$\frac{\tau_{\text{w}}}{\rho}\left(\frac{\upsilon}{M_{\text{o}}}\right)^2 = A_\tau\left(\frac{xM_{\text{o}}}{\upsilon^2}\right)^{\alpha_\tau}, \tag{2.15}$$

where M_{o} is the inlet momentum flux per unit mass defined as $M_{\text{o}} = U_{\text{o}}^2 H$. A_τ and α_τ are constants defined by the following relations:

$$A_\tau = -\lambda\left(2\alpha_2 + \alpha_1\right) A_1 \left(A_2\right)^2 \tag{2.16}$$

$$\alpha_\tau = 2\alpha_2 + \alpha_1 - 1 \tag{2.17}$$

$$\lambda = \int_0^\infty \left(\frac{U}{U_{\text{m}}}\right)^2 d\left(\frac{y}{\left(y_{1/2}\right)_{\text{out}}}\right) \tag{2.18}$$

$$\frac{\left(y_{1/2}\right)_{\text{out}} M_o}{\upsilon^2} = A_1\left(\frac{xM_{\text{o}}}{\upsilon^2}\right)^{\alpha_1} \tag{2.19}$$

$$\frac{U_{\mathrm{m}}\upsilon}{M_o} = A_2\left(\frac{xM_{\mathrm{o}}}{\upsilon^2}\right)^{\alpha_2}. \tag{2.20}$$

The coefficients λ, α_1 and α_2 can be calculated using the data from measurements or numerical simulations. Wygnanski *et al.* (1992) reported values of A_τ = 0.146 and α_τ = -1.07, while Rostamy *et al.* (2011b) reported A_τ = 0.161 and α_τ = -1.05, which differ by approximately 10% and 2%, respectively.

By comparing the fitted data obtained from the composite profile, i.e. Equation (2.13), with those from the classical logarithmic law, i.e.

$$U^+ = \frac{1}{\kappa}\ln(y^+) + B \tag{2.21}$$

with κ = 0.41 and B = 5.0 for a canonical turbulent boundary layer, Rostamy *et al.* (2011b) observed a good collapse of their data in the overlap region with the classical logarithmic law. In addition, by comparing the friction velocities on the smooth surface calculated using the above three methods, they concluded the results from Equation (2.13) and Equation (2.14) are in close agreement with each other with a maximum difference of 1.1%, while the friction velocities from Equation (2.15) and those from the other two methods have a higher discrepancy (as much as 6%) over the same downstream extent.

Based on the same data set, Rostamy *et al.* (2011a) used both the classical logarithmic law and the composite profile of George *et al.* (2000) for the profile fitting to compare the friction velocity results. Where the classical logarithmic law with constants of κ = 0.41 and B = 5.0, and the constants given by George *et al.* (2000) were used, these two methods led to approximately the same friction velocity. However, it should be noted that George *et al.* (2000) stated some of the constants in their composite profile relation have different values for a

canonical turbulent boundary layer and a plane turbulent wall jet, and the constants for the latter flow were obtained based only on the data of Eriksson *et al*. (1998). This uncertainty in the profile constants limits the universality of the composite profile of George *et al.* (2000) for calculating the friction velocity in a plane wall jet.

Given the above, in the present study, profile fitting using the classical logarithmic law was adopted to determine the friction velocities in a plane wall jet on a smooth surface. In addition, the profile fitting process also included the simultaneous correction in the wall-normal coordinate of the velocity data, denoted as ε_y, so as to compensate for the experimental error in this coordinate. More specifically, the profile fitting process was comprised of two stages: first an approximate range of the U_τ and ε_y were determined by adjusting their values in a spreadsheet to make the slope as well as the general shape of the fitted data roughly match those of the classical logarithmic law curve in the overlap region, then the Univariate Search Method based on Raju (2014) was used as a refining algorithm to converge the profile fitting to the optimum values of U_τ and ε_y such that the root-mean-square of the distances between the fitted data and the classical logarithmic law curve in the overlap region was minimized.

As for the wall jet on the rough surface, Raupach *et al.* (1991) proposed the following modified logarithmic law as

$$U^+ = \frac{1}{\kappa}\ln(y^+) + B - \Delta U^+ \tag{2.22}$$

typically in the overlap region of a zero-pressure-gradient turbulent boundary layer. The parameter ΔU^+ is the downshift from the classical log law and is referred to as the roughness shift. A simultaneous correction in the wall-normal coordinate of the velocity data, ε_{yk}, was again performed but for a different purpose, i.e. to locate the wall-normal virtual origin of the velocity profile a distance of ε_{yk} below the nominal top of the roughness elements. Similar to the smooth

surface case, the profile fitting process had two steps: first the values of the U_τ and ε_{yk} were determined by adjusting their values in a spreadsheet to make the slope of the fitted data match that of the classical log law curve in the overlap region, then the optimum roughness shift ΔU^+ was determined such that the root-mean-square of the distances between the fitted data and the modified logarithmic law curve in the overlap region was minimized.

It should be noted that as an additional check on the estimated values of U_τ, the results from profile fitting have been constrained to ensure that the near-wall peak of the non-dimensionalized Reynolds shear stress profile, i.e. $-\langle uv \rangle / U_\tau^2$ versus y^+, is less than unity in magnitude. In addition, in the rest of this thesis, unless stated otherwise, the wall-normal coordinate of the velocity data has already incorporated the appropriate correction, i.e. ε_y and ε_{yk} for the smooth and rough surface data, respectively.

2.4.2 Surface Roughness

Nikuradse (1933) was the first to present a comprehensive experimental study on turbulent rough-wall flow inside a pipe. He simulated roughness by gluing uniform sand grains of diameter k on the inner walls of a pipe. His results, together with the study covering the transitionally rough flow condition by Colebrook (1939), were plotted by Moody (1944) in what came to be known as the Moody chart for the friction factor in a pipe. As presented by White (2011), based on the value of the roughness Reynolds number defined as $k^+ = kU_\tau/\upsilon$, the pipe flow can be divided into three flow conditions: if $k^+ < 5$, the flow is hydraulically smooth and there is no effect of surface roughness on the wall friction; if $5 \leq k^+ \leq 70$, the flow is transitionally rough; and finally, if $k^+ > 70$, the flow is fully rough. In this case the viscous

sublayer is totally broken by the roughness elements and the wall friction is now independent of Reynolds number.

In order to provide a common measure of the effect of surface roughness in various types of flow, e.g. pipe flow, boundary layer flow or a plane wall jet, the concept of equivalent sand grain roughness k_s was introduced. This parameter is defined as the roughness height of the uniform sand grain surface as used in the experiment of Nikuradse (1933) that gives the same wall resistance effect on the flow as the rough surface under consideration. Such wall resistance effect is usually expressed by the Darcy friction factor f or the skin friction coefficient C_f. Another equivalent definition for k_s is presented by Flack *et al*. (2007) as the comparable uniform sand grain height that gives the same roughness shift, i.e. ΔU^+, in Equation (2.22). This second definition for k_s is more precise and thus is adopted in this study to determine the value of k_s.

An equivalent sand grain roughness Reynolds number k_s^+, defined as $k_s^+ = k_s U_\tau / \upsilon$, is a characteristic parameter for flows over rough surfaces. It is equivalent in meaning to the roughness Reynolds number k^+ described above. For the transitionally and fully rough flows, a relation curve between k_s^+ and ΔU^+ was plotted by Raupach *et al.* (1991) based on the results of Prandtl and Schlichting (1934). Note that the experimental results for a sand grain surface by Colebrook and White (1937) match favorably with this correlation curve. Specifically, for the fully rough flow condition, White (2011) gave the explicit relation of Nikuradse (1933) as follows:

$$\Delta U^+ = \frac{1}{\kappa} \ln(k_s^+) - 3.5 \ . \tag{2.23}$$

This relation is the same as presented in the correlation curve plotted by Raupach *et al.* (1991), and is further supported by the review of Flack and Schultz (2010) on recent experimental results on rough-wall turbulent boundary layers. The correlation curve and the relation referenced here are adopted in this study to obtain k_s^+ through ΔU^+.

2.4.3 Two-dimensionality

The most direct method to estimate the two-dimensionality of a plane wall jet is by conducting off-centerline measurements as performed by Dunn (2010). Experimenting in the same facility as used in the present study, he took measurements along both the streamwise centerline of the ground plane and a line that was 0.275 m away from the centerline in the spanwise direction. By comparing the experimental data along these two streamwise lines, he concluded that the facility was able to produce a two-dimensional plane wall jet up to $x = 100H$.

A second method is the two-dimensional momentum integral equation suggested by Launder and Rodi (1981) as an indirect yet crucial test on the two-dimensionality. Such a momentum integral equation can be expressed as

$$\left(M_{\text{jet}} + M_{\text{reverse}}\right) \Big/ M_{\text{o}} = 1 - M_{\text{loss}} / M_{\text{o}} , \tag{2.24}$$

where M_{jet} is the momentum of the wall jet, M_{reverse} is the momentum of the reverse flow, M_{o} is the initial momentum of the jet, and M_{loss} is the loss of momentum due to the wall shear stress and is defined as

$$M_{\text{loss}} = \int_0^X \left(\tau_{\text{w}} / \rho\right) \mathrm{d}x , \tag{2.25}$$

where X is the downstream location under consideration. According to Launder and Rodi (1981) and Eriksson *et al*. (1998), if a plane wall jet sustains two-dimensionality, M_{reverse} should be

minimal. This method requires high-precision measurements for the wall shear stress τ_w over the entire flow field under study, which was possible in the LDA measurements of Eriksson *et al*. (1998) with sufficiently high spatial resolution that enabled τ_w to be resolved directly. By using this method they reported their plane wall jet on a smooth surface remained two-dimensional up until $x = 150H$.

A third method is by comparing the measured data under consideration with other established two-dimensional wall jet results in terms of self-similarity. As presented by George *et al.* (2000) and Eriksson *et al*. (1998), a two-dimensional plane turbulent wall jet on a smooth surface features a single similarity profile when scaled by outer scales, i.e. U_m and $(y_{1/2})_{out}$. Rostamy *et al*. (2011a, 2011b) observed similar results for a plane wall jet on a rough surface. Therefore, if the experimental data compare favorably with previous studies in terms of self-similarity using outer scales, these data are two-dimensional.

In the present study, the first method above is not feasible since no off-centerline measurements were conducted. The second method is also inapplicable due to the data resolution limit which will be described in the following chapters. Hence the third method, i.e. comparing the present results with previous studies, is adopted for estimating the two-dimensionality in the present study.

2.4.4 Scaling Laws for the Mean Velocity Field

For the plane wall jet on a smooth surface, Wygnanski *et al.* (1992) provided a comprehensive review of several classical scaling laws for the mean velocity field. They found that the law of the wall, i.e. the linear relation $U^+ = y^+$, applies only to the viscous sublayer of the wall jet, and the rest of the inner layer can be scaled in an analogous fashion to the canonical

turbulent boundary layer by using their proposed defect law that scales ($U - U_m$) with U_τ and y with $(y_{1/2})_{out}$ up to $y/y_m \approx 4$ (or $y/(y_{1/2})_{out} \approx 0.6$). For the outer layer, the mean velocity profile was found to be self-similar when scaled by the conventional outer scales, i.e. U_m and $(y_{1/2})_{out}$, in the region of $0.15 < y/(y_{1/2})_{out} < 1.3$, and was independent of the slot Reynolds number Re_o. Furthermore, they found that the ratio $y_m/(y_{1/2})_{out}$ remains a constant of approximately 0.15 for a plane turbulent wall jet on the smooth surface regardless of slot Reynolds number Re_o and other details of the flow conditions.

More recently, George *et al.* (2000) presented a theoretical analysis on the scaling laws for the plane turbulent wall jet based on the asymptotic invariance principle (AIP). They indicated that the AIP shows that the similarity solutions for the plane wall jet in fact depend on the finite local half-width Reynolds number $\left(y_{1/2}\right)_{out}^{+}$ and only lose this dependence at infinite $\left(y_{1/2}\right)_{out}^{+}$. In other words, such similarity solutions are only asymptotically independent of the local Reynolds number based on the outer half-width. They concluded that for the mean streamwise velocity profiles in the inner layer the appropriate velocity scale is the friction velocity U_τ, and the length scale is υ/U_τ. As for the outer layer, the appropriate velocity scale is the local maximum velocity U_m, and the length scale is the outer half-width $(y_{1/2})_{out}$. This set of outer and inner scales has been validated by many previous experimental results, e.g. George *et al.* (2000) found their scales compare favorably with the LDA data of Karlsson *et al.* (1992, 1993) and the hot-wire anemometry (HWA) data of Abrahamsson *et al.* (1994). Recent numerical studies, e.g. the study using large-eddy simulation (LES) by Banyassady and Piomelli (2014) and the study using direct numerical simulation (DNS) by Naqavi *et al.* (2015), also supported such a set of inner and outer scales for the mean streamwise velocity profiles on the smooth surface. It

should be noted that this scaling law has in fact been used for decades but without comprehensive theoretical support until the work of George *et al.* (2000).

The most relevant scaling laws to the present study were proposed by Barenblatt *et al.* (2005) based on a triple-layered structure model. Their study was among the first to emphasize the role of the inner half-width as a parameter for characterizing the mean velocity profile in the inner region. There are two major differences from the conventional scaling law, i.e. the scaling law validated by George *et al.* (2000). One is that the previous velocity scale for the inner layer, i.e. U_τ, is replaced by the local maximum velocity U_m which now is the same as the outer layer. The other is the length scales for both layers are changed, i.e. $(y_{1/2})_{out}$ is replaced by $\left(y_{1/2}\right)_{out}/A_o$ for the outer layer and υ/U_τ is replaced by $\left(y_{1/2}\right)_{in}/A_i$ for the inner layer. By using these new scaling laws, they found that the inner and outer layer exhibit different self-similar structures and they each retain a dependence on the slot height H, which is evidence of incomplete similarity. Recent experimental studies by Rostamy *et al.* (2011c) provided similar observations based on LDA data.

In contrast to the smooth surface case, relatively few studies have considered the scaling laws for the plane wall jet on a rough surface. Rostamy *et al*. (2011a, 2011b) observed that the conventional outer scales, i.e. the velocity scale U_m and the length scale $(y_{1/2})_{out}$, apply to the profiles in the outer layer of a plane wall jet on a transitionally rough surface. The scaling law for a plane wall jet on a fully rough surface has not yet been studied in detail. However, it is worth noting that for the case of a turbulent boundary layer on a fully rough surface, Flack *et al.* (2007) observed that the conventional velocity-defect scaling, i.e. normalizing $(U - U_e)$ with U_τ, and y with δ, where U_e is the free stream velocity and δ is the boundary layer thickness, collapsed the data well in the outer part of the boundary layer for smooth, transitionally rough and fully rough

surfaces with k_s^+ ranging over 0 to 1,150. From this, they concluded that the mean velocity in the outer layer is largely insensitive to surface condition. In terms of scaling the inner layer profiles on the rough surface, by using Equation (2.22) Raupach *et al.* (1991) indicated that the conventional inner scales, i.e. the velocity scale U_τ and the length scale υ/U_τ, are still applicable to the rough surface case. This scaling method has been frequently adopted in recent studies, e.g. Banyassady and Piomelli (2014). Although the length scale associated with the surface roughness is not explicitly included in previous scaling laws for the mean velocity field in the inner layer, for the scaling law used in the present study, i.e. the scaling law of Barenblatt *et al.* (2005), the length scale associated with the rough surface is indirectly considered through the procedure to determine the inner half-width. This will be discussed later in Section 2.4.5. In addition, Tang *et al.* (2015) showed that the scaling laws of Barenblatt *et al.* (2005) are valid for the outer and inner layers of a transitionally rough plane wall jet.

2.4.5 Inner Half-Width

Similar to the case of the friction velocity, determining the inner half-width is often challenging in experiments due to the resolution limit near the wall. Previous studies usually adopted extrapolation as the method to estimate the inner half-width which is typically located in the buffer layer of the plane wall jet, i.e. in the range of $3 < y^+ < 30$ defined by George *et al.* (2005). Here the inner half-width Reynolds number is defined to be $\left(y_{1/2}\right)_{\text{in}}^+ = \left(y_{1/2}\right)_{\text{in}} U_\tau / \upsilon$.

For the smooth surface case, Rostamy *et al*. (2011c) used the composite profile of George *et al*. (2000), i.e. Equation (2.13) above, for extrapolation. The profile coefficients presented by George *et al*. (2000) are as follows:

$$\frac{C_{\mathrm{o}}}{C_{\mathrm{i}}}=\frac{C_{\mathrm{o}\infty}}{C_{\mathrm{i}\infty}}\exp\left(\frac{(1+\alpha)A}{\left(\ln\left(D\left(y_{1/2}\right)_{\mathrm{out}}^{+}\right)\right)^{\alpha}}\right) \tag{2.26}$$

$$\gamma=\gamma_{\infty}+\frac{\alpha A}{\left(\ln\left(D\left(y_{1/2}\right)_{\mathrm{out}}^{+}\right)\right)^{1+\alpha}} \tag{2.27}$$

where $\alpha = 0.46$, $A = 2.90$, $D = 1.0$, $C_{\mathrm{o}} = C_{\mathrm{o}\infty} = 1.30$ and $C_{\mathrm{i}\infty} = 56.7$ for the wall jet. As mentioned above, the coefficients C_{i} and γ are functions of $\left(y_{1/2}\right)_{\mathrm{out}}^{+}$ only.

For the case of a transitionally rough surface, Rostamy *et al*. (2013) modified the power-law velocity profiles for the overlap region of a transitionally rough turbulent boundary layer proposed by Seo and Castillo (2004) for application to the buffer layer of a transitionally rough wall jet. This power-law can be expressed as follows:

$$U^{+}=\widetilde{C}_{\mathrm{i}}\left(y^{+}+a^{+}\right)^{\tilde{\gamma}} \tag{2.28}$$

where

$$\widetilde{C}_{\mathrm{i}}=C_{\mathrm{i}}/\left(1+C_{\mathrm{ik}}\right) \tag{2.29}$$

$$\tilde{\gamma}=\gamma+\gamma_{\mathrm{k}} \tag{2.30}$$

$$C_{\mathrm{ik}}=0.03551\left(k_{s}^{+}\right)^{0.88647} \tag{2.31}$$

$$\gamma_{\mathrm{k}}=0.0065\left(k_{s}^{+}\right)^{0.60126} \tag{2.32}$$

and C_{i} and γ are the same as in Equations (2.26) and (2.27). Note that the coefficients C_{ik} and γ_{k} are functions of k_{s}^{+} only.

Tang *et al*. (2015) provided a summary review of the extrapolation techniques adopted by Rostamy *et al*. (2011c) and Rostamy *et al*. (2013), and found that the coefficients in the smooth-

wall composite profile changed less than 5% over the streamwise extent considered by Rostamy *et al*. (2011c), i.e. $30 < x/H < 80$, while the coefficients in the rough-wall power-law profile changed approximately 40% over the same range of x/H. This was expected since the modified log-law also varies at different downstream locations, i.e. ΔU^+ varies for different x/H and accordingly k_s^+ varies.

Finally, for a fully rough plane wall jet, thus far no specific profile for the buffer layer has been proposed. However, considering that the friction velocity U_τ for a fully rough wall jet will be significantly larger than for the smooth or transitionally rough cases, the inner half-width $\left(y_{1/2}\right)_{\text{in}}^+$ will most likely be located in the overlap region. Therefore, the modified logarithmic law, i.e. Equation (2.22), may be valid for extrapolating the mean velocity profile to the wall in the fully rough wall jet. This will be further discussed in Chapter 5.

2.4.6 Streamwise Development and Skin Friction

For the smooth surface wall jet, Bradshaw and Gee (1960) proposed an empirical power-law relation between the skin friction coefficient C_f and the local maximum-velocity Reynolds number $Re_{\text{m}} = U_{\text{m}} y_{\text{m}} / \upsilon$ based on their measurements using surface Pitot tubes and platinum–rhodium hot wires. George *et al*. (2000) proposed a theoretical relation between C_f and Re_{m} which showed a remarkable match to the relation of Bradshaw and Gee (1960) as well as the experimental data of Karlsson *et al*. (1992, 1993).

Tachie *et al*. (2004) were among the first to use LDA to study plane wall jets on both a smooth and transitionally rough surface. Their slot Reynolds numbers were in the range of $5{,}900 < Re_{\text{o}} < 12{,}500$. They observed that the surface roughness barely changed the spread rate of outer half-width, i.e. $\mathrm{d}(y_{1/2})_{\text{out}}/\mathrm{d}x$, or the decay rate of the maximum mean velocity U_{m} using the

momentum-viscosity scaling of Narasimha *et al*. (1973). The momentum-viscosity scaling removed the Reynolds number dependence seen in conventional scaling which normalizes U_m with U_o and x with H. However, the skin friction coefficient increased noticeably by 15% - 30% on the rough surface compared to the smooth surface case. More recently, the LDA data of Rostamy *et al*. (2011b) for Re_o = 7,500 was used to investigate the effect of surface roughness on a plane wall jet on both a smooth and transitionally rough surface. They observed a distinct change in the shape of the mean velocity profile due to roughness when using conventional outer scales, i.e. U_m and $(y_{1/2})_{out}$. In addition, there was a significant increase, as much as 140%, in the skin friction coefficient on the transitionally rough surface compared to the smooth surface. Tang *et al.* (2015) observed that the surface roughness modifies the development of the mean velocity profile in both the inner and outer regions, although the effect on the outer region is relatively small. The LES study of Banyassady and Piomelli (2014) for a plane turbulent wall jet on both smooth and transitionally rough surfaces at a slot Reynolds number of Re_o = 7500, which was similar to the experimental study of Rostamy *et al.* (2011b), concluded that the effects of surface roughness were confined to the inner layer and that the magnitude of the decay rate of maximum velocity, dU_m/dx, increased, while the growth rate of the maximum velocity location, dy_m/dx, decreased on the rough surface compared to the smooth one. Table 3 of their paper, which summarizes the effects of surface roughness observed in several previous wall jet studies, indicates that there is still some disagreement on the effect of roughness on the streamwise development of the mean velocity field.

Although there are few scaling laws that used a length scale relevant to the surface roughness for the development of the wall jet, Hogg *et al.* (1997) developed scaling laws for the spatial variation of the maximum velocity U_m and its wall-normal location y_m for a plane wall jet

on a rough surface based on the scaling for the smooth surface proposed by Wygnanski *et al.* (1992). Their scaling laws took the average height of roughness elements k_e into account. They observed only a weak dependence of the variations of U_m and y_m on the k_e by comparing their scaling laws with the experimental data of Rajaratnam (1967), i.e. the variations of U_m and y_m remained approximately the same for a wide range of the ratio k_e/H from 0.00455 to 0.126 over a slot Reynolds number extent of $1.91\times10^4 \leq Re_o \leq 1.02\times10^5$.

From the summary presented above, there still appear to be some questions related to the effects of surface roughness on the streamwise development of the plane turbulent wall jet, especially for the case of fully rough flow. Although most studies conclude that the effects of surface roughness are confined to the inner layer, most of these studies only considered the case of a transitionally rough surface. Furthermore, there are very few experimental measurements of the skin friction coefficient for a plane turbulent wall jet on a fully rough surface. Therefore, the effect of surface roughness on the streamwise development of the mean velocity field as well as the skin friction coefficient will be a focus of the present study.

2.5 Chapter Summary

This chapter provides a review of previous studies that are directly relevant to the specific topics investigated in this thesis. First, the theory on incomplete similarity and the relevant criteria of investigation were elucidated. Next, established studies on the features of the developing and fully developed region of a plane wall jet on both smooth and rough surfaces were documented. The points highlighted in this chapter will serve to guide the analysis of the experimental results presented in this thesis.

CHAPTER 3

APPARATUS AND INSTRUMENTATION

3.1 Introduction

This chapter presents the specifics of the experimental facility used for the present study. The measurements were carried out in the Department of Mechanical Engineering at the University of Saskatchewan. The facility was designed to produce a two-dimensional plane wall jet with a uniform streamwise velocity profile and a low level of the relative streamwise turbulence intensity at the inlet slot.

In this chapter, an overview of the apparatus is presented first. Next, the direct measurement of the surface roughness and the installation of it in the facility are introduced. Then, a description of the PIV instrumentation and uncertainty analysis are provided. Next the measurement of the flow rate is explained. Finally, the run matrix is presented.

3.2 Apparatus

A schematic of the experimental facility is shown in Figure 3.1. The experimental facility consists of a glass-walled water tank, a pump and a piping system which recirculates the water, an orifice plate flow meter to measure the flow rate, a glass ground plane, and a specially designed flow conditioner to generate a uniform inlet wall jet. As shown in Figure 3.1, the water is drawn from one end of the tank and pumped through the orifice plate flow meter and then into the back of the flow conditioner through four inlet holes. The water then flows through three screens and multiple straightening vanes, and is eventually discharged from the slot and flows across the ground plane. The water tank is 4.0 m long, 1.0 m wide and 0.7 m deep. The glass

ground plane was used as the smooth surface. The rough surface was created by attaching a layer of traction tapes on the ground plane. One major change in the facility from Dunn's experiments (2010) is a newly installed pump that provides a wide range of flow rates. The new pump is a Goulds G&L Series SSH pump which is connected to a TOSHIBA VF-AS1 digital pump controller. This system produces a flow rate which varies continuously from zero to approximately 600 L/min. This provided a slot exit bulk velocity U_o as high as 2.23 m/s. The slot exit on the front of the flow conditioner has a width of W = 750 mm and height of H = 6 mm, resulting in a width-to-height ratio of 125. The slot has a contraction ratio no less than 36 to 1, i.e. the ratio of the internal height of the flow conditioner to the slot height. The inside corner of the slot has a convex profile with a radius of curvature equal to 9.5 mm, and the section preceding the slot is a flat vertical wall. These structures were designed to achieve the desired initial conditions in the present study. The ground plane is held in place with a steel frame that is suspended from angled brackets that rest on the side walls of the water tank. The steel frame and brackets are connected by four threaded steel rods, which allows the height of the steel frame to be finely adjusted. For smooth surface experiments, the top of the ground plane was adjusted to align with the bottom of the slot exit. This setup and the piping system are the same as used by Dunn (2010).

The global coordinate system established in the facility is a Cartesian coordinate system positioned with the origin at the midpoint point of the bottom of the slot exit. The x direction is the streamwise direction and the y direction is the wall-normal direction as shown in Figure 3.1.

To renovate the facility after its last operation several years ago, the walls of the tank and the equipment in the tank (flow conditioner and glass plate with its steel frame) were thoroughly cleaned. After cleaning and re-installing the flow conditioner and the glass plate, but before

filling the tank with water, the slot exit height was directly measured by a ruler (with 1 mm graduation) assisted with several special metal gauge blocks. The measured slot height was H = 5.5 ± 0.5 mm. This value was monitored throughout the measurements by checking with the gauge blocks when the slot was immersed in water.

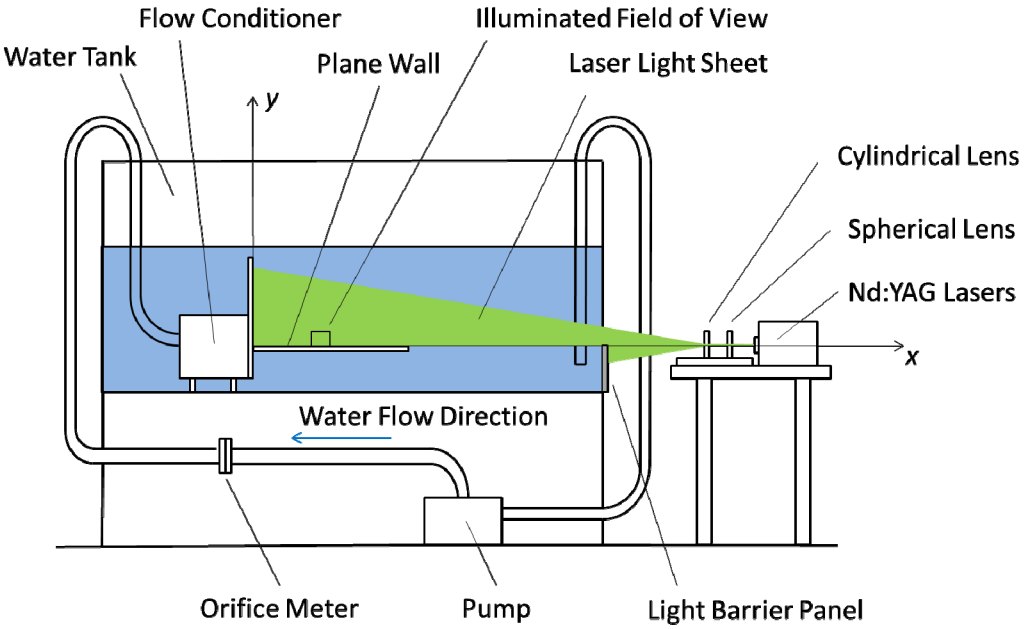

Figure 3.1: Schematic of the facility showing the layout of the water tank components and the position of the laser sheet (not to scale)

3.3 Rough Surface

The rough surface in these experiments was created by gluing a 36-grit traction tape onto the surface of the glass plate. This anti-slip tape was manufactured by Gator Grip ™ and has a nominal roughness element size of 0.53 mm. To determine the actual protrusion height of the roughness elements, a CyberScan Vantage 50 surface profilometer was used to conduct a direct

measurement. This device has a measurement resolution of 0.01 μm and a measurement range up to 8 mm which is well above the nominal roughness element size of 0.53 mm. Ten groups of measurements were conducted. The results were averaged to give an estimate of the roughness protrusion height as $k = 435$ μm or $k \approx 0.44$ mm.

The installed rough surface is shown in Figure 3.2. To help prevent the detachment of the rough surface from the glass plate when immersed in water, the traction tapes were bonded to the ground plane with double-sided tape. After attaching the traction tapes, the ground plane position was adjusted to make the top of the rough surface align the bottom of the slot exit.

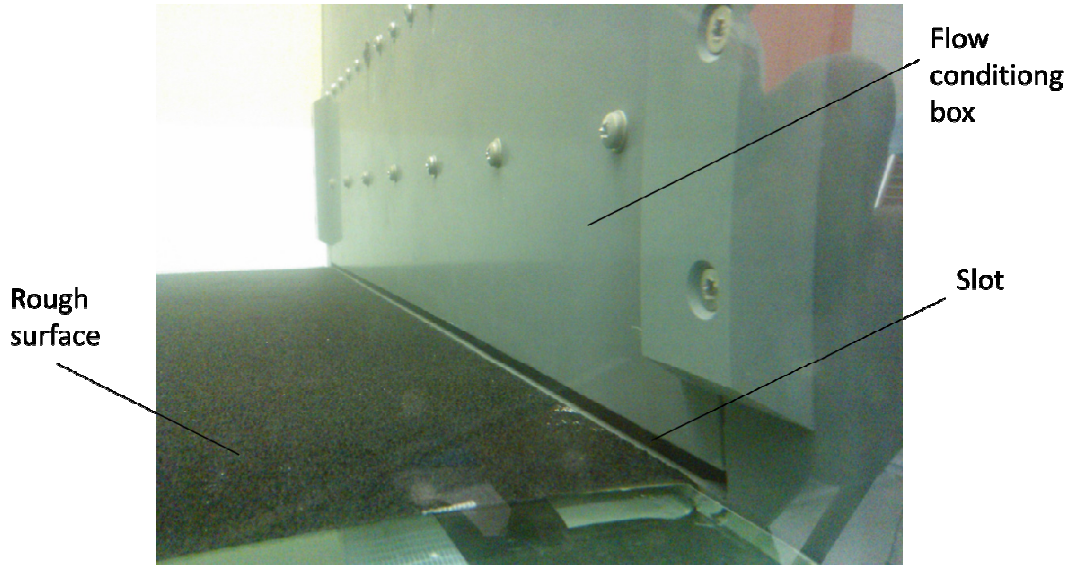

Figure 3.2: The installation of the rough surface

3.4 Particle Image Velocimetry System

The velocity field was measured by a particle image velocimetry (PIV) system. The system was comprised of four major components: the dual Nd:YAG lasers of Model 25350 manufactured by New Wave Research with a pulse energy of 200 mJ; a BNC Model 505

pulse/delay generator; a MegaPlus ES 4020 digital camera with a 2048 x 2048 pixel resolution sensor and a Nikon lens with a focal length of 105 mm; and a computer used for monitoring and controlling the aforementioned components using in-house software. Particles seeded in the water were hollow glass beads with diameter of 8-12 μm and a specific gravity of 1.1. The lasers were used to illuminate the seeding particles that were added in the water and the camera was used to capture pairs of images of the illuminated particles. A spherical and a cylindrical lens were used next to the aperture of the lasers to modify the laser beam into a light sheet that was positioned vertical to the ground plane. The focal length of them is 3,000 mm and 25 mm, respectively. A barrier paper panel was used to trim the lower half part of the light sheet, as shown in Figure 3.1, to reduce undesirable light that might cause problem in capturing PIV images. The Nd:YAG lasers were fixed on a table with adjustable height and were positioned such that the centre of the laser beam pointed at the midpoint of the bottom of the slot exit. The camera was mounted on a tripod and positioned to image the laser light sheet through the glass side wall of the tank.

In order to transform the local camera coordinate system to the global system as defined in Figure 3.1, two calibration images were taken before and after the measurement for each field of view. To do so, a steel ruler was first placed on top of the ground plane in the stationary water in the tank and an image was taken. This procedure was repeated after the measurement. The two calibration images were then compared with each other to ensure the facility setup remains reasonably unchanged during the measurements. The calibration image, normally the one taken after the measurement, was then used to calculate scaling parameters to facilitate the coordinate transformation.

The PIV field of view was nominally 115 mm × 115 mm, corresponding to 2048 × 2048 pixels. The in-house "PIVAnalysis" software began with an interrogation area (IA) size of 32 × 32 pixels. After a preliminary analysis with 32 × 32 IAs, a second pass with 16 × 16 IAs was performed. The second pass used particle displacements from the first pass to refine the process of extracting IA images from the original images. The overlap ratio of neighboring IAs was set to be 50% in both streamwise and wall-normal directions. The overall result from this combination of settings is that the processed data grid equals 1/4 of the starting interrogation area size, i.e. the spacing between the neighboring velocity data points is

$$\frac{115 \text{ mm}}{2048 \text{ pixel}} \times 32 \text{ pixel} \times \frac{1}{4} \approx 0.45 \text{ mm}.$$

This is the spatial resolution limit of the processed PIV data in this study. Post-correlation rejection of outlier velocity vectors was done using a dynamic threshold neural network technique as describe in Shinneeb *et al.* (2004).

For the facility and PIV apparatus used in this study, Shinneeb (2006) and Dunn (2010) concluded that the measurement uncertainty for the particle displacement has an absolute value of 0.29 pixels and is independent of the particle displacement. Since the present study used the same experimental facility, seeding particles, in-house software and mostly identical software settings as used by Dunn (2010), this measurement uncertainty was used in this study. Also following Dunn (2010), the time delay between the two images in a pair was set to make the particle displacement approximately 8 pixels and 1 pixel for the streamwise and wall-normal directions, which corresponds to a relative uncertainty of 3.6% and 34% for the measured streamwise and wall-normal instantaneous velocity, respectively. Further analysis on the uncertainties of other relevant variables of this study can be found in Appendix A.

3.5 Flow Rate Measurement

The flow rate was determined using an orifice plate flow meter, the same as used by Dunn (2010). The orifice plate flow meter was connected to a P855 differential pressure transducer manufactured by Validyne Engineering and the pressure transducer was connected to a multimeter. To identify the relationship between the voltage output from the pressure transducer and the pressure differential, a calibration was conducted using a DPI 605 Druck Pressure Calibrator. The calibration data is shown in Figure 3.3. Using a linear fit based on these data, a relationship with $R^2 = 1$ was established as:

$$P = 20,000\,V + 49.4 \tag{3.1}$$

where P is the pressure differential in Pa and V is the voltage. The pressure differential was then used to calculate the flow rate through the orifice plate flow meter by using ISO 5167-1 (1999) as done by Dunn (2010).

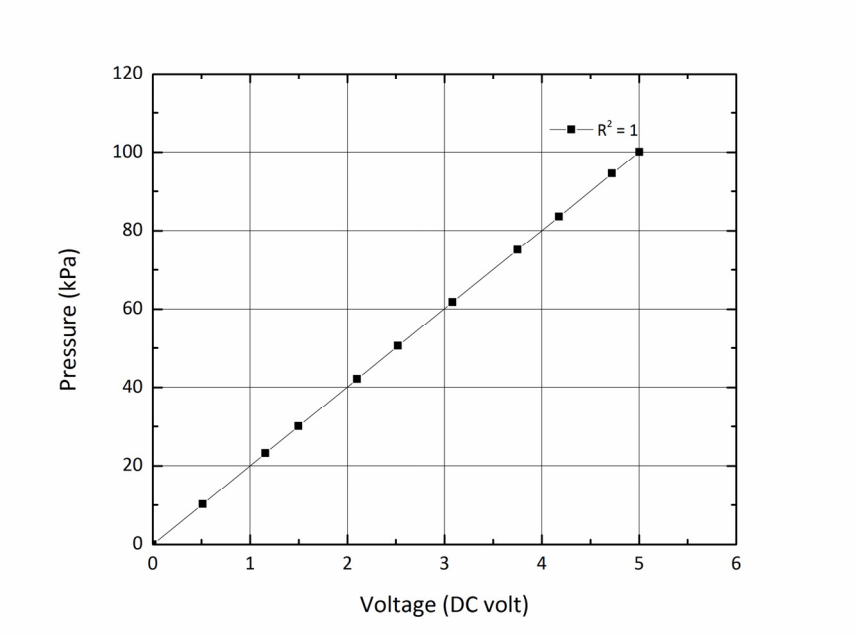

Figure 3.3: Calibration data for the differential pressure transducer

3.6 Run Matrix

To design the measurement matrix for this study, the first parameter to determine was the flow rate range. To fully use the capabilities of the new pump, the maximum flow of 600 L/min was used in the present experiments. A second lower flow rate equal to one half of the maximum, i.e. 300 L/min, was also used. These two flow rates will hereafter be referred to as High Flow Rate (HFR) and Low Flow Rate (LFR), respectively.

Four series of measurements were conducted along the centerline, i.e. $z = 0$, with the slot height being kept as $H = 5.5 \pm 0.5$ mm. Two series of measurements were first taken on the smooth surface at two inlet flow rates. Then the rough surface was installed and two series of measurements were taken at the same two inlet flow rates. Each series covered the streamwise distance from the slot exit to $x = 110H$ with seven fields of view (FOV). At each FOV, 2,000 and 4,000 pairs of instantaneous PIV raw images were captured at a sampling frequency of 4 Hz (Dunn, 2010) for the smooth and rough surface case, respectively. Similar to the procedures followed by Dunn (2010), the water temperature and the flow rate were monitored throughout each set of measurements. Among all measurements, the temperature ranged between 20.0 ^{o}C and 23.5 ^{o}C with an overall average of 22.0 ^{o}C. For the LFR series, the flow rate ranged from 300 L/min to 304 L/min with an overall average of 302 L/min. For HFR series, the flow rate ranged from 600 L/min to 604 L/min with an overall average of 602 L/min. These correspond to a streamwise bulk velocity at the slot exit of $U_o = 1.12$ m/s and $U_o = 2.23$ m/s for the LFR and HFR cases, respectively. The corresponding slot Reynolds number are $Re_o = 6{,}930$ and $Re_o = 13{,}900$. The series of measurements are summarized in Table 3.1.

Table 3.1: Outline of measurement series

Series Number	Surface	Flow Rate	Average Temperature (^{o}C)	Average Volume Flow Rate Q (L/min)	Average Slot Bulk Velocity U_o (m/s) based on Q	Average Slot Reynolds Number Re_o
1	smooth	LFR	23.43	301.82	1.12	7,190
2	smooth	HFR	23.39	603.40	2.23	14,300
3	rough	LFR	19.76	301.37	1.12	6,660
4	rough	HFR	20.38	601.13	2.23	13,400

3.7 Chapter Summary

This chapter aims to document the experimental facility and the instrumentation used for the present study. First the setup of the facility was described. Second the measurement of the surface roughness element and how the rough surface was installed were presented. Next the PIV equipment and the related adjustments were detailed, followed by uncertainty analysis on velocity measurements. Then the method to measure the flow rate was provided. Finally, the run matrix for conducted measurements and the recorded key experimental parameters were summarized.

CHAPTER 4

INLET BOUNDARY CONDITIONS AND INITIAL DEVELOPMENT

4.1 Introduction

The flow structure at the inlet as well as the initial development stage are analyzed in this chapter. The inlet flow condition is first investigated by plotting the mean velocity profiles for the range of $0 \le x \le H$. The mean streamwise velocity profile near the slot exit is used to assess the uniformity of the inlet velocity profile, the slot height H and the accuracy of the estimated bulk mean streamwise velocity obtained from the orifice plate flow meter. The corresponding wall-normal mean velocity profile is also presented to show the effects of the surface roughness and the inlet flow rate on the inlet flow structure. Next, the mean streamwise velocity profiles in the initial development region defined as $x \le 10H$ are plotted to display the early spatial development of the wall jet. Finally, the decay of the maximum streamwise velocity in the initial development region is investigated.

One issue to be noted before discussing these velocity profiles is the wall-normal coordinate correction, i.e. the estimation of ε_y and ε_{yk} as introduced in Chapter 2. This parameter is used to correct the wall-normal coordinate. Unlike the fully developed region that will be extensively discussed in Chapter 5, in the initial development region there is no reference formula which would allow profile fitting to be implemented. Instead, the following measures are adopted: for the smooth surface, the wall-normal coordinate correction caused solely by the uncertainty of the ruler height, $\varepsilon_y \approx 0.4$ mm, is adopted. For the rough surface, the estimation of

ε_{yk} is more complex due to the presence of the roughness elements. Since there is no method to determine ε_{yk}, the wall-normal coordinate is left unmodified for the rough surface case, $\varepsilon_{yk} = 0$.

4.2 Inlet Boundary Conditions

The inlet boundary conditions determine key parameters, such as the initial bulk velocity U_o, the slot height H, the initial momentum per unit mass M_o ($= \int_0^H U^2 \mathrm{d}y$) and the inlet turbulence levels. The mean streamwise velocity profiles near the slot exit for both flow rates on the smooth surface are shown in Figure 4.1, with their counterparts on the rough surface given in Figure 4.2. Dunn (2010) concluded that the data at the location $x = 2/3\,H$ were valid as an approximation of the inlet boundary condition. He chose this location because the velocity measurements at the slot, i.e. at $x = 0$, were inaccurate due to PIV resolution limit and the light scattering caused by the reflection of the illuminating laser from the front panel of the flow conditioner. These two issues were also encountered in the present measurements. As can be seen in Figure 4.1, the discrete grid size of Dunn's data is approximately 0.25 mm, while this value in the present study is approximately 0.45 mm as presented in Chapter 3. This indicates that the spatial resolution of Dunn's data is better than that of the present data. Given that the physical configuration of the slot exit in this study is exactly the same as in Dunn's experiment, it is reasonable to consider the flow at the location $x = 2/3H$ as representative of the inlet boundary condition. It should also be noted that the location $x = 2/3H$ is close enough to the slot exit such that effects of the wall and entrainment are still negligible.

Figures 4.1 and 4.2 show that unrealistic results were obtained at $x = 0$ and $x = 1/6H$. The velocity profiles at $x = 2/3H$ are very close to the profiles at $x = H$. These observations agree

with Dunn (2010) for a smooth surface wall jet in the same facility. Figures 4.1 and 4.2 also show that at $x = 2/3H$, in the region around the upper edge of wall jet (i.e. $y > 5$ mm) the mean streamwise velocity monotonically and quickly drops to zero due to shear in the mixing region. This is also observed in Dunn's data (2010) for a smooth surface wall jet. As for the near-wall region (i.e. for $y < 0.5$ mm), a rapid decrease in the mean streamwise velocity is also shown in Dunn's data (2010) due to the wall shear stress. This is not explicitly observed in the present smooth surface data due to the resolution limitations.

Profiles of the mean and fluctuating streamwise velocity profiles on smooth and rough surfaces for both flow rates at $x = 2/3\,H$ are presented in Figures 4.3 to 4.6. For the smooth surface, at $x = 2/3H$ the mean streamwise velocity profile over the central 70% of the slot height has a root-mean-square deviation from the average velocity of 0.7% and 0.2% for the LFR and HFR, respectively. For the rough surface, these velocity deviations are 0.6% and 0.3% for the LFR and HFR, respectively. These velocity deviations indicate that the flow becomes more uniform as the slot Reynolds number Re_o increases on both surfaces. For comparison, Dunn (2010) reported a velocity deviation of 0.3% over 71% of the slot height for a smooth surface wall jet. For the smooth surface cases, the boundary layer thickness within the wall jet at the slot exit, defined as the wall-normal location where U reaches $0.99U_m$, is $y = 0.7$ mm ($y/H = 0.12$). In comparison, in the study of Eriksson *et al*. (1998) for a smooth surface wall jet this value was $y =$ 1.4 mm or $y/H = 0.15$ while $H = 9.6$ mm.

Figure 4.3 shows a noticeable difference from Dunn's data (2010) in terms of the mean velocity profile. In the region of 6.0 mm $< y <$ 9.0 mm, the mean velocity is of negative values, and this is enhanced by increasing the flow rate as shown in Figure 4.4. This may be evidence of a local recirculating flow located above the inlet slot, possibly due to a slight change in the

surface smoothness of the front panel of the flow conditioner caused by the reinstallation of the experimental facility as compared to the original installation used by Dunn (2010), but the exact reason is yet unknown. Note that this feature is not observed in Figures 4.5 and 4.6 for the rough surface cases.

From the fluctuating velocity profiles in Figure 4.3 to 4.6, at $x = 2/3H$ the maximum relative streamwise turbulence intensity based on the mean streamwise velocity is 3.3% and 3.0% for the LFR and HFR, respectively, on the smooth surface, and 2.9% and 3.2% for the LFR and HFR, respectively, on the rough surface. These turbulence levels are about twice the value of 1.45% measured by Dunn (2010), and also higher than the level of 1% measured by Eriksson *et al*. (1998), but are slightly less than the values of 3% ~ 5% measured by Tachie *et al*. (2004). It can also be seen that, for all four flow cases, the fluctuating streamwise velocity peaks at the upper edge of the wall jet where the mean streamwise velocity has a large gradient in the wall-normal direction. This is consistent with the data of Dunn (2010) for a smooth surface wall jet.

Figure 4.3 shows that in the same region of 6.0 mm < y < 9.0 mm where the present mean velocity profiles deviate from Dunn's data (2010), the fluctuating velocity profiles also differ from Dunn's profiles (2010). A sharp peak in the fluctuating velocity is observed in the region of 6.5 mm < y < 8.0 mm where the mean streamwise velocity outside the wall jet changes rapidly along the wall-normal direction.

As mentioned in the introduction to this chapter, one of the reasons for examining the inlet boundary condition is to estimate the slot height H and the initial bulk mean streamwise velocity U_0. Recall that Chapter 3 gives the directly measured slot height before commencing the experiment as $H = 5.5 \pm 0.5$ mm. The mean velocity profiles shown in Figures 4.1 to 4.6 indicate the slot height H is around 5.8 mm. Due to the measurement resolution limits, a more

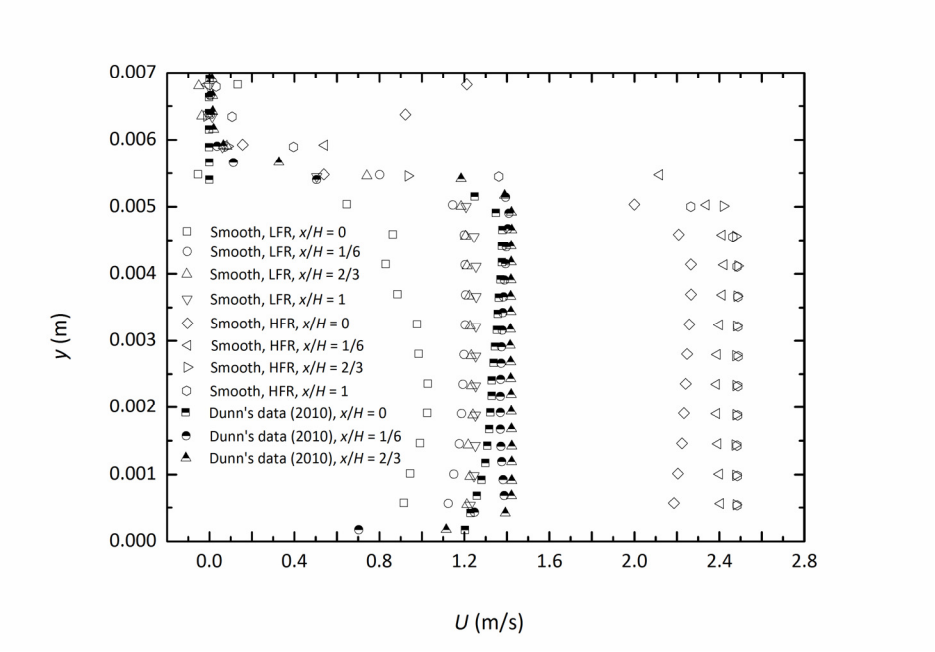

Figure 4.1: Smooth surface, mean streamwise velocity development for $0 \leq x \leq H$

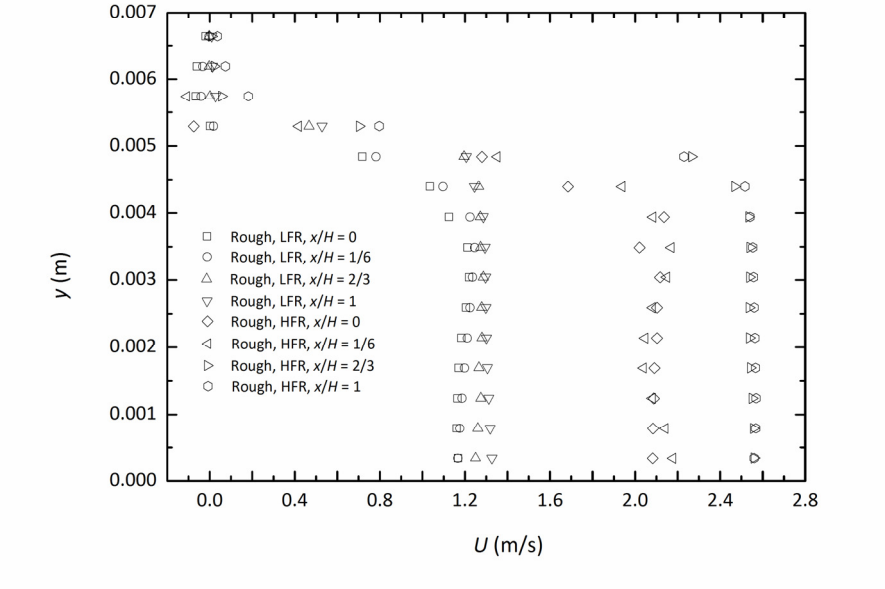

Figure 4.2: Rough surface, mean streamwise velocity development for $0 \leq x \leq H$

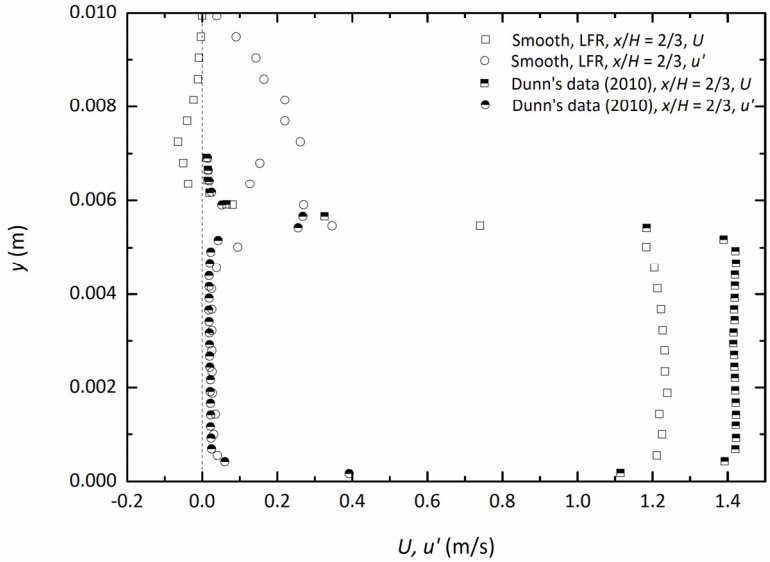

Figure 4.3: Smooth surface, LFR, streamwise mean and fluctuating velocity profiles at $x = 2/3H$

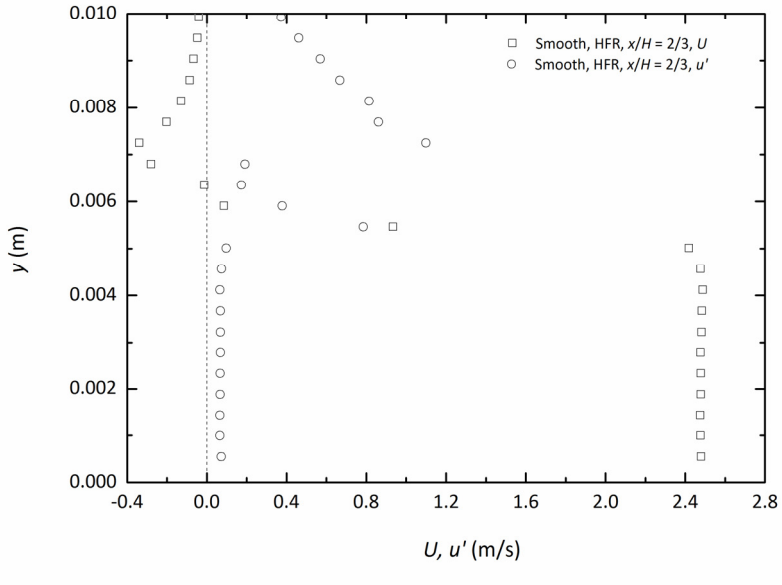

Figure 4.4: Smooth surface, HFR, streamwise mean and fluctuating velocity profiles at $x = 2/3H$

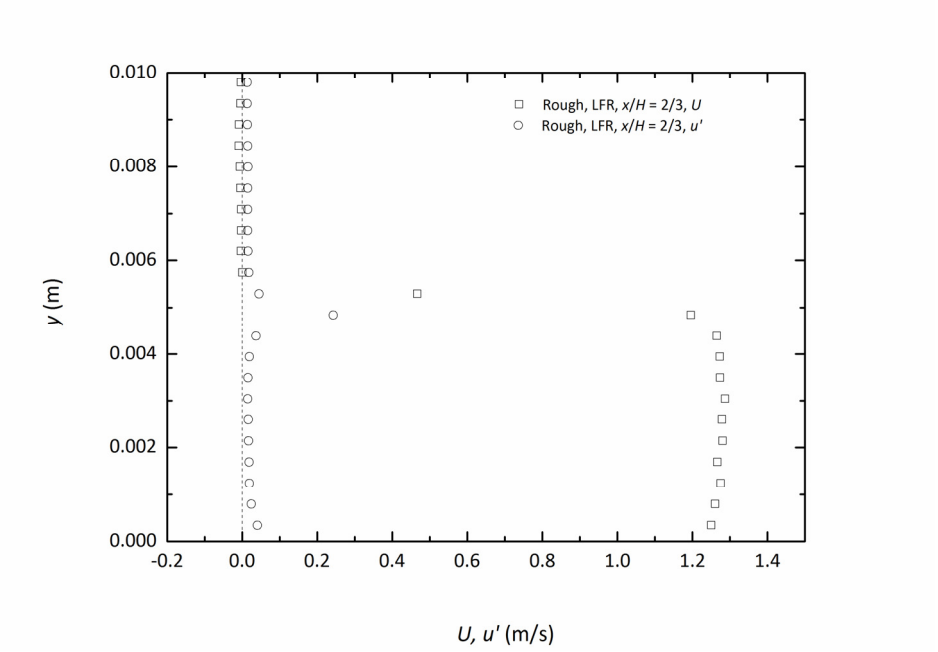

Figure 4.5: Rough surface, LFR, streamwise mean and fluctuating velocity profiles at $x = 2/3H$

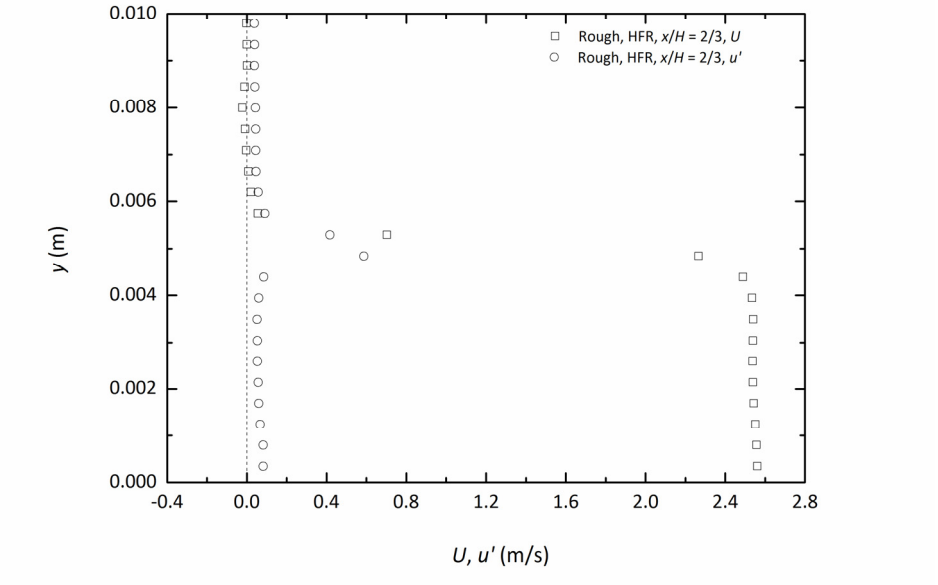

Figure 4.6: Rough surface, HFR, streamwise mean and fluctuating velocity profiles at $x = 2/3H$

precise value for H could not be determined during the PIV experiments. Therefore, following the result of H adopted by Dunn (2010) who used the same slot setting, a slot height of H = 6.0 mm is used in this study.

As for the initial bulk streamwise velocity U_o, Table 4.1 gives the values calculated from the representative mean velocity profiles at $x = 2/3H$ as well as those determined from the volume flow rate measured by the orifice plate flow meter. Since the difference between the two values is less than 2.3%, it is reasonable to use the U_o values based on the orifice plate flow meter for the analyses in this study. That the value of $U_{o,calculated}$ determined by the orifice plate flow meter was larger than the value of $U_{o,measured}$ based on the velocity profile at $x = 2/3H$ for all four flow conditions may be attributed to a small amount of leakage from the flow conditioner device. This explanation is supported by the observation that some air bubbles were pushed out of the flow conditioner when the flow conditioner was first filled with water after it was reinstalled in the water tank.

Table 4.1: Bulk inlet velocity U_o from two different methods

Surface type	Flow rate	$U_{o,calculated}$ (m/s) calculated from the orifice plate flow meter	$U_{o,measured}$ (m/s) from the PIV data at the slot exit ($x = 2/3H$)	Percent difference $\frac{U_{o,calculated} - U_{o,measured}}{U_{o,measured}}$	$U_{m,o}$ (m/s) from the PIV data at the slot exit ($x = 2/3H$)
Smooth	Low	1.12	1.10	1.82%	1.24
	High	2.23	2.18	2.29%	2.49
Rough	Low	1.12	1.11	0.90%	1.29
	High	2.23	2.20	1.36%	2.56

Table 4.1 also documents the maximum mean streamwise velocity $U_{m,o}$ at $x = 2/3H$, which is typically 10% - 15% larger than the calculated $U_{o,calculated}$ values from the orifice plate

flow meter for all four flow conditions. This is a result of the lower mean streamwise velocity in the near-wall region and around the upper edge of the wall jet, which was similar to the observation of Dunn (2010) for a smooth surface wall jet.

Figures 4.7 to 4.10 present profiles of the wall-normal mean and fluctuating velocity fields at $x = 2/3\,H$. For the same type of surface, the magnitude of the mean wall-normal velocity is increased with the doubling in the flow rate. Figures 4.7 and 4.8 indicate that the mean wall-normal velocity is close to zero across most of the slot height on the smooth surface. The positive wall-normal mean velocity near the wall (y < 3.0 mm) on the smooth surface indicates the decrease of the streamwise mass flux across a unit wall-normal extent due to the wall shear stress. This is enhanced on the rough surface as shown in Figures 4.9 and 4.10, indicating that even at $x = 2/3H$ the change in surface roughness has already increased the wall shear stress and began to impact the wall jet structure. In contrast, the mean wall-normal velocity beyond the outer edge of the wall jet (y > 6.0 mm) generally has a negative value, which is the evidence of the flow above the slot being entrained into the jet. This entrained flow is reduced on the rough surface due to the overall upward displacement of the jet caused by the rough surface. For comparison, Dunn's data (2010) for the smooth surface show positive values for the mean wall-normal velocity across most of the slot height, i.e. for approximately $y \leq 5.5$ mm, and show negative values above $y \approx 5.5$ mm, which is generally in conformity with the present study.

Figure 4.7 also shows a major difference from Dunn's data (2010) in the wall-normal mean velocity profiles on the smooth surface: in the region above the slot, i.e. for 6.0 mm < y < 9.0 mm, the mean wall-normal velocity deviates strongly from Dunn's profile (2010). Recalling that a similar phenomenon is also observed in the mean streamwise velocity profile as shown in

Figure 4.3 for the LFR on the smooth surface, it could be evident that a local recirculating flow region occurs above the slot in the present measurements on the smooth surface.

For all four flow cases, the wall-normal fluctuating velocity has approximately the same magnitude as the streamwise fluctuating velocity across most of the slot height, but the wall-normal relative turbulence intensity based on the wall-normal mean velocity is clearly much higher than the streamwise counterpart, which was similar to the observation of Dunn (2010) for a smooth surface wall jet. Similar to the mean wall-normal velocity, the magnitude of the fluctuating velocity is also increased with the increase in flow rate. As for the effect of surface roughness, the magnitude of the wall-normal fluctuating velocity near the surface, i.e. for $y \leq 1$ mm, remains approximately the same for LFR cases but increases significantly for HFR cases when the rough surface is used. In contrast, for both flow rates, near the outer edge of the jet, the magnitude of the wall-normal fluctuating velocity is significantly reduced for a rough ground plane.

Similar to the wall-normal mean velocity profiles for LFR on the smooth surface, Figure 4.7 shows that the wall-normal fluctuating velocity profiles are also different from Dunn's data (2010) in the region above the slot, i.e. for 6.0 mm $< y <$ 9.0 mm. In addition, similar to the streamwise fluctuating velocity, the peak of the wall-normal fluctuating velocity is also located in the region of 6.5 mm $< y <$ 8.0 mm where both of the mean streamwise and wall-normal velocity components change rapidly in the wall-normal direction. As for the wall-normal fluctuating velocity profiles within the wall jet, i.e. for $y <$ 5.0 mm, the fluctuating velocity magnitudes measured for LFR on the smooth surface in the present study are generally much smaller than the data reported by Dunn (2010), and the magnitude reaches a peak near where the wall-normal mean velocity changes rapidly.

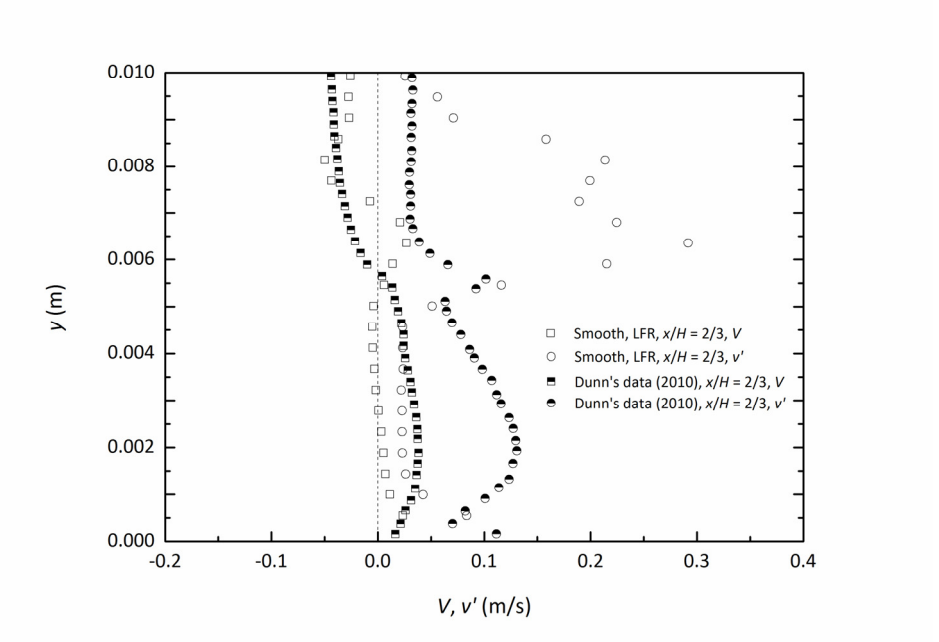

Figure 4.7: Smooth surface, LFR, wall-normal mean and fluctuating velocity profiles at $x = 2/3H$

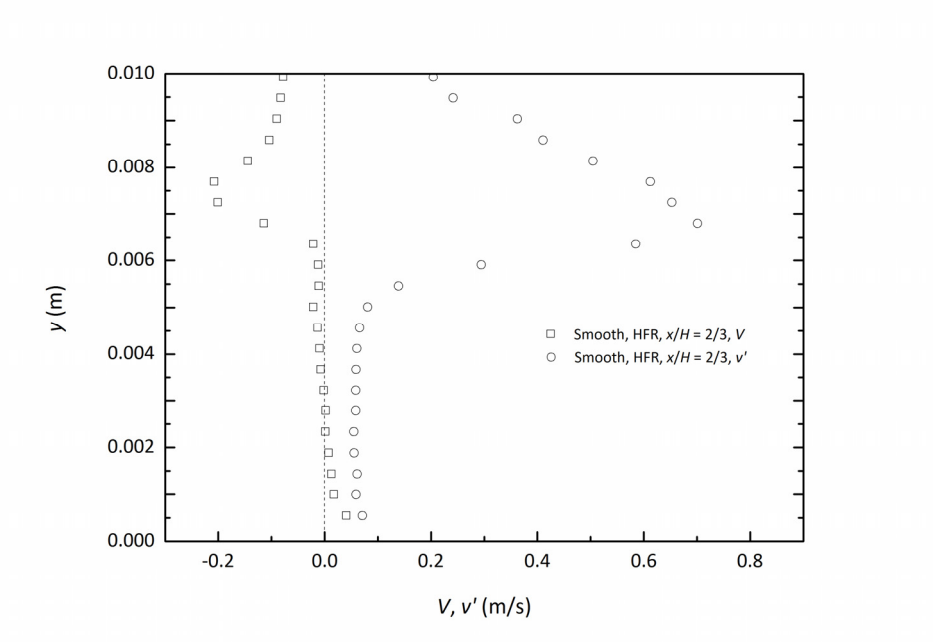

Figure 4.8: Smooth surface, HFR, wall-normal mean and fluctuating velocity profiles at $x = 2/3H$

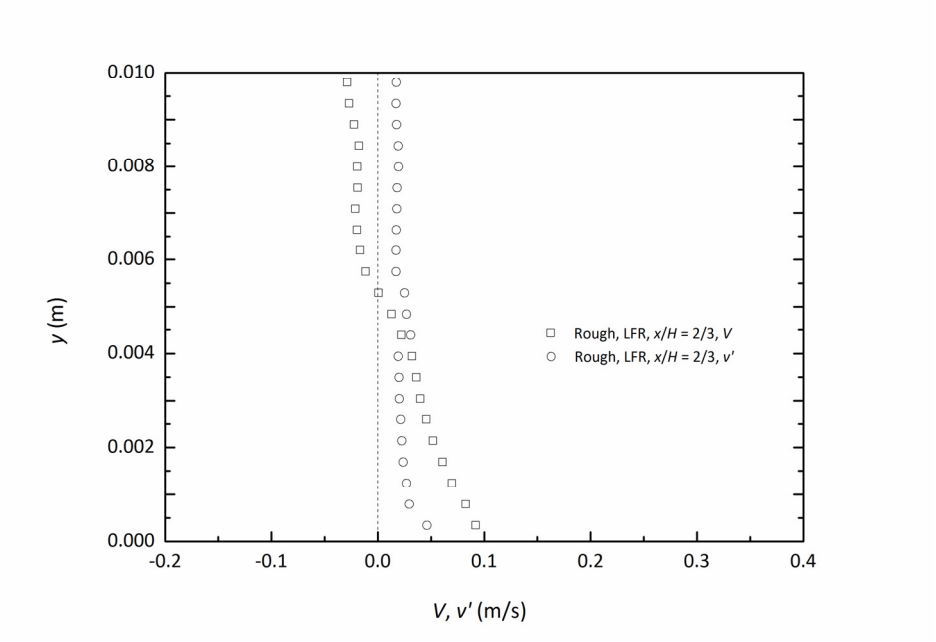

Figure 4.9: Rough surface, LFR, wall-normal mean and fluctuating velocity profiles at $x = 2/3H$

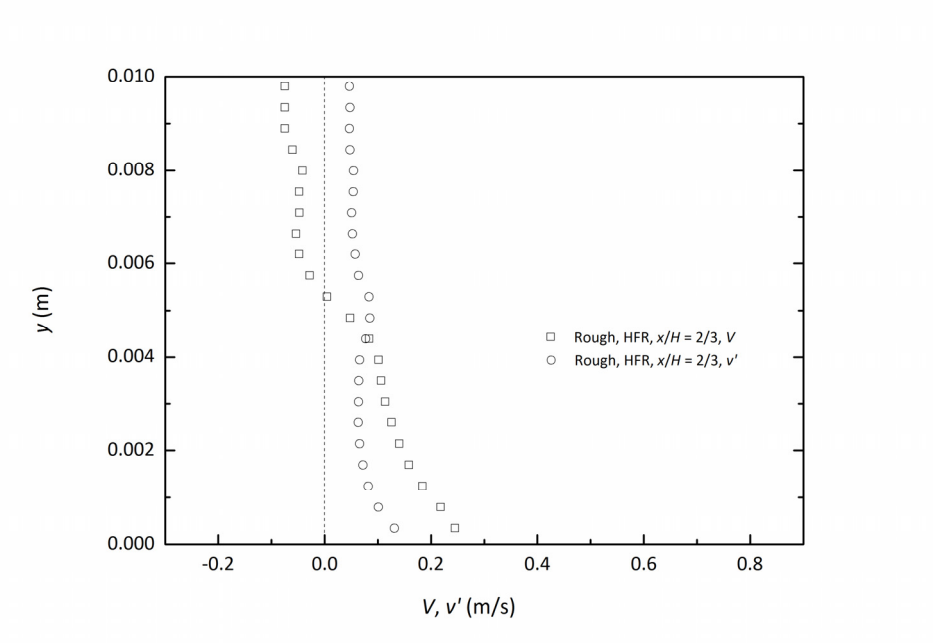

Figure 4.10: Rough surface, HFR, wall-normal mean and fluctuating velocity profiles at $x = 2/3H$

The streamwise and wall-normal velocity profiles discussed above indicate that the mean and fluctuating velocity fields are closely coupled, especially outside the wall jet where the fluctuating velocity is observed to respond to the gradient of the mean velocity.

4.3 Initial Development

4.3.1 Mean Velocity Profile

The initial development of the mean streamwise velocity profile in the region near the slot exit is shown in Figures 4.11 to 4.14. Within the first ten slot heights, the velocity profile transitions from mostly uniform to non-uniform which is characteristic of a wall jet. This transition is caused by the wall shear stress consuming the momentum near the wall as well as the turbulent mixing at the outer edge of the wall jet. The former effect is dominant for the rough surface cases, while the latter effect is more significant for the smooth surface cases. As shown in these figures, the major result of this transition is a gradual decrease of the maximum streamwise velocity and an enlargement of the wall-normal extent of the wall jet. Dunn (2010) observed a similar behavior for a smooth surface wall jet. Figures 4.11 and 4.12 also show a peculiar feature of the profile at $x = H$ on the smooth surface, i.e. a region of negative mean streamwise velocity occurs in the region 6.0 mm < y < 9.0 mm for the present measurements. As discussed above, this may be the indication of a local recirculating flow above the slot exit. The subsequent spatial development of the wall jet on the smooth surface as shown in Figures 4.11 and 4.12 suggests that the effect of the local recirculating flow on the streamwise velocity profiles is quickly attenuated as the wall jet develops downstream, and becomes negligible from $x = 2H$ onwards. As for the effect of surface roughness, the reduction in streamwise momentum of the wall jet is greatly accelerated by the rough surface, as shown in Figures 4.13 and 4.14.

Using the velocity deviation at $x = 2/3H$ as the criterion for uniformity, for both flow rates on the smooth surface, the mean streamwise velocity profile remained uniform up to $x = H$. In contrast, on the rough surface the profile had already lost uniformity by $x = H$, which illustrates the significant effect of the surface roughness in reducing the initial momentum of the wall jet. Note that in Figure 4.14, the data near the wall for the HFR on the rough surface have a much larger measurement error than the other three flow conditions. More specifically, the profiles at $x = 6H$, $7H$ and $8H$ show anomalies near the location of $y = 0.001$ m. This may be due to a strong mechanical vibration of the ground plane induced by the pump at the HFR for the rough surface case or due to ε_{yk} not being accounted for in the initial developing region, however, the exact source of such error is yet unclear.

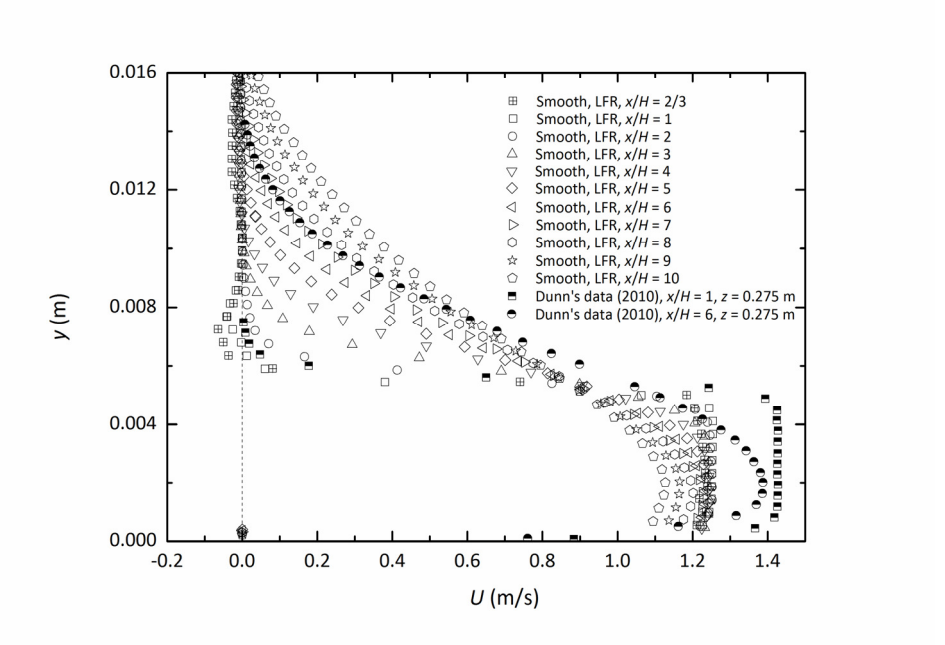

Figure 4.11: Smooth surface, LFR: initial development region of streamwise velocity profiles for $2/3H \leq x \leq 10H$

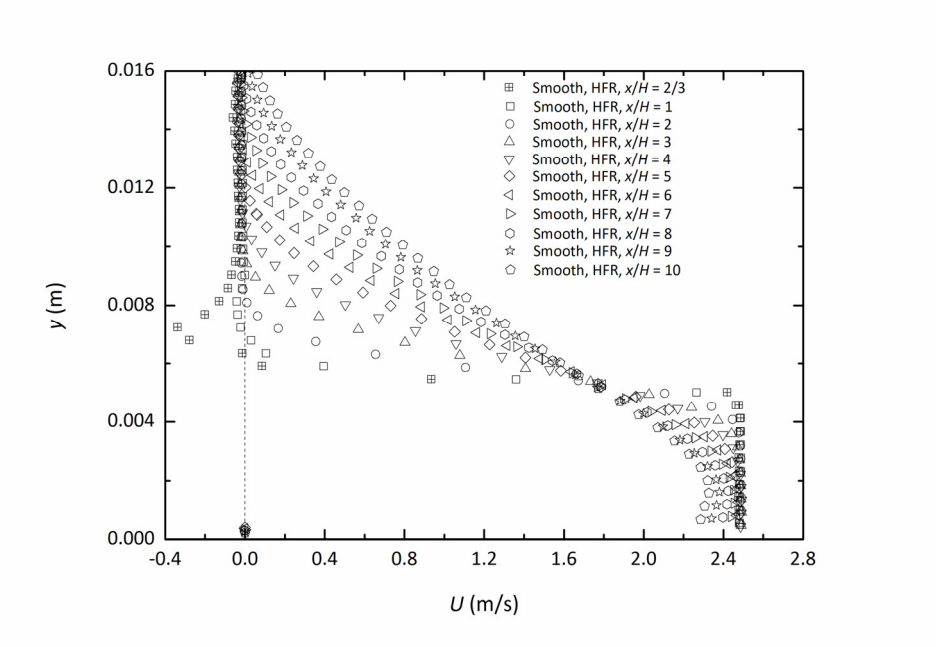

Figure 4.12: Smooth surface, HFR: initial development region of streamwise velocity profiles for $2/3H \leq x \leq 10H$

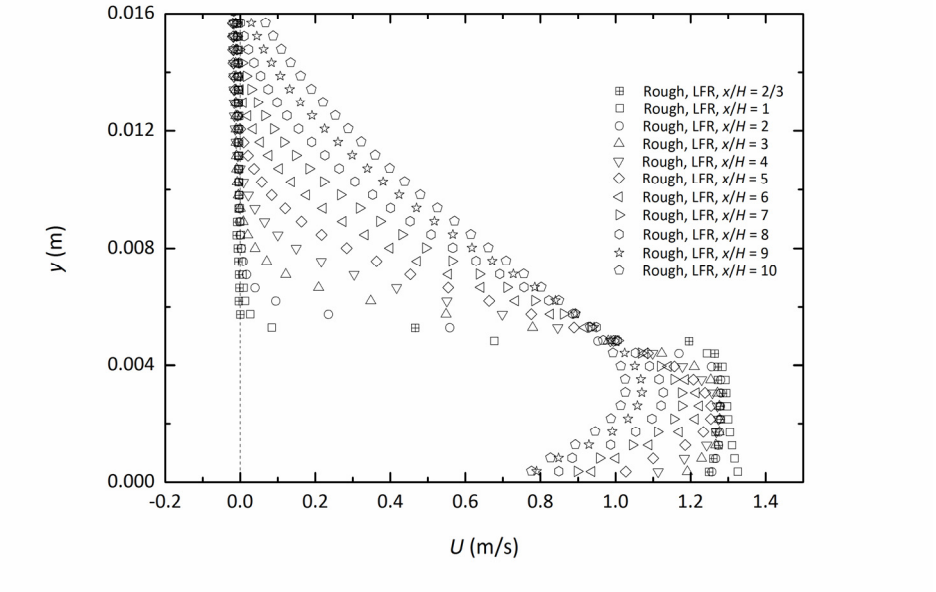

Figure 4.13: Rough surface, LFR: initial development region of streamwise velocity profiles for $2/3H \leq x \leq 10H$

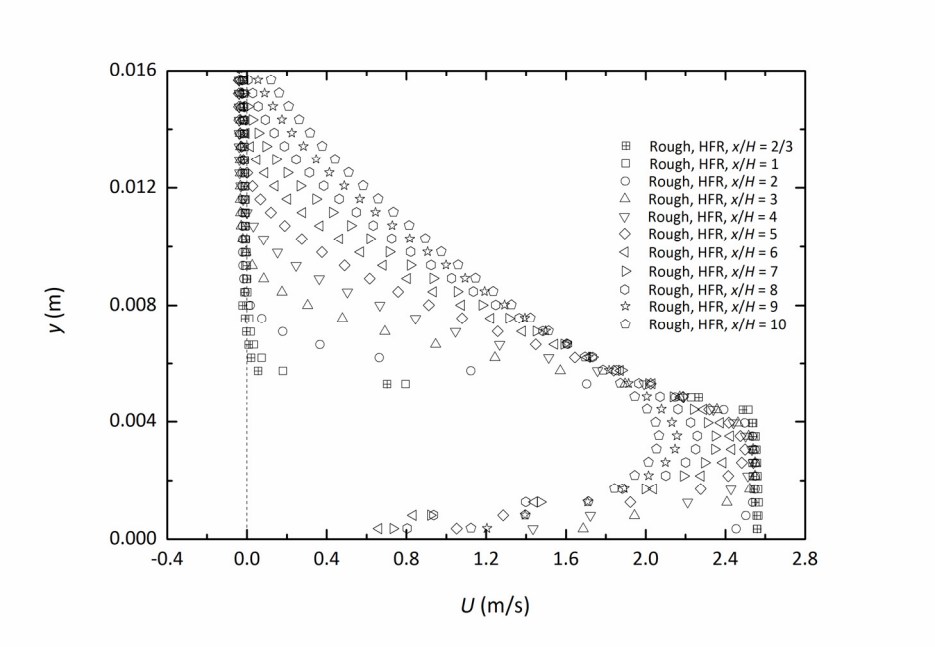

Figure 4.14: Rough surface, HFR: initial development region of streamwise velocity profiles for $2/3H \leq x \leq 10H$

4.3.2 Decay of the Maximum Mean Velocity

Figure 4.15 presents the decay of the maximum mean streamwise velocity with increasing downstream distance. Figure 4.16 presents the decay of non-dimensionalized U_m in terms of $U_{m,o}$ with uncertainty bars added at $x = 10H$ for the LFR cases to illustrate the magnitude of uncertainty in the data. For the smooth surface cases there is a noticeable decrease in the maximum velocity at $x = 7H$ for both flow rates, while a similar decrease occurs as early as $x = 3H$ for both flow rates on the rough surface. This implies that the potential core length is approximately $6H$ and $2H$ for both flow rates on the smooth and rough surface, respectively. By comparison, Dunn (2010) reported a value of $x_p = 6H$ for a smooth surface wall jet. Note that the length of the potential core is significantly shortened by the roughening of the surface, which is

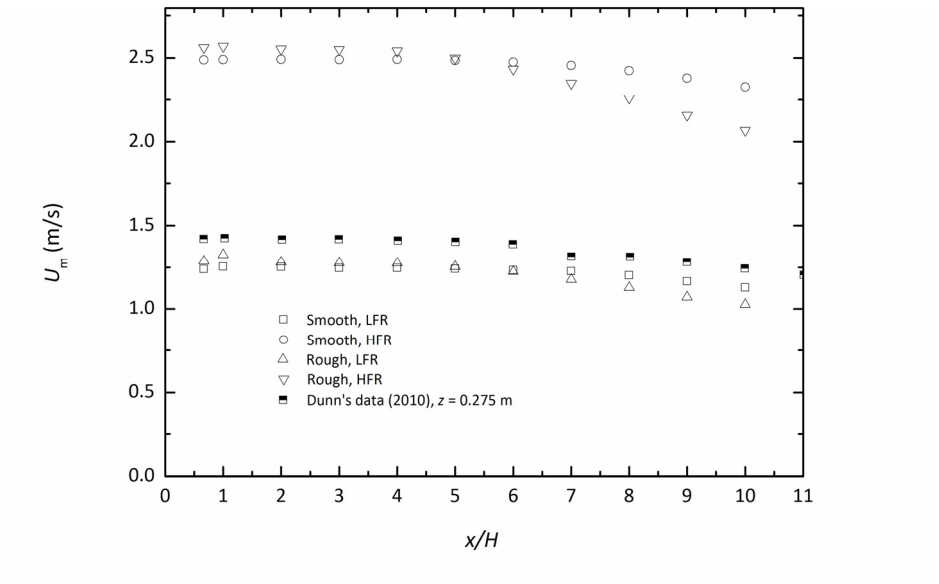

Figure 4.15: Decay of the maximum velocity for $2/3H \leq x \leq 10H$

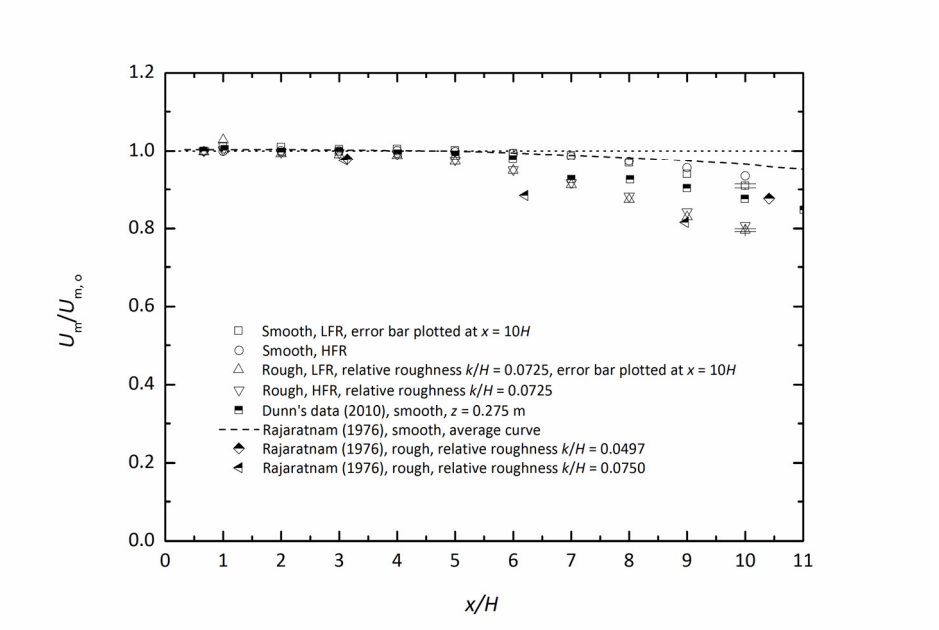

Figure 4.16: Decay of the maximum velocity for $2/3H \leq x \leq 10H$, with U_{m} normalized by the initial maximum mean streamwise velocity $U_{\mathrm{m,o}}$

consistent with the observations of Rajaratnam (1976). Figure 4.16 also shows that, in the initial development region of $2/3H \leq x \leq 10H$ considered in this study, the decays of U_m on both the smooth and rough surface are affected by the increasing flow rate. Such an effect is shown from $x \approx 9H$ onwards for the smooth surface cases but from $x \approx 7H$ onwards for the rough surface cases. This indicates that the increase of slot Reynolds number has a more significant effect on the decay pattern of U_m on the rough surface than on the smooth surface.

4.4 Chapter Summary

This chapter examines the inlet boundary conditions as well as the initial development of the plane wall jet. The inlet streamwise velocity profile is found to be reasonably uniform with a low turbulence intensity level which compares favorably with previous studies. The values of the slot height H and the initial bulk streamwise velocity U_o are estimated for use in subsequent parts of the thesis. The wall-normal velocity profile is also investigated. The mean and fluctuating velocity fields are found to be closely coupled. A local recirculating flow region is identified for the smooth surface cases only, the effect of which on the streamwise mean velocity profiles is quickly attenuated as the wall jet develops downstream. In the initial development region, the surface roughness has a significant effect on the reduction of the streamwise momentum of the wall jet as well as the potential core length. It is also observed that the increase in the slot Reynolds number has a more significant effect on the decay pattern of U_m on the rough surface than on the smooth surface. The next chapter will present the analysis of the mean velocity field in the fully developed region.

CHAPTER 5

MEAN VELOCITY FIELD IN THE FULLY DEVELOPED REGION

This chapter discusses the mean velocity field in the fully developed region. First, the fully developed region will be identified based on the establishment of the self-similar profile in the outer layer of the plane wall jet. Then, features of the mean velocity field will be analyzed in detail. The main purpose of this chapter is to examine the general features of the wall jet in comparison to other documented results, as well as to investigate the effects of surface roughness and slot Reynolds number.

5.1 Identification of Fully Developed Region

Figures 5.1 to 5.12 show the streamwise development of the wall jet for all four cases considered in this study. Focus is given to the region $x > 20H$, because it is widely observed that the critical location where the plane turbulent wall jet on the smooth surface becomes fully developed is in the range of $20H \leq x \leq 40H$, e.g. Narasimha *et al*. (1973) reported such a location to be $x = 30H$, Eriksson *et al*. (1998) reported $x = 40H$, and Hall and Ewing (2005) reported a range of $20H \leq x \leq 25H$. For a rough surface Smith (2008) observed that such a critical location is further downstream than the smooth surface case for the same boundary conditions. For each case considered in this study, the dimensional profiles are presented first, followed by two corresponding non-dimensionalized plots both of which include the uncertainty bars for the profile at $x = 100H$. The second non-dimensionalized plot presents an enlarged view of the wall jet region. It can be seen from the dimensional profiles, i.e. Figures 5.1, 5.4, 5.7 and 5.10, that as

the wall jet develops in the downstream direction its lateral extent increases, while the maximum velocity decreases.

As noted by George (1989), self-preservation or self-similarity is an asymptotic state which the flow attains once its internal adjustments are complete. As described by George *et al*. (2000) (and many other studies) for a smooth wall jet, this state is typically reflected by a self-similar profile obtained by using the outer length scale $(y_{1/2})_{out}$ and outer velocity scale U_m to scale the mean streamwise velocity profiles. Once self-preservation is established, the wall jet is considered to be fully developed. Smith (2008) noted that this criterion is also applicable for the rough surface case. In addition, as shown in the non-dimensionalized mean streamwise velocity profiles, i.e. Figures 5.2, 5.5, 5.8 and 5.11, beyond the outer edge ($y/(y_{1/2})_{out} \approx 2.0$) the wall jet exhibits negative velocities. This was also observed by Dunn (2010) and was attributed to the effect of the reverse flow. By analyzing the non-dimensionalized mean streamwise velocity profiles, i.e. Figures 5.2, 5.3, 5.5, 5.6, 5.8, 5.9, 5.11 and 5.12, it is clear that for all flow conditions, at $x = 100H$ a similarity profile has formed. Then, by using the dimensionless profile at $x = 100H$ as the reference profile for the fully developed state, it is found that the characteristic shape of the self-similarity profile exhibits as far upstream as $x = 40H$ on the smooth surface and $x = 70H$ on the rough surface. More specifically, it was determined that for both flow cases on the smooth surface the velocity profiles for $x \geq 40H$ remain within 1.1% from the reference profile at $x = 100H$ over more than 90% of the wall-normal extent of the velocity profiles. Note that the deviation of 1.1% is less than the uncertainty of U/U_m at $x = 100H$ which is 1.3% - 6.0% for the smooth surface cases. As for the rough surface cases, the velocity profiles for $x \geq 70H$ remain within a deviation of 0.8% from the reference profile at $x = 100H$ over more than 90% of the wall-normal extent of velocity profiles. The deviation is less than the uncertainty of U/U_m at

$x = 100H$ which is 0.9% - 5.6% for the rough surface cases. These observations indicate that the onset of the fully developed region is $x = 40H$ for both flow rates on the smooth surface and $x = 70H$ for both flow rates for the rough surface. This is consistent with the observation by Smith (2008) that the wall jet, especially its inner layer, is slower to reach a fully developed state on the rough surface compared to the smooth surface. In addition, for the smooth surface, the location of $x = 40H$ for onset of the fully developed region matches that observed by Eriksson *et al.* (1998).

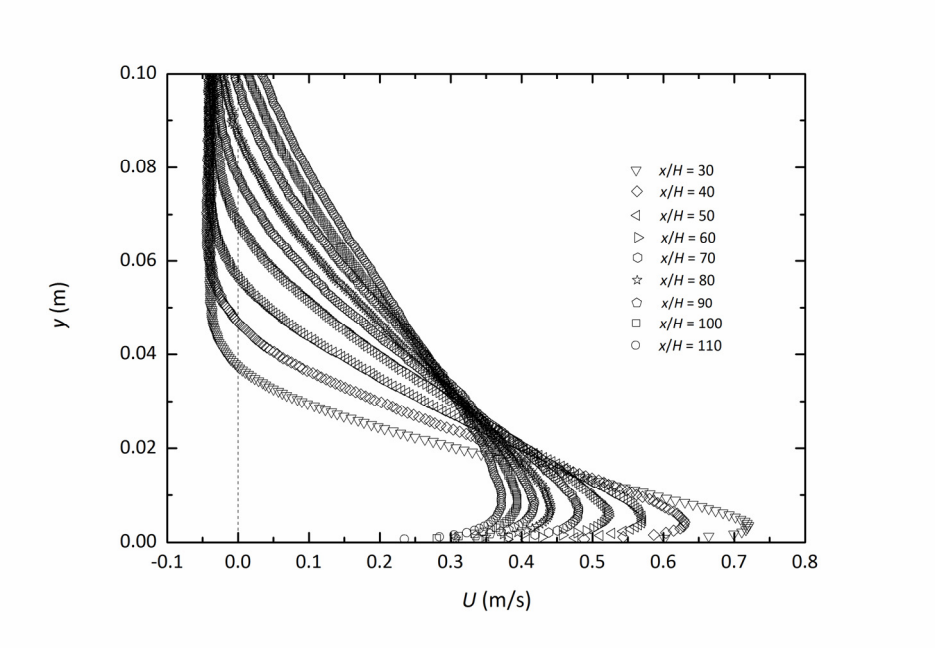

Figure 5.1: The development of the mean streamwise velocity profiles for the smooth surface, LFR (U_o = 1.12 m/s, Re_o = 7,190)

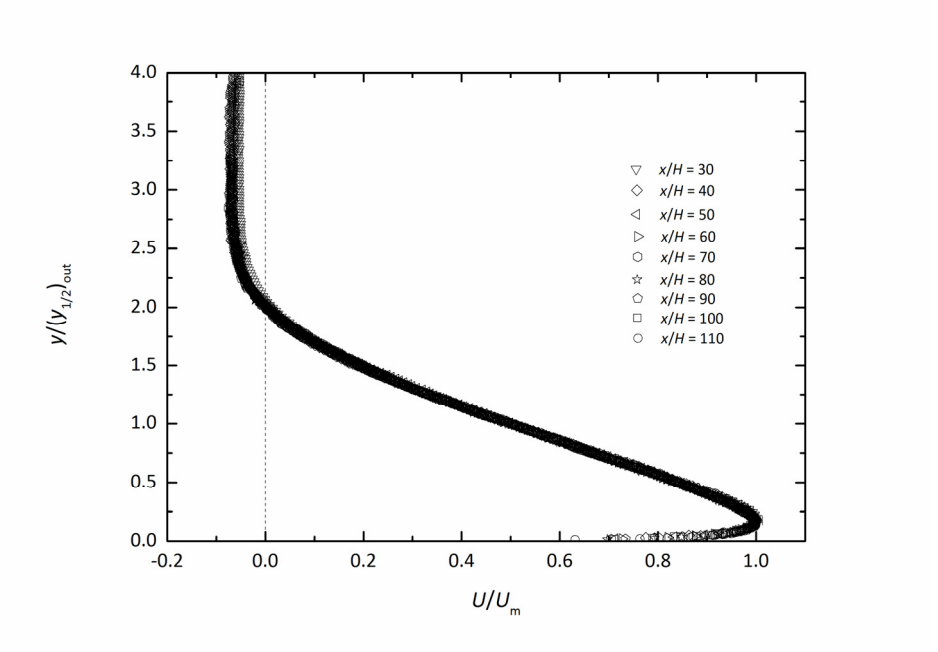

Figure 5.2: Non-dimensionalized mean streamwise velocity profiles for the smooth surface, LFR

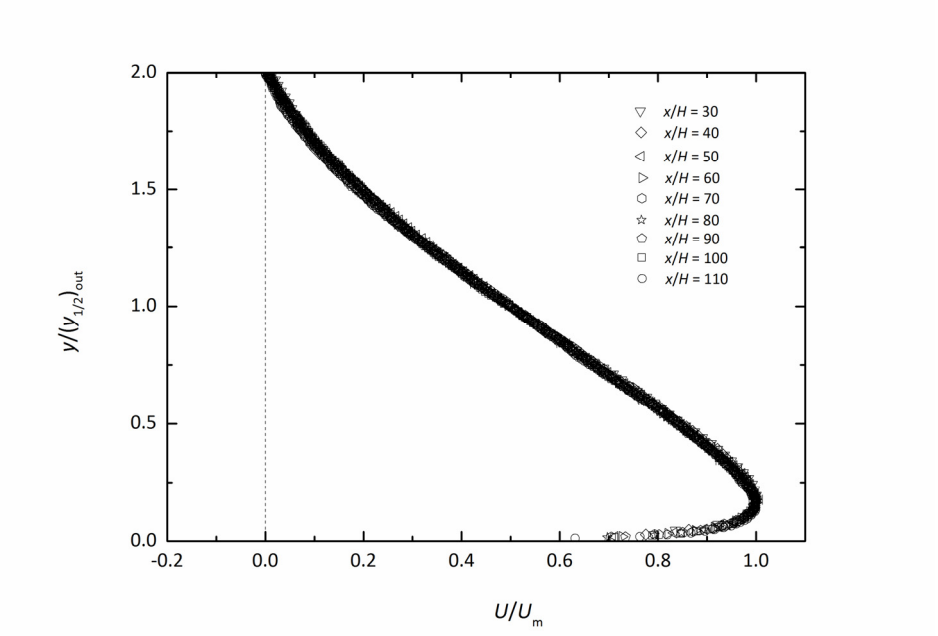

Figure 5.3: Non-dimensionalized mean streamwise velocity profiles for the smooth surface, LFR (enlarged view of the wall jet region)

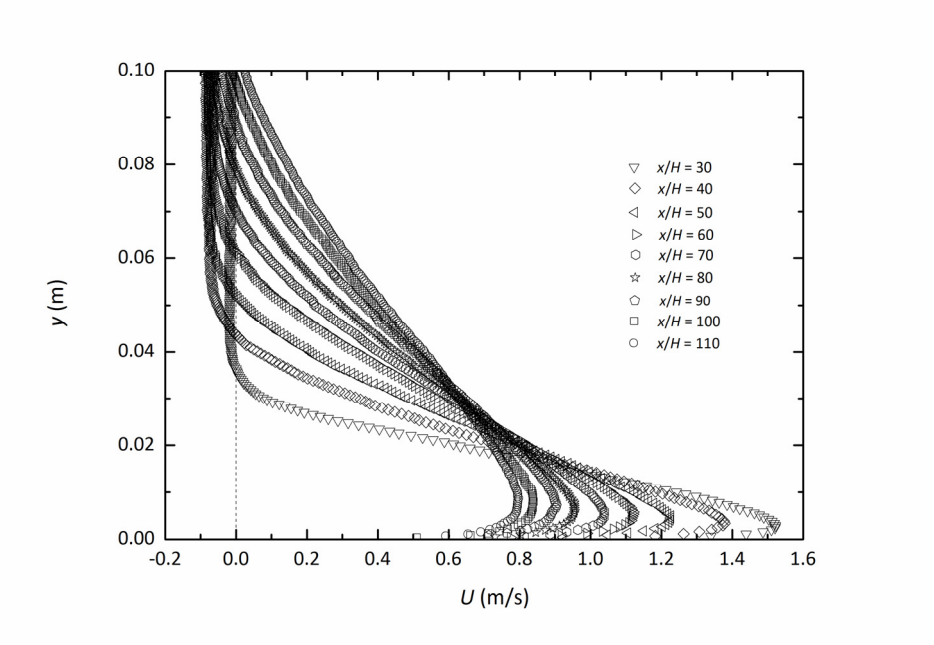

Figure 5.4: The development of the mean streamwise velocity profiles for the smooth surface, HFR (U_o = 2.23 m/s, Re_o = 14,300)

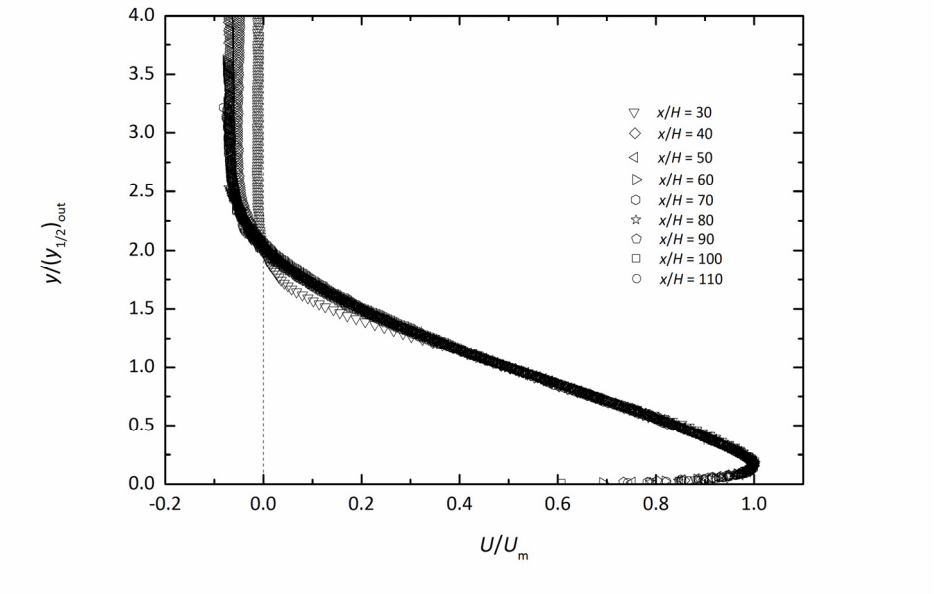

Figure 5.5: Non-dimensionalized mean streamwise velocity profiles for the smooth surface, HFR

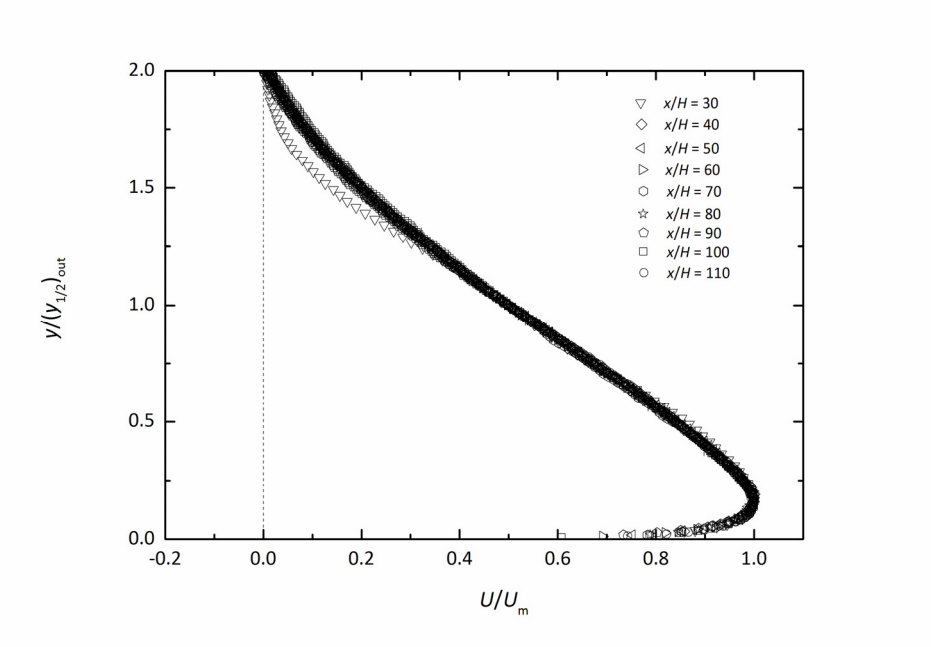

Figure 5.6: Non-dimensionalized mean streamwise velocity profiles for the smooth surface, HFR (enlarged view of the wall jet region)

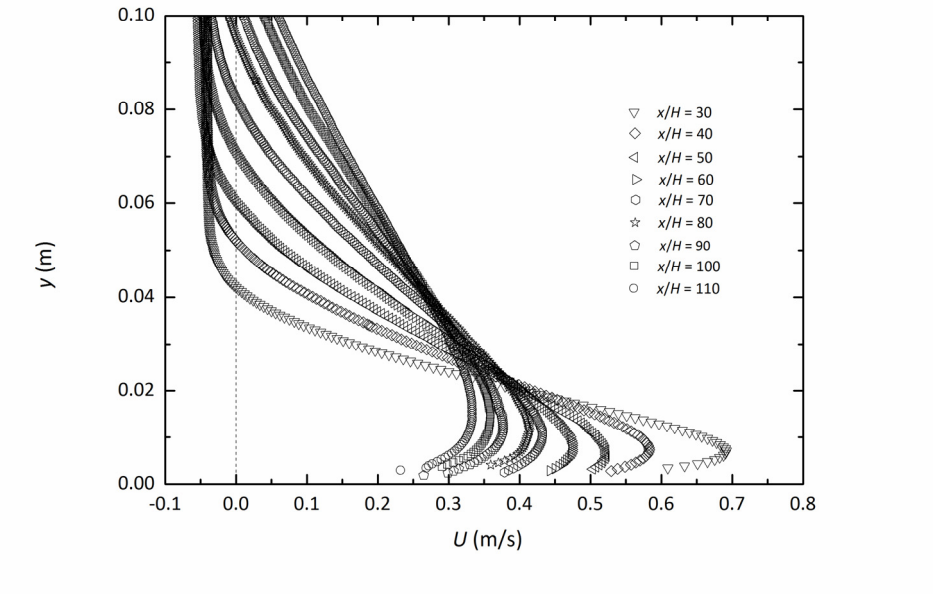

Figure 5.7: The development of the mean streamwise velocity profiles for the rough surface, LFR (U_o = 1.12 m/s, Re_o = 6,660)

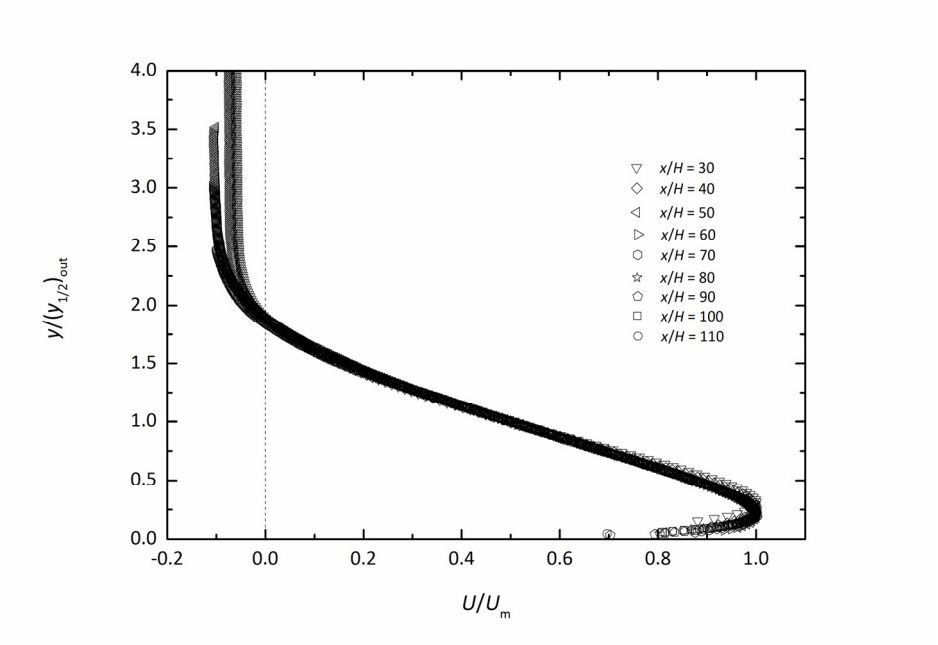

Figure 5.8: Non-dimensionalized mean streamwise velocity profiles for the rough surface, LFR

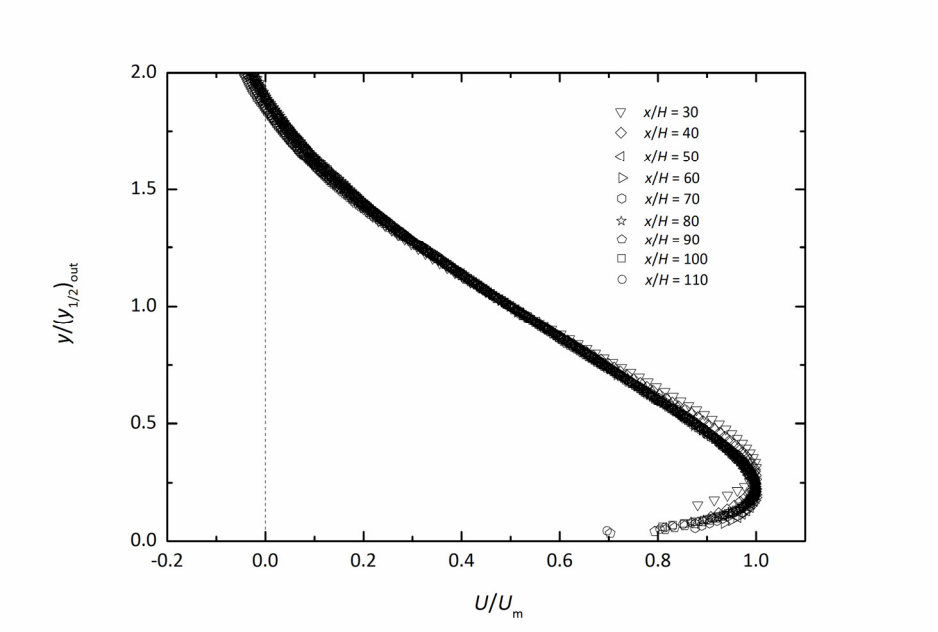

Figure 5.9: Non-dimensionalized mean streamwise velocity profiles for the rough surface, LFR (enlarged view of the wall jet region)

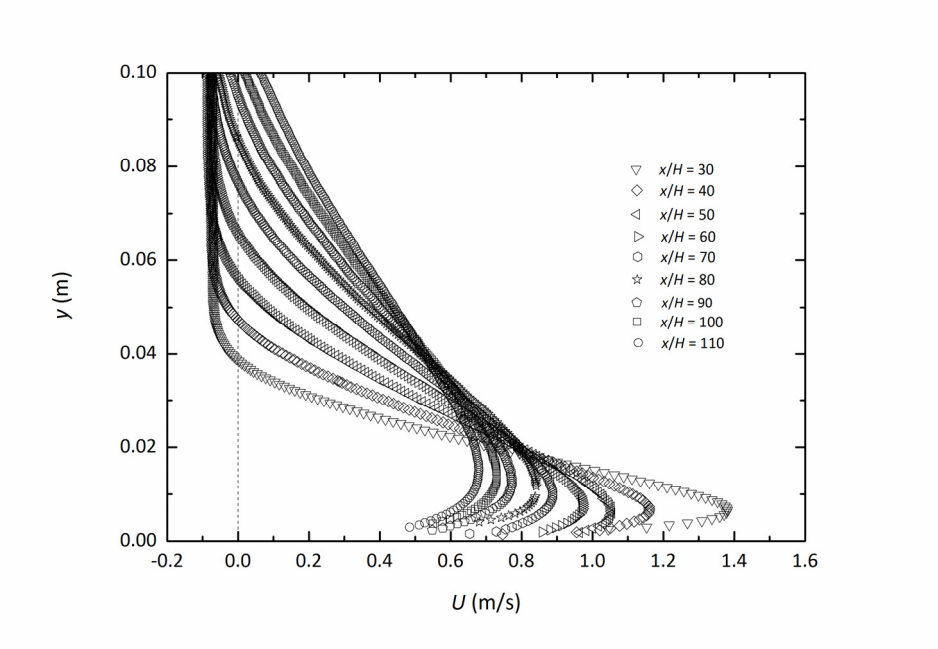

Figure 5.10: The development of the mean streamwise velocity profiles for the rough surface, HFR (U_o = 2.23 m/s, Re_o = 13,400)

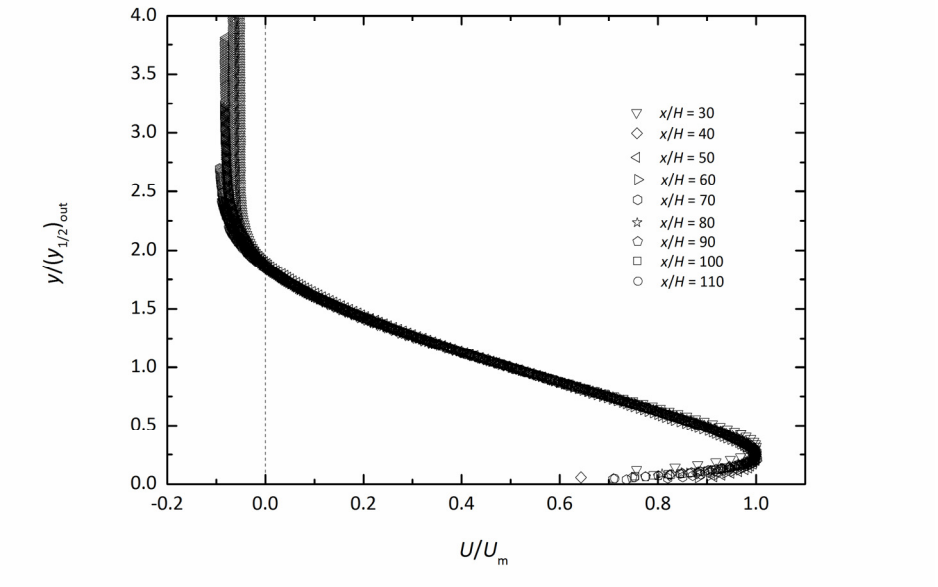

Figure 5.11: Non-dimensionalized mean streamwise velocity profiles for the rough surface, HFR

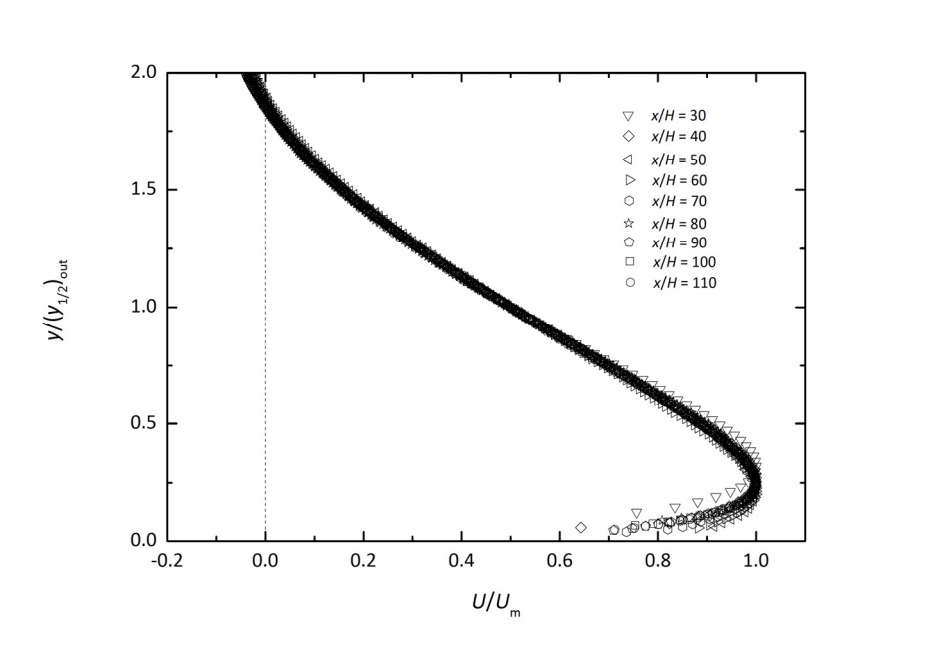

Figure 5.12: Non-dimensionalized mean streamwise velocity profiles for the rough surface, HFR (enlarged view of the wall jet region)

5.2 Analysis of the Fully Developed Region

This section presents a detailed discussion of the mean velocity field in the fully developed region. Note that in the following analysis, the wall-normal corrections ε_y and ε_{yk}, which were introduced in Chapter 2, are included wherever the wall-normal coordinate y is specified.

5.2.1 Mean Velocity Profiles in Outer Scales

Figure 5.13 shows the mean streamwise velocity profiles on the smooth and rough surface. Every fifth data point is plotted for better legibility. For the smooth surface case, Figure 5.13(a) shows that the profiles collapse well within the present data in the outer layer for both

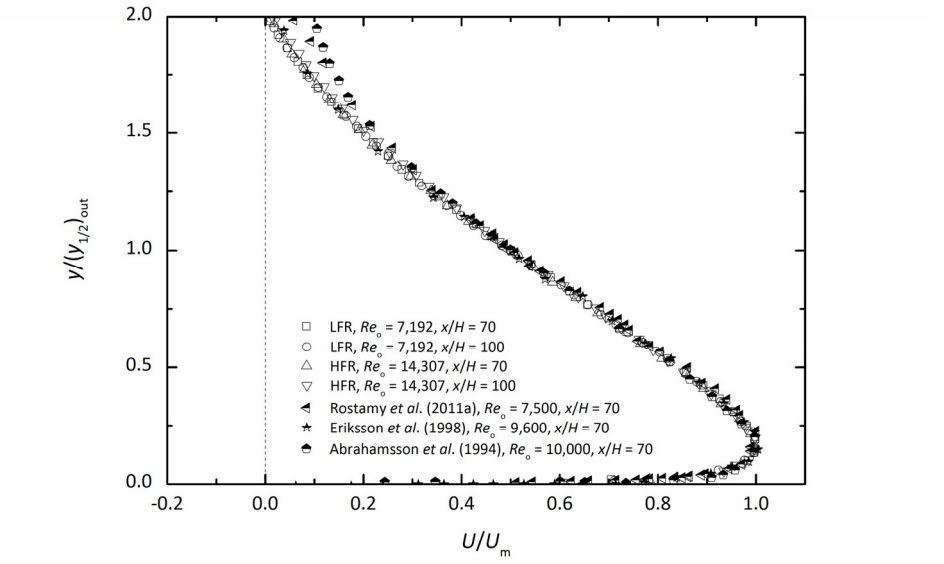

(a)

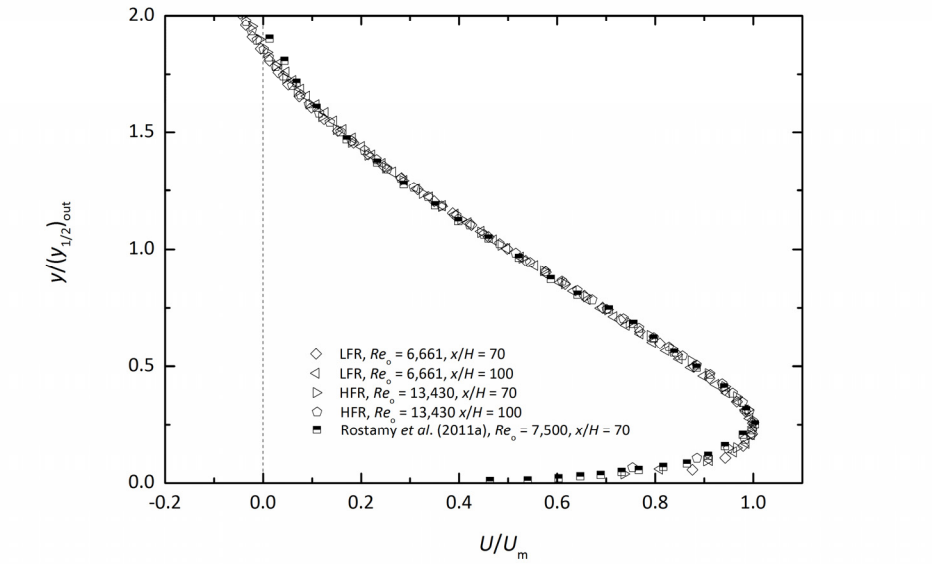

(b)

Figure 5.13: Non-dimensionalized mean velocity profiles on (a) the smooth surface, and (b) the rough surface

flow rates, except for the region beyond the outer edge of the wall jet, i.e. $y/(y_{1/2})_{out} > 1.5$, where the reverse flow appears and the structure of the wall jet is accordingly altered. This indicates independence of the nominally self-similar profile on the slot Reynolds number Re_o, which was also observed by George *et al*. (2000) as they examined several representative studies. Comparison with results of other studies, i.e. Rostamy *et al*. (2011a), Eriksson *et al*. (1998) and Abrahamsson *et al*. (1994) which were cited by George *et al*. (2000), shows a favorable match for the region of $0.2 \leq y/(y_{1/2})_{out} \leq 1.3$. For both flow rates on the smooth surface, the present data in the fully developed region yield a constant of $y_m/(y_{1/2})_{out} \approx 0.17$ with a deviation of less than 5.6% for all downstream locations considered in this study. Recall that Tachie *et al.* (2004) reported this value to be $0.16 \leq y_m/(y_{1/2})_{out} \leq 0.18$ and Wygnanski *et al.* (1992) reported $y_m/(y_{1/2})_{out} \approx 0.15$.

As for the rough surface, Figure 5.13(b) leads to a similar conclusion, i.e. the nominally self-similar profile for the rough surface is independent of the slot Reynolds number Re_o, and the present rough surface data compare favorably with the previous study of Rostamy *et al.* (2011a). More specifically, the present data for the transitionally and fully rough surface collapse well in the outer layer, i.e. $0.3 < y/(y_{1/2})_{out} < 1.5$. However, it should be noted that the transitionally rough and fully rough profiles in the region $y/(y_{1/2})_{out} < 0.3$ do not collapse, i.e. the deviation between profiles is larger than the uncertainty of U/U_m. This indicates that within the inner layer the transitionally rough and fully rough wall jet in outer scales are distinct.

Figure 5.14 shows a comparison between the profiles for the smooth and rough surfaces. Again only every fifth data point is plotted, and uncertainty bars are included. The figure shows that the rough surface results in a noticeable increase in the thickness of the inner layer, i.e. y_m, and a systematic difference between the smooth and rough self-similar profiles near the outer

edge of the wall jet. Tachie *et al*. (2004) and Rostamy *et al*. (2011a) both observed similar phenomena when comparing their data for smooth and transitionally rough surfaces. This indicates that the smooth and rough surface lead to distinct self-similar profiles in the outer layer.

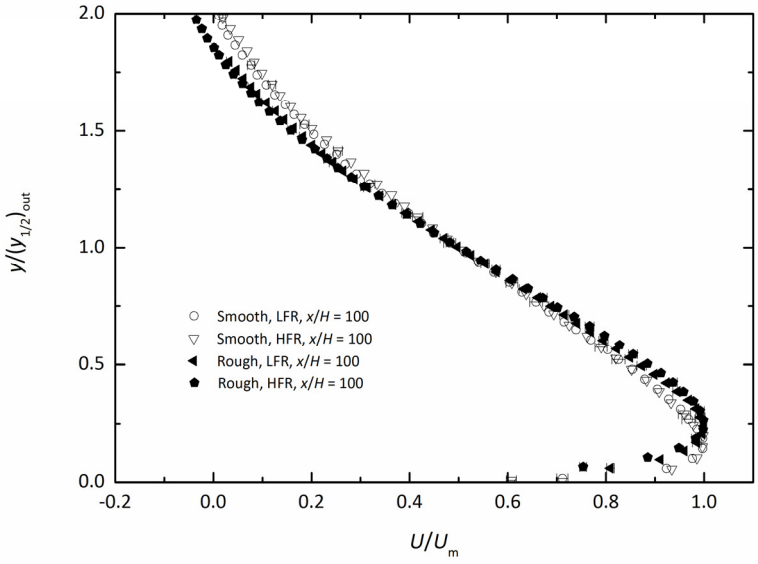

Figure 5.14: Comparison of profiles on smooth and rough surface

As discussed above, each of the four flow cases in the present study exhibits a self-similar profile using the outer scales, and these self-similar profiles show a favorable comparison to other established two-dimensional data in most of the outer layer. More specifically, for each flow case, in this region more than 65% of the present U/U_m data points have a deviation from the other results that is less than the corresponding uncertainty of U/U_m. Based on the review in Chapter 2, this also indicates that the wall jets for all four flow cases maintain two-dimensionality in the fully developed region.

5.2.2 Mean Velocity Profiles in Inner Scales

This section focuses on the mean velocity profile non-dimensionalized by inner scales, i.e. the friction velocity U_τ and the viscous length scale υ/U_τ, based on results of profile fitting as described in Section 2.4.1. Figures 5.15 and 5.16 show the mean streamwise velocity using inner scales for all four flow cases considered in this study. For the smooth and transitionally rough wall jet conditions, Figures 5.15 and 5.16(a), the values of the constants used for both the classical log-law and modified log-law profiles are $\kappa = 0.41$ and $B = 5.0$. For the fully rough case, preliminary profile fitting using the same constants showed problematic behavior in the region of $100 < y^+ < 300$ compared to other studies. Therefore, a different value was used for κ for the fully rough case, i.e. the value of $\kappa = 0.38$ as suggested by Osterlund *et al*. (2000) based on their experimental study of a zero-pressure-gradient turbulent boundary layer. It should be noted that the issue of the value of the constants in the classical and modified log- law profile is still an ongoing topic of research and there is not yet any consensus on which values of these constants are optimal. Based on this concern, the κ value of Osterlund *et al*. (2000) is adopted for the fully rough case, but the value of B remains the same as for the other flow cases. The change in κ value was found to change the friction velocity by less than 2%, and slightly improve the profile fitting result by decreasing the root-mean-square of the deviation between the fitted data and the modified log-law by 2% ~ 8% for different downstream locations. Note that Rostamy *et al*. (2011b) found that the classical and modified log- law profiles with a value of $\kappa = 0.41$ fitted the smooth and transitionally rough data reasonably well. However, the LES study of Banyassady and Piomelli (2015) on plane and radial wall jets on a smooth surface indicated that the slope of the logarithmic law was a function of the local Reynolds number, which was a measure of the penetration of the outer layer into the inner layer. To summarize, although the optimal value for

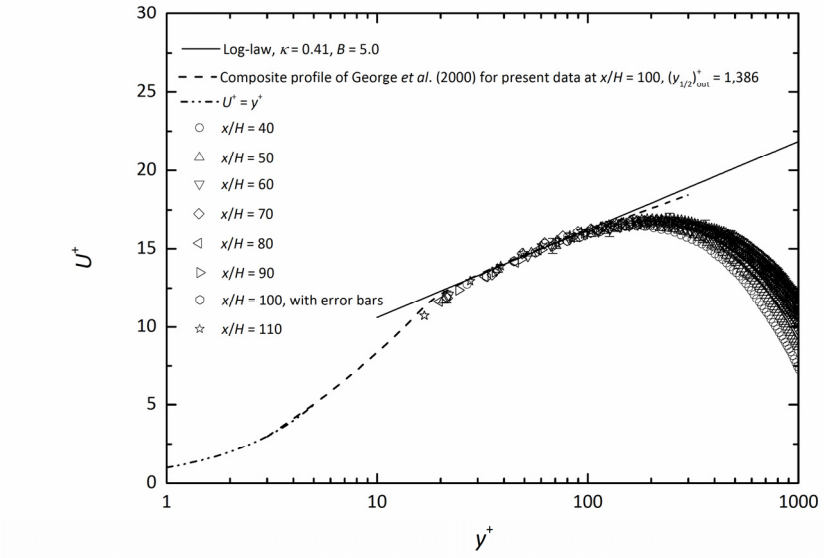

(a)

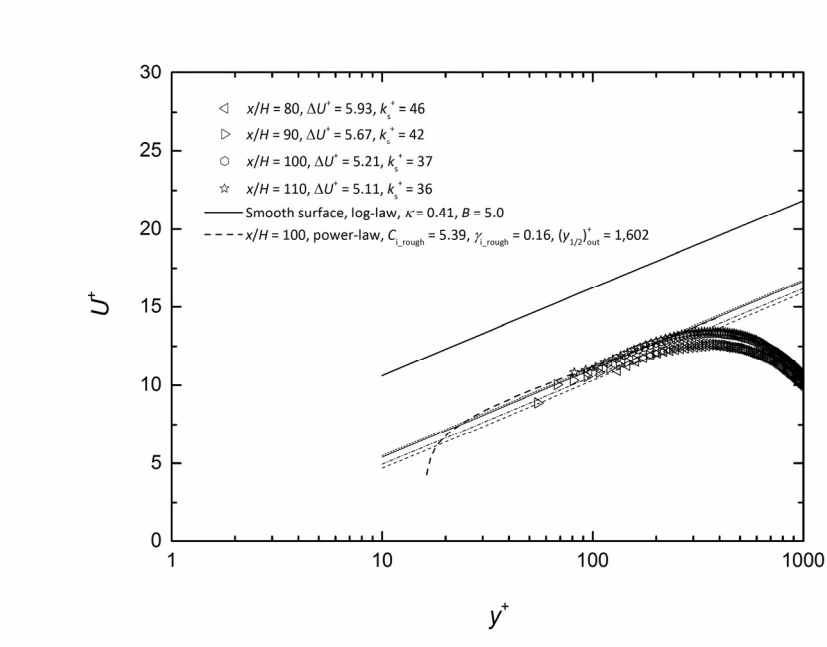

(b)

Figure 5.15: Mean streamwise velocity in inner coordinates for the LFR on (a) a smooth surface, and (b) a rough surface

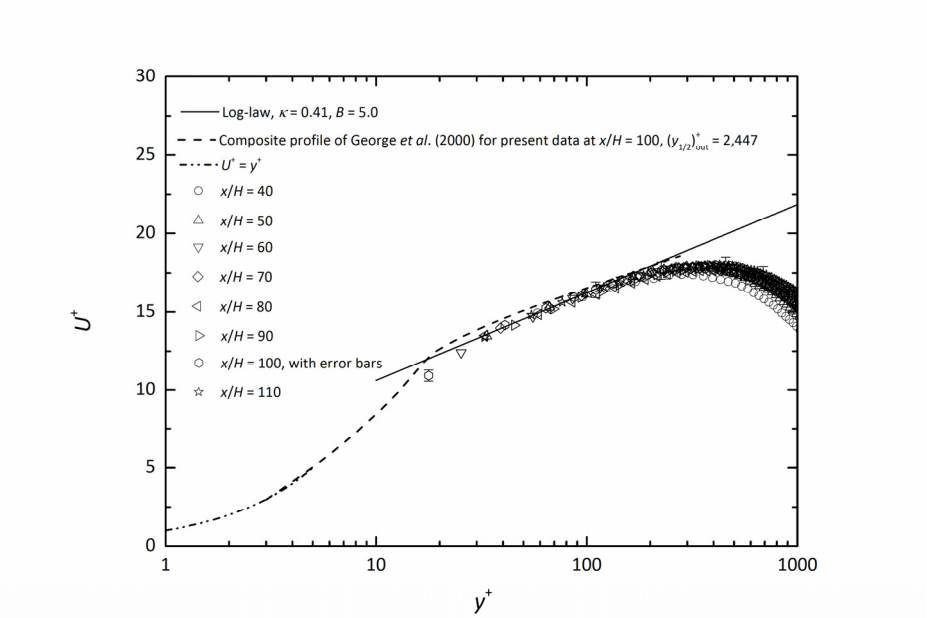

(a)

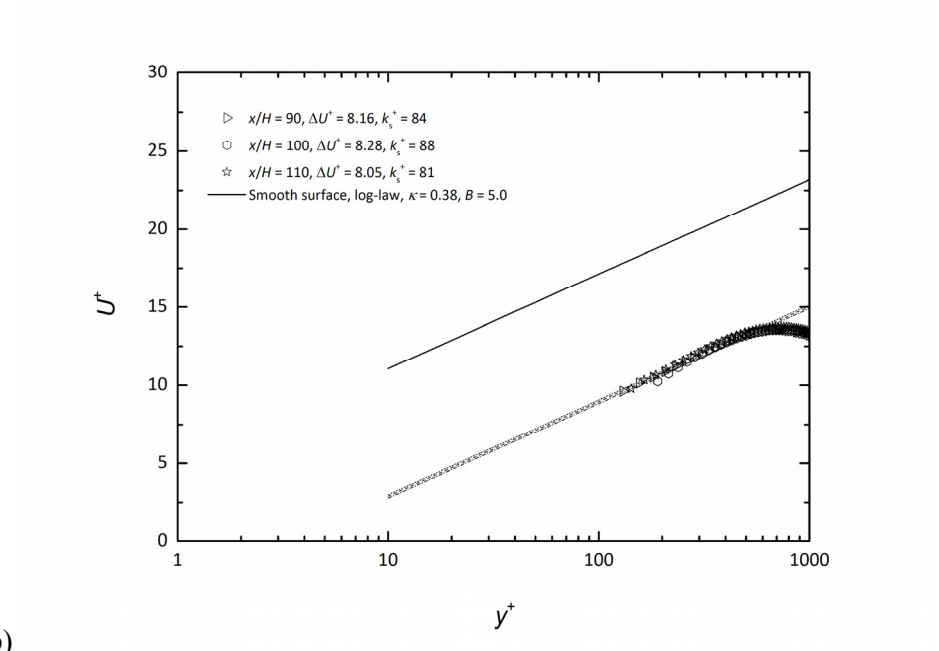

(b)

Figure 5.16: Mean streamwise velocity in inner coordinates for the HFR on (a) a smooth surface with $\kappa = 0.41$, and (b) a rough surface with $\kappa = 0.38$

κ in the log-law relation for the plane wall jet has been studied recently using both experimental and numerical results, the outcome is inconclusive. Therefore, the conventional value of $\kappa = 0.41$ was adopted in this study for the smooth and transitionally rough cases, and a revised value of $\kappa = 0.38$ was used for the fully rough case.

For the smooth surface cases, i.e. Figures 5.15(a) and 5.16(a), the present profiles for different downstream locations collapse well with each other in the region of $y^+ \leq 100$ with a deviation of less than 8%. This adds credibility to the present estimations of the friction velocity since any errors in these values would tend to separate these profiles in inner scales (Eriksson *et al*., 1998). Note that the increase of slot Reynolds number is observed to expand the upper boundary of this region of collapse from $y^+ \approx 100$ up to $y^+ \approx 200$. The figures also show that for both flow rates on the smooth surface, there are systematic differences between the data at different downstream locations above the overlap region, i.e. $y^+ > 0.1\left(y_{1/2}\right)^+_{\text{out}}$, which is to be expected since the inner scaling fails for the outer layer velocity profiles according to George *et al*. (2000) and Rostamy *et al*. (2011b). In addition, in the overlap region, the classical logarithmic law profile fits the dimensionless velocity profile well with a deviation in U^+ to be less than 10%.

For more detailed quantitative results, Tables 5.1 and 5.2 present the characteristic parameters determined from profile fitting. Table 5.1 shows that the friction velocity decreases monotonically with distance from the slot for both flow rates, which was also observed by Rostamy *et al*. (2011b). The friction velocity approximately doubles at the same downstream location with the doubling of the slot Reynolds number. The correction for the wall-normal location, ε_y, is partly due to the limitation of using a horizontal ruler to determine the wall-normal coordinates in the PIV calibration image. This correction is as large as 1/64 inch or 0.397 mm which occurred near the locations of $x = 40H$ and $x = 50H$.

Table 5.1: Profile fitting results for the smooth surface cases

	LFR (Re_o = 7,190)			HFR (Re_o = 14,300)		
x/H	U_τ (m/s)	ε_y (mm)	$\varepsilon_y^+ \left(=\frac{\varepsilon_y U_\tau}{\upsilon}\right)$	U_τ (m/s)	ε_y (mm)	$\varepsilon_y^+ \left(=\frac{\varepsilon_y U_\tau}{\upsilon}\right)$
40	0.0383	0.430	17.2	0.0792	0.460	38.4
50	0.0347	0.460	17.1	0.0685	0.355	26.2
60	0.0315	0.270	9.11	0.0624	0.255	17.2
70	0.0285	0.240	7.31	0.0582	0.165	10.2
80	0.0264	0.325	9.30	0.0541	0.200	11.7
90	0.0248	0.315	8.46	0.0504	0.245	13.3
100	0.0235	0.175	4.59	0.0467	0.150	7.77
110	0.0219	0.265	6.47	0.0442	0.245	12.0

For the rough surface cases, i.e. Figures 5.15(b) and 5.16(b), the non-dimensionalized velocity profiles show the characteristic downward shift ΔU^+ as reported by Raupach *et al.* (1991) and Rostamy *et al*. (2011b). In the overlap region, the modified logarithmic law profile fits the collapsed velocity profile well with a deviation of U^+ less than 12% and 7% for the LFR and HFR cases, respectively.

Table 5.2 gives the profile fitting results for the rough surface cases. Similar to the smooth surface cases, the friction velocity for the rough surface decreases monotonically with distance from the slot for both flow rates. This was also observed by Rostamy *et al*. (2010) for a transitionally rough plane wall jet. Also similar to the smooth surface cases, the friction velocity approximately doubles with the increase in the slot Reynolds number. Based on the analysis of ε_y for the smooth surface data, a new calibration method was used for the PIV image, which set the level of the top of the rough surface directly by using a second vertically positioned ruler rather than the previous horizontal ruler. This new method leads to a value for ε_{yk} between

Table 5.2: Profile fitting results for the rough surface cases

	LFR (Re_o = 6,660)					HFR (Re_o = 13,400)				
x/H	U_τ (m/s)	ε_{yk} (mm)	$\varepsilon_{yk}^+ \left(=\frac{\varepsilon_{yk}U_\tau}{\upsilon}\right)$	ΔU^+	k_s^+ rough surface	U_τ (m/s)	ε_{yk} (mm)	$\varepsilon_{yk}^+ \left(=\frac{\varepsilon_{yk}U_\tau}{\upsilon}\right)$	ΔU^+	k_s^+ rough surface
80	0.0329	0.080	2.57	5.93	46.2	-	-	-	-	-
90	0.0298	0.080	2.33	5.67	42.4	0.0570	0.060	3.38	8.16	84.0
100	0.0269	0.090	2.33	5.21	36.6	0.0538	0.030	1.59	8.28	87.9
110	0.0248	0.090	2.15	5.11	35.5	0.0495	0.040	1.95	8.05	80.6

0.03 mm and 0.09 mm, thus the ratio of ε_{yk} over the average roughness protrusion height, i.e. $k_g \approx$ 0.44 mm, varies from 7% to 21% which is smaller than the ratio of 25% reported by Rostamy *et al*. (2011a) who used the same type of surface. For the LFR case, the roughness shift, ΔU^+, decreases monotonically with distance from the slot, which indicates that the effect of surface roughness on the mean velocity profile is decreasing. This was also observed by Rostamy *et al*. (2011b). Such a systematic change is not observed for the HFR case. Based on the introduction in Section 2.4.2, by using the relation between k_s^+ and ΔU^+ given by Raupach *et al.* (1991), k_s^+ is determined to be in the range of $35 < k_s^+ < 47$ for the LFR case. For the HFR case, using Equation (2.23) gives a value of k_s^+ to be in the range of $81 < k_s^+ < 88$. This indicates that at the downstream sections on the rough surface considered in this study, the LFR case corresponds to the transitionally rough flow condition and the HFR case corresponds to the fully rough flow condition.

5.2.3 Extrapolation for Inner Half-width

The representative extrapolation curves as introduced in Section 2.4.5 for obtaining the inner half-width, $(y_{1/2})_{in}$, are also included in Figures 5.15 and 5.16. Tables 5.3 and 5.4 give the calculated coefficients of the extrapolation relations. Note that for the fully rough case, ΔU^+ is the only relevant coefficient for the extrapolation relation and its values have been presented in Table 5.2. The results for $(y_{1/2})_{in}$ are presented in Tables 5.5 and 5.6. Recall that the coefficients C_i and γ are functions of $\left(y_{1/2}\right)^+_{out}$ only, and the coefficients $\widetilde{C}_i$ and $\tilde{\gamma}$ are functions of k_s^+ and $\left(y_{1/2}\right)^+_{out}$.

Table 5.3: Coefficients of extrapolation formula for the smooth surface cases

	LFR (Re_o = 7,190)			HFR (Re_o = 14,300)		
x/H	$\left(y_{1/2}\right)^+_{out}$	C_i	γ	$\left(y_{1/2}\right)^+_{out}$	C_i	γ
40	934	9.46	0.117	1782	10.2	0.107
50	1050	9.59	0.115	1907	10.2	0.106
60	1146	9.68	0.113	2037	10.3	0.105
70	1185	9.72	0.113	2135	10.3	0.104
80	1242	9.77	0.112	2252	10.4	0.104
90	1308	9.83	0.111	2353	10.4	0.103
100	1386	9.89	0.110	2447	10.5	0.103
110	1430	9.92	0.110	2544	10.5	0.102

Table 5.4: Coefficients of extrapolation formula for the transitionally rough case

x/H	$\left(y_{1/2}\right)^+_{out}$	k_s^+	$\widetilde{C}_i$	$\tilde{\gamma}$
80	1611	46.2	4.88	0.173
90	1638	42.4	5.08	0.170
100	1602	36.6	5.39	0.165
110	1618	35.5	5.46	0.164

Table 5.5: Results of $(y_{1/2})_{in}$ from extrapolation for the smooth surface cases

	LFR (Re_o = 7,190)		HFR (Re_o = 14,300)	
x/H	$(y_{1/2})_{in}$ (mm)	$(y_{1/2})^+_{in}$	$(y_{1/2})_{in}$ (mm)	$(y_{1/2})^+_{in}$
40	0.243	9.73	0.128	10.7
50	0.261	9.72	0.153	11.3
60	0.292	9.85	0.169	11.3
70	0.331	10.1	0.181	11.2
80	0.348	9.96	0.188	11.0
90	0.377	10.1	0.209	11.3
100	0.383	10.0	0.220	11.4
110	0.419	10.2	0.233	11.4

Table 5.6: Results of $(y_{1/2})_{in}$ from extrapolation for the rough surface cases

	LFR (Re_o = 6,660)		HFR (Re_o = 13,400)	
x/H	$(y_{1/2})_{in}$ (mm)	$(y_{1/2})^+_{in}$	$(y_{1/2})_{in}$ (mm)	$(y_{1/2})^+_{in}$
80	0.631	20.3	-	-
90	0.672	19.5	0.773	43.6
100	0.760	19.7	0.861	45.7
110	0.819	19.6	0.883	43.1

Table 5.3 shows that for the LFR case on the smooth surface, the local half-width Reynolds number $(y_{1/2})^+_{out}$ increases monotonically from 934 to 1,430, i.e. an increase of 53%, over the streamwise extent of $40 < x/H < 110$. Accordingly, the composite profile coefficient C_i varies from 9.46 to 9.92, i.e. a monotonic increase of 4.9%, and the coefficient γ varies from 0.117 to 0.110, i.e. a monotonic decrease of 6.0%. Similarly, for the HFR case on the smooth surface, $(y_{1/2})^+_{out}$ increases monotonically by 43%, and accordingly the coefficient C_i increases

by 2.9% and the coefficient γ decreases by 4.7%. This indicates that the values of the composite profile coefficients do not change significantly over the streamwise extent considered in the present study. For comparison, Rostamy *et al*. (2013) indicated an increase of 2.9% for the coefficient C_i and a decrease of 5.3% for the coefficient γ over the streamwise extent of $30 < x/H < 80$ for a smooth surface plane wall jet with Re_o = 7,500, which are similar to the magnitudes of change observed for the smooth surface cases in this study.

As for the transitionally rough surface case, Table 5.4 shows that $\left(y_{1/2}\right)^+_{out}$ varies in a range from 1,602 to 1,638 but without any monotonic pattern over the streamwise extent of $80 < x/H < 110$ considered in this study. Another parameter that the power law coefficients $\widetilde{C}_i$ and $\tilde{\gamma}$ rely on, i.e. k_s^+, decreases monotonically from 46.2 to 35.5. As a result, the coefficients $\widetilde{C}_i$ increases monotonically from 4.88 to 5.46 (12%) and the coefficient $\tilde{\gamma}$ drops monotonically from 0.173 to 0.164 (5.2%). Note that Rostamy *et al*. (2013) indicated a monotonic increase of 39% for the coefficient $\widetilde{C}_i$ and a monotonic decrease of 15% for the coefficient $\tilde{\gamma}$ over the streamwise extent of $30 < x/H < 80$. The reason for the noticeable difference between the present variation in the coefficients and those of Rostamy *et al*. (2013) is not clear.

Based on the discussions above, the coefficients in the extrapolation relations used in this study have a narrow range of change which is between 2.9% and 12% over the streamwise extent considered in this study, i.e. $40 < x/H < 110$ for the smooth surface cases and $80 < x/H < 110$ for the transitionally rough surface case, respectively. The representative curves for the extrapolation relations shown in Figure 5.15 and Figure 5.16(a) are indicative of the characteristic shapes of those relations. In addition, it is found that in the overlap region for the smooth surface cases, the difference between the classical logarithmic law and the composite profile is within 3.2% and

8.3% for all downstream locations for the LFR and HFR, respectively, while for the transitionally rough case the difference between the modified logarithmic law and the power law profile of Rostamy *et al*. (2013) is within 11.5%.

Table 5.5 presents the calculated inner half-width $(y_{1/2})_{in}$ for the smooth surface cases. For the LFR, the dimensionless inner half-width $\left(y_{1/2}\right)_{in}^{+}$ varies from 9.72 to 10.2, and for the HFR it varies from 10.7 to 11.4, all of which are in the buffer layer and hence add validity to the use of the composite profile to extrapolate for $\left(y_{1/2}\right)_{in}^{+}$. Table 5.6 shows results for the rough surface cases. The dimensionless inner half-width varies from 19.5 to 20.3 for the LFR, which is in the buffer layer, and from 43.1 to 45.7 for the HFR, which is in the overlap region. Therefore, similar to the smooth surface case, these $\left(y_{1/2}\right)_{in}^{+}$ results add credibility to the extrapolation using the power law of Rostamy *et al*. (2013) in the buffer layer for the transitionally rough case, and the modified logarithmic law in the overlap region for the fully rough case.

5.2.4 Development of the Outer and Inner Layers

Tables 5.7 and 5.8 present the values of the outer and inner half-widths non-dimensionalized by the slot height H for the LFR and HFR, respectively. In terms of the effect of the slot Reynolds number Re_o on the smooth surface flow, the outer half-width decreases from 8% to 11% with the increase in Re_o, while the inner half-width decreases from 42% to 47%. As for the rough surface, the outer half-width decreases 9% with the increase in Re_o, while the inner half-width increases from 7% to 15%. This shows that the increase in Re_o decreases the size of both the outer and inner layers of the smooth surface wall jet, while such an effect is only observed for the outer layer of the rough surface wall jet. This is most likely because, for the

smooth surface case, the increase in Re_o does not change the flow condition, i.e. the wall jet remains hydraulically smooth. However, for the rough surface case, the increase in Re_o makes the wall jet transition from a transitionally rough flow to a fully rough flow, which makes the effects of the slot Reynolds number on the rough surface wall jet different from on the smooth surface case.

In terms of the effect of surface roughness, Table 5.7 shows that for the LFR the outer half-width increases by 15.6% to 16.9% over the streamwise extent of $80 < x/H < 110$, while the inner half-width increases by 78.0% to 98.6%. This indicates that the surface roughness enlarges the thicknesses of both the outer and inner layer, though such an effect is much more significant for the inner layer than for the outer layer. This is in agreement with the observations of Rostamy *et al*. (2011b) and Banyassady and Piomelli (2014) for a transitionally rough wall jet in terms of the effect of surface roughness on the thickness of the outer half-width. A similar phenomenon is also observed for the HFR but with a much more noticeable effect of surface roughness as shown by Table 5.8. More specifically, the outer half-width increases by 18.3% to 19.0% over the streamwise extent of $90 < x/H < 110$, while the inner half-width increases by 271% to 292%.

Table 5.7: The spatial development of the wall jet for the LFR

x/H	$(y_{1/2})_{out}/H$ (smooth surface)	$(y_{1/2})_{out}/H$ (rough surface)	Increase (%)	$(y_{1/2})_{in}/H$ (smooth surface)	$(y_{1/2})_{in}/H$ (rough surface)	Increase (%)
40	3.90	-	-	0.0405	-	-
50	4.70	-	-	0.0436	-	-
60	5.66	-	-	0.0487	-	-
70	6.46	-	-	0.0552	-	-
80	7.23	8.36	15.6	0.0580	0.105	81.4
90	8.12	9.38	15.6	0.0629	0.112	78.0
100	8.81	10.3	16.9	0.0638	0.127	98.6
110	9.76	11.3	15.6	0.0699	0.137	95.4

Table 5.8: The spatial development of the wall jet for the HFR

x/H	$(y_{1/2})_{out}/H$ (smooth surface)	$(y_{1/2})_{out}/H$ (rough surface)	Increase (%)	$(y_{1/2})_{in}/H$ (smooth surface)	$(y_{1/2})_{in}/H$ (rough surface)	Increase (%)
40	3.55	-	-	0.0213	-	-
50	4.30	-	-	0.0255	-	-
60	5.05	-	-	0.0281	-	-
70	5.73	-	-	0.0301	-	-
80	6.43	-	-	0.0314	-	-
90	7.22	8.55	18.3	0.0348	0.129	271
100	7.88	9.37	19.0	0.0366	0.144	292
110	8.65	10.3	18.6	0.0388	0.147	279

After investigating the magnitude of the outer and inner half-widths, focus is turned to the change rate of these variables. Figures 5.17, 5.18, 5.19 and 5.20 present the outer and inner half-widths as well as the fitted coefficients based on power law relations of Equations (2.8) and (2.9) to illustrate the spread of the outer and inner layers of the wall jet. Data from select previous studies are also shown for comparison. It should also be noted that the power law coefficients reported by Barenblatt *et al*. (2005) are based on the data of Eriksson *et al*. (1998).

For all these plots, the uncertainty of the coefficients is given at a confidence level of 95%. Note that the presented uncertainty level of the coefficients is much higher for the rough surface data than for the smooth surface data, which was expected due to the limited amount of valid data available for curve fitting.

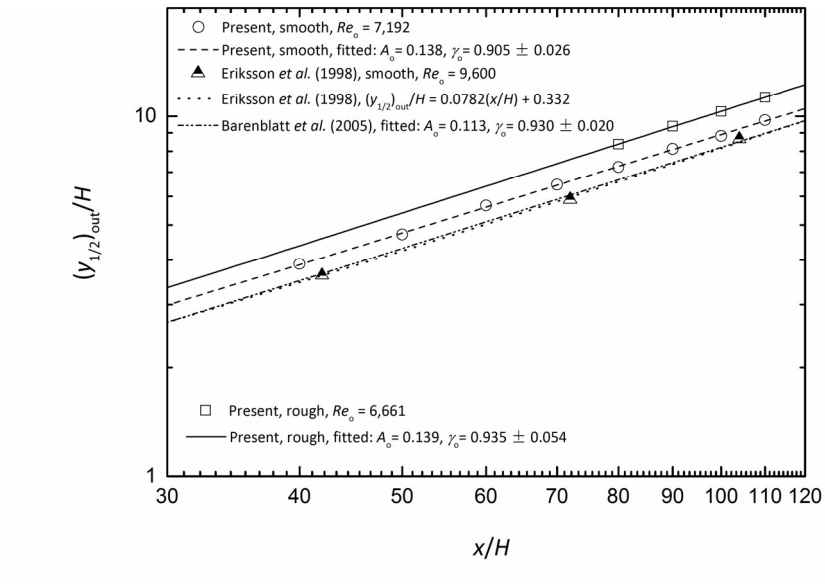

Figure 5.17: Spread of wall jet in the outer region for the LFR

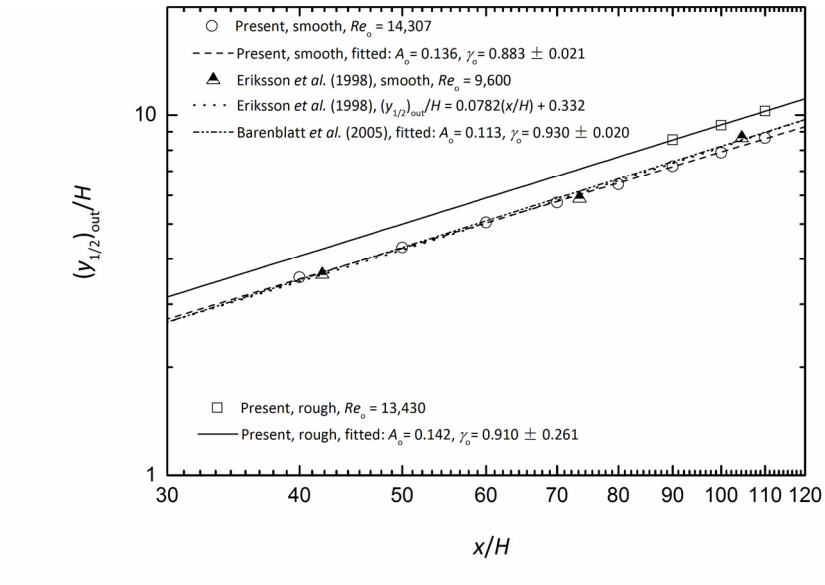

Figure 5.18: Spread of wall jet in the outer region for the HFR

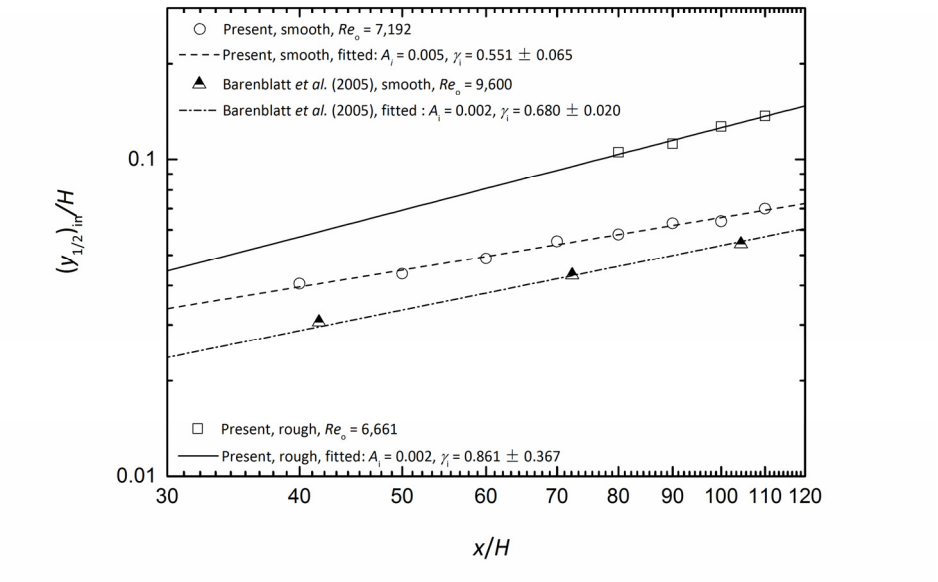

Figure 5.19: Spread of wall jet in the inner region for the LFR

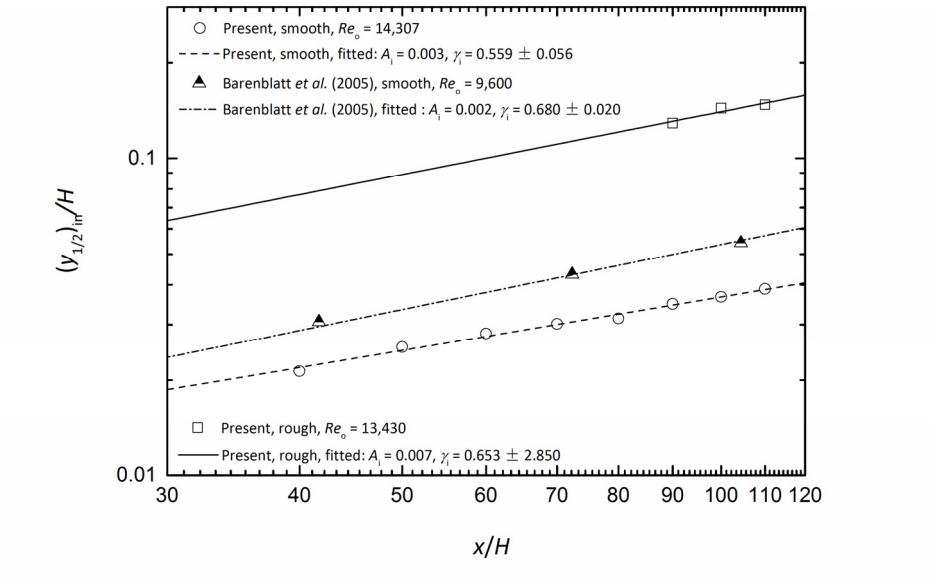

Figure 5.20: Spread of wall jet in the inner region for the HFR

For the outer half-width for the smooth surface cases, the present non-dimensionalized outer half-width data for the HFR compare relatively well with the data of Eriksson *et al*. (1998) as shown in Figure 5.18, while a more noticeable discrepancy is observed between the present and other data as shown in Figure 5.17. Consequently, it is seen that the power law coefficients, A_o and γ_o, are different between the present results and other studies. More specifically, for the LFR case, Figure 5.17 shows a difference of 22% in the coefficient A_o from the reference data of Barenblatt *et al*. (2005), and a difference of 2% in the coefficient γ_o from the reference data. For the HFR case, Figure 5.18 shows a difference of 20% in the coefficient A_o from the reference data, and a difference of 5% in the coefficient γ_o from the reference data. As for the inner half-width, differences between the present smooth-wall results and those of Barenblatt *et al*. (2005) are observed for both the LFR and HFR. For the LFR case, Figure 5.19 shows a difference of 150% in the coefficient A_i from the reference data of Barenblatt *et al*. (2005), and a difference of 19% in the coefficient γ_i from the reference data. For the HFR case, Figure 5.20 shows a difference of 50% in the coefficient A_i from the reference data of Barenblatt *et al*. (2005), and a difference of 18% in the coefficient γ_i from the reference data.

Table 5.9 summarizes the power law exponential coefficients in Figures 5.17 to 5.20. The differences in these coefficients are supposedly due to the dependence on the slot Reynolds number Re_o, as suggested by Barenblatt *et al*. (2005). Their assumed relation of $\gamma = 1 - \text{Constant}/\ln(Re_o)$ based on analogy with the pipe flow and the boundary layer is not supported by the present results.

In addition, as shown in Figure 5.17, Eriksson *et al*. (1998) proposed a linear relation for the streamwise growth (spread rate) of the outer half-width, whereas the power-law relations

adopted in this study admit the possibility of a non-linear growth rate. Note that for the outer half-width, the linear relation proposed by Eriksson *et al*. (1998) compares favorably with the power law relation of Barenblatt *et al*. (2005) in terms of fitting the experimental data of Eriksson *et al*. (1998). This illustrates that different functional relations can result in similar curves for specific sets of data.

Table 5.9: The effect of slot Reynolds number on exponential coefficients γ_o and γ_i

Study		Re_o	γ_o	γ_i
Barenblatt *et al*. (2005)		9,600	0.930	0.680
Present smooth surface	LFR	7,190	0.905	0.551
	HFR	14,300	0.883	0.559
Present rough surface	LFR	6,660	0.935	0.861
	HFR	13,400	0.910	0.653

Next, attention will be turned to comparison within the new PIV data in terms of the effects of slot Reynolds number Re_o and surface roughness on the power law coefficients. Note that in this study the exponential coefficients of γ_o and γ_i represent the wall jet spread rates for the outer and inner layer, respectively. The physical meaning of the coefficients A_o and A_i, if any, has not yet been identified.

In terms of the effect of slot Reynolds number Re_o on the outer half-width, comparing Figure 5.17 and 5.18 shows that for the smooth surface case the coefficient A_o changes by less than 2% and the coefficient γ_o changes by less than 3% with the increase in Re_o, while for the rough surface case both A_o and γ_o change less than 3% with the increase in Re_o. This indicates that the effect of slot Reynolds number on the spread rate of the outer layer is minimal. As for the inner half-width, comparison between Figures 5.19 and 5.20 shows that for the smooth

surface case the coefficient A_i changes by 40% and the coefficient γ_i changes by less than 2% with the increase of the Re_o, while for the rough surface case A_i changes by 250% and the coefficient γ_i decreases by 24% with the increase in Re_o. This shows that for the smooth surface the effect of slot Reynolds number on the spread rate of the inner layer is still minimal as expected, but for the rough surface such an effect is not negligible due to the fact that the wall jet transitions from a transitionally rough flow condition to a fully rough one with the increase in Re_o.

In terms of the effect of surface roughness, Figure 5.17 shows that for the LFR the coefficient A_o changes by less than 1% with the roughening of the wall surface, and the coefficient γ_o increases by 3%. Figure 5.18 shows that for the HFR the coefficient A_o changes by less than 5% with the roughening of the wall surface, and the coefficient γ_o increases by 3%. In contrast, Figure 5.19 shows that for the LFR the coefficient A_i decreases by 150% with the roughening of the wall surface, and the coefficient γ_i increases by 56%. Figure 5.20 shows that for the HFR the coefficient A_i increases by 133% with the roughening of the wall surface, and the coefficient γ_i increases by 17%. This clearly shows that the surface roughness significantly increases the spread rate of the inner layer, and the effect of surface roughness penetrates into the outer layer though the impact is much less than for the inner layer. In terms of the effect of surface roughness on the spread rates of outer and inner layers, this observation is consistent with the conclusions of Banyassady and Piomelli (2014) and Tang *et al.* (2015).

5.2.5 Decay of the Maximum Mean Streamwise Velocity

Figures 5.21 and 5.22 show the decay of the maximum mean streamwise velocity U_m with distance from the slot by fitting the data to Equation (2.7). In this study the decay rate of U_m is represented by the magnitude of the exponential coefficient γ_m. For the LFR for the smooth surface, the coefficient A_m is 13% lower than the value based on the data of Eriksson *et al*. (1998) and the magnitude of coefficient γ_m is 7% lower than the reference value. For the HFR, the coefficient A_m is 2% higher than the reference value and the magnitude of coefficient γ_m is 4% lower than the reference value. This is similar to the case of the power law coefficients for the outer and inner half-width development as discussed above, i.e. the power law coefficients for the decay of U_m are dependent on the slot Reynolds number Re_o. However, again no specific correlation between the coefficients and Re_o is identified.

In terms of the effect of slot Reynolds number Re_o, comparing Figures 5.21 and 5.22 shows that for the smooth surface case the coefficient A_m increases by 17% with the increase in Re_o, and the magnitude of coefficient γ_m increases by 4%. For the rough surface case, the coefficient A_m increases by 22% with the increase in Re_o, and the magnitude of coefficient γ_m increases by 7%. This indicates that the increase in Re_o slightly increases the magnitude of the decay rate for both the smooth and rough surface cases, i.e. the increase in Re_o slightly accelerates the attenuation of U_m/U_o, although the magnitude of U_m/U_o increases by approximately 8% for the smooth surface case and by approximately 3% for the rough surface case with the increase in Re_o.

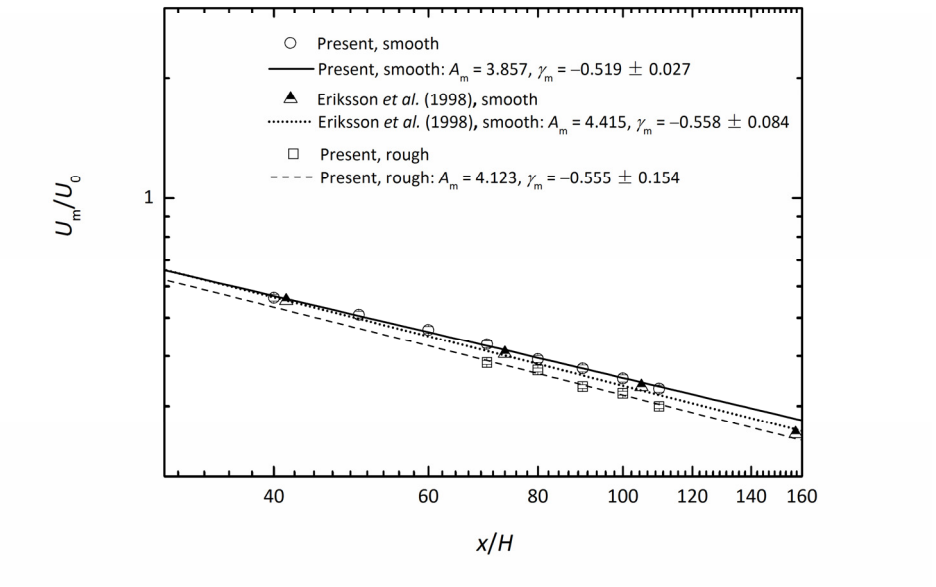

Figure 5.21: Decay of maximum velocity with streamwise distance from slot for the LFR

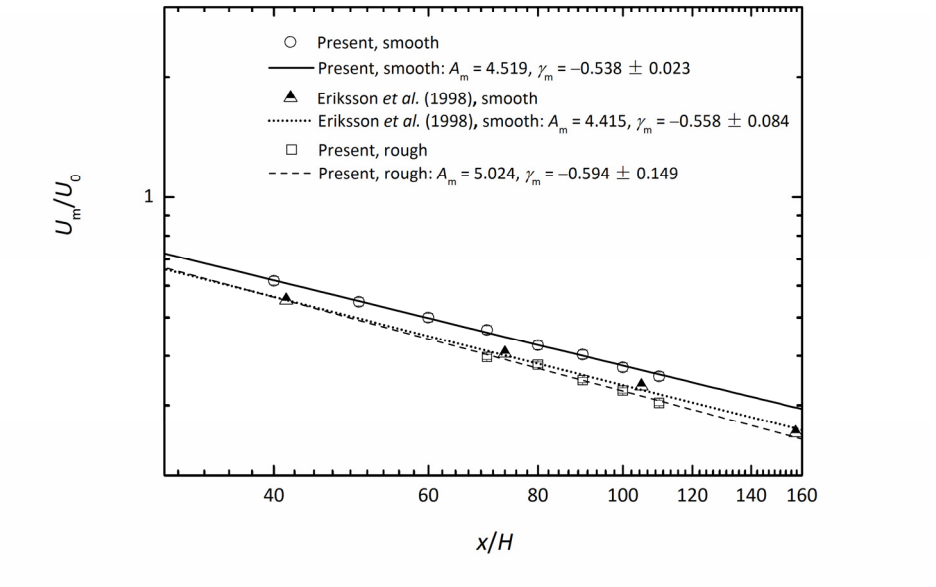

Figure 5.22: Decay of maximum velocity with streamwise distance from slot for the HFR

In terms of the effect of surface roughness, Figure 5.21 shows that for the LFR the coefficient A_{m} increases by 7% due to the rough surface, and the magnitude of coefficient γ_{m} increases by 7%. For the HFR, Figure 5.22 shows that the coefficient A_{m} increases by 11% due to the rough surface, and the magnitude of coefficient γ_{m} increases by 10%. This indicates that the rough surface slightly accelerates the attenuation of $U_{\mathrm{m}}/U_{\mathrm{o}}$, which is expected considering the enhanced wall shear stress on the rough surface. As for the magnitude of $U_{\mathrm{m}}/U_{\mathrm{o}}$, it decreases by approximately 9% for the LFR case and by approximately 13% for the HFR due to the rough surface. These observations which relate to the effect of surface roughness on the decay rate and the magnitude of U_{m} agree with the conclusions of Rostamy *et al*. (2011a, b) and Banyassady and Piomelli (2014).

In addition to the scaling law for the decay of U_{m} that was introduced in Section 2.1, George *et al*. (2000) observed that U_{m} and the outer half-width $(y_{1/2})_{\mathrm{out}}$ satisfy the following power law relation based on their similarity analysis:

$$\frac{U_{\mathrm{m}}}{U_{\mathrm{o}}} = B_{\mathrm{o}}\left(\frac{(y_{1/2})_{\mathrm{out}}}{H}\right)^{n} \tag{5.1}$$

Figures 5.23 and 5.24 present the decay of U_{m} using the above scaling law. Note that the coefficients presented by George *et al*. (2000) were obtained based on previous established data with slot Reynolds numbers ranging from 10,000 up to 20,000. More specifically, George *et al*. (2000) concluded that a value of n = -0.528 was nearly the same for various slot Reynolds numbers but B_{o} was found to increase from 1.09 to 1.18 monotonically over the range of 10,000 $\leq Re_{\mathrm{o}} \leq$ 20,000. Figures 5.23 shows that for the LFR case, the coefficient B_{o} is 5% higher than the value based on the data of Eriksson *et al*. (1998) and 14% higher than the value reported by

George *et al*. (2000), and the magnitude of the coefficient *n* is 3% lower than the value based on the data of Eriksson *et al*. (1998) and 9% higher than the value reported by George *et al*. (2000). As for the HFR case, the coefficient B_o is 15% higher than the value based on the data of Eriksson *et al*. (1998) and 24% higher than the value reported by George *et al*. (2000), and the magnitude of the coefficient *n* is 4% higher than the value based on the data of Eriksson *et al*. (1998) and 17% higher than the value reported by George *et al*. (2000). This indicates a slot Reynolds number dependence of the power law coefficients in Equation (5.1). However, the pattern of change in these coefficients with slot Reynolds number is not yet clear.

In terms of the effect of slot Reynolds number Re_o, comparing Figures 5.23 and 5.24 shows that for the smooth surface case the magnitude of coefficients increases by 9% with the increase in Re_o, and for the rough surface case the magnitude of coefficients increases by 10%. This indicates that the increase in Re_o slightly increases the magnitude of the decay rate for both the smooth and rough surface cases, which is the same as observed in Figures 5.21 and 5.22. In addition, the comparison within the present PIV data support the observation of George *et al*. (2000) that the coefficient B_o increases with the increase in Re_o.

In terms of the effect of surface roughness, Figure 5.23 shows that for the LFR the magnitude of the coefficient *n* increases by 6% due to the rough surface, and for the HFR Figure 5.24 shows that the magnitude of the coefficient *n* increases by 7%. This indicates that the rough surface slightly accelerates the attenuation of U_m/U_o, which is also observed in Figures 5.21 and 5.22.

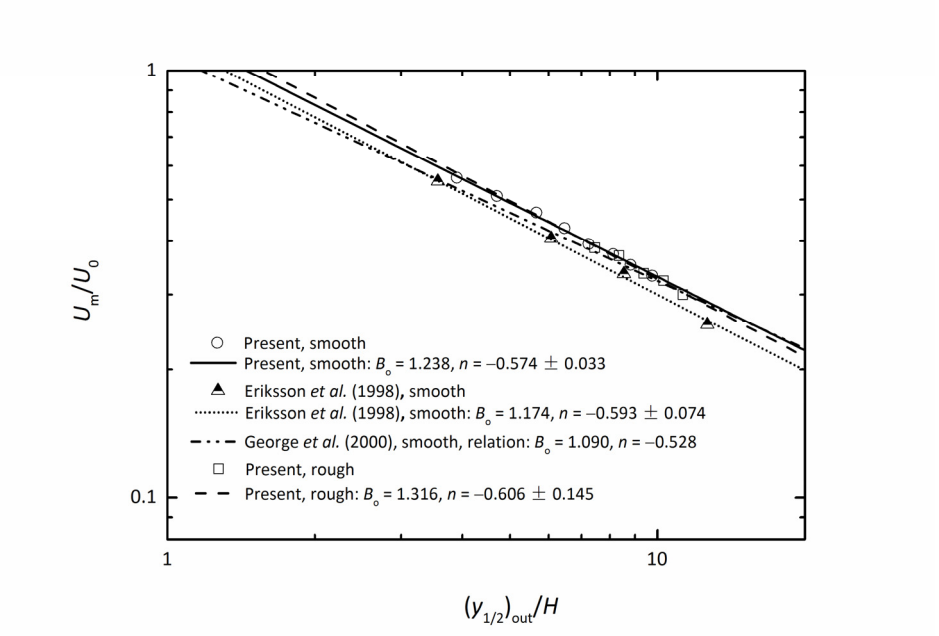

Figure 5.23: Dependence of maximum velocity on the outer half-width for the LFR

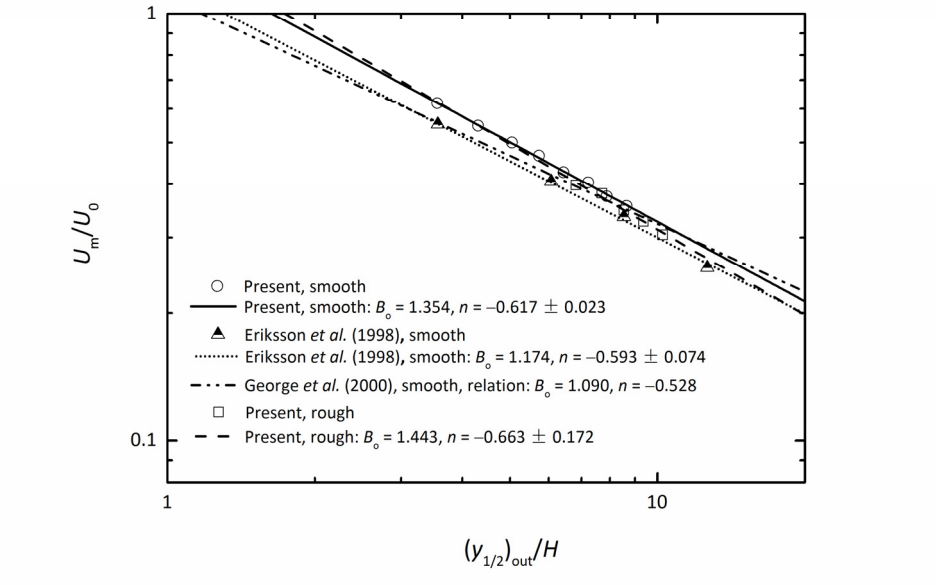

Figure 5.24: Dependence of maximum velocity on the outer half-width for the HFR

5.2.6 Change in the Height of the Maximum Mean Streamwise Velocity

Based on the results of Tachie *et al*. (2004) and Tang *et al*. (2015), a power law relation is used to correlate the parameter y_m and the distance from the slot as follows:

$$\frac{y_m}{H} = A_{ym}\left(\frac{x}{H}\right)^{\gamma_{ym}} \tag{5.2}$$

Figures 5.25 and 5.26 present the change of y_m with distance from the slot. Comparison between these two figures shows that for the smooth surface case, the coefficient A_{ym} increases 17% with the increase of the slot Reynolds number Re_o, while γ_{ym} decreases 6%. As for the rough surface case, the coefficient A_{ym} decreases 59% with the increase in Re_o, while γ_{ym} increases 19%. A pattern of slot Reynolds number dependence of the power law coefficients is again observed, but it is distinct for the smooth and rough surface cases, i.e. the increase of the slot Reynolds number slightly decreases the spread rate of y_m on the smooth surface but increases it on the rough surface. As for the effect of surface roughness, Figure 5.25 shows that for the LFR there is a 24% decrease in A_{ym} due to the surface roughness but a 19% increase in γ_{ym}. Figure 5.26 shows that for the HFR there is a 74% decrease in A_{ym} due to the surface roughness but a 52% increase in γ_{ym}. This indicates that the surface roughness has a significant impact on increasing the spread rate of y_m, especially for the HFR in this study. As for the magnitude of y_m, Figure 5.25 shows an 65% increase due to the rough surface for the LFR and Figure 5.26 shows this increase to be 67% for the HFR; both indicate that roughening the surface significantly increases the magnitude of y_m. These observations with respect to the effect of surface roughness on the spread rate and the magnitude of y_m are consistent with the conclusions of Banyassady and Piomelli (2014).

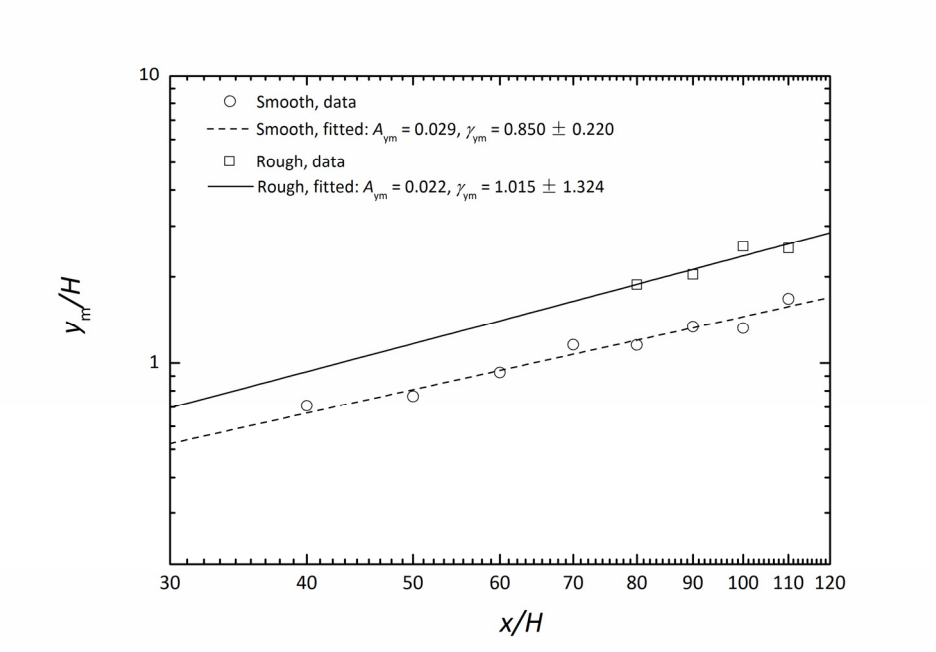

Figure 5.25: Streamwise development of the height of the maximum velocity for the LFR

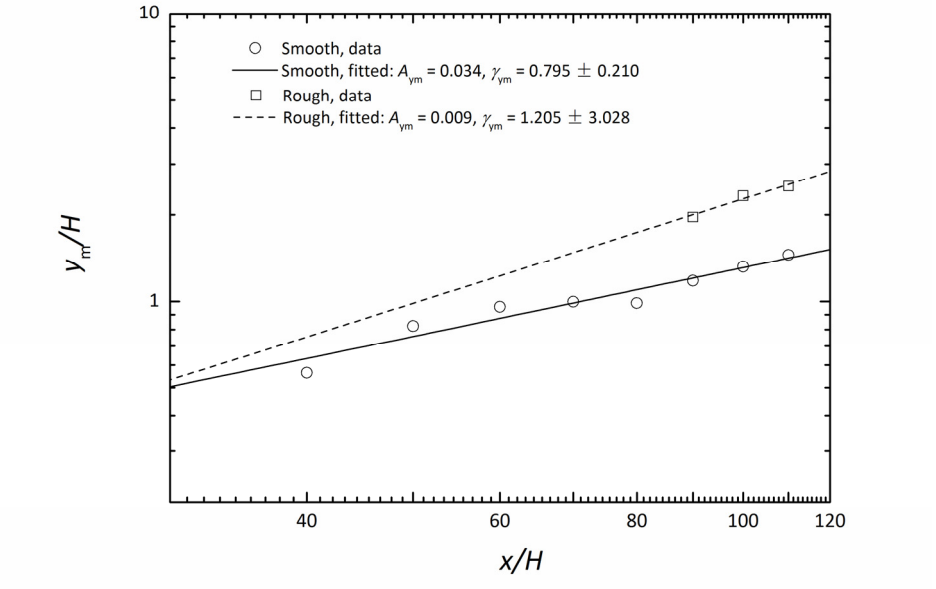

Figure 5.26: Streamwise development of the height of the maximum velocity for the HFR

The results of the effect of surface roughness on the streamwise growth of the mean velocity field, as illustrated above, are summarized in Table 5.10. It shows that for the LFR, while in general the surface roughness tends to increase the streamwise growth rate of the inner and outer half-widths as well as the height of the maximum velocity, the magnitude of such an effect becomes stronger as the wall-normal distance to the surface decreases. Such a pattern is not observed for the HFR, and the reason is not clear.

Table 5.10: The effect of surface roughness on the streamwise development of the wall jet

Case	Increase of γ_o (%)	Increase of γ_{ym} (%)	Increase of γ_i (%)
LFR	3	19	56
HFR	3	52	17

5.2.7 Skin Friction Coefficient

One of the primary contributions of the present study is to add to the existing state of knowledge on the skin friction characteristics of a fully rough plane wall jet. Tables 5.11 and 5.12 present the values of the skin friction coefficient C_f with the local maximum-velocity Reynolds number Re_m, which also are plotted in Figures 5.27 and 5.28. The skin friction coefficient is calculated based on the local friction velocity and the maximum mean streamwise velocity as

$$C_f = 2\left(\frac{U_\tau}{U_m}\right)^2 . \tag{5.3}$$

The present values of C_f for both smooth surface cases compare favorably with previous studies. The present results for the transitionally rough case compare well to the data of Rostamy *et al*.

(2011b) with the exception of the values of C_f for Re_m = 4,850 corresponding to the downstream location x = 110H. As for the fully rough case, Figure 5.28 shows a small deviation of less than 3% in the values of C_f over the range of 9,000 ≤ Re_m ≤ 10,100, which indicates that over the streamwise extent considered in this study the variable C_f is approximately independent of Re_m or the distance from the slot. Based on the values of C_f for a fully rough turbulent boundary layer presented by Brzek *et al*. (2009), the condition of C_f being independent of Re_m is evidence of a fully rough flow condition being formed in the present HFR case for the rough surface. For the effect of slot Reynolds number Re_o, Tables 5.11 and 5.12 show that C_f decreases by 10% - 16% due to the increase in Re_o for the smooth surface case and by 3% - 13% for the rough surface case. For the effect of surface roughness, Tables 5.11 and 5.12 show that C_f increases by 58% - 78% due to the surface roughness in the LFR case and by 72% - 75% in the HFR case. This noticeable increase of skin friction due to the surface roughness was also observed in previous studies on the transitionally rough plane wall jet, e.g. Tachie *et al*. (2004) and Rostamy *et al*. (2011b).

Table 5.11: The skin friction coefficient for the LFR

x/H	Re_m (smooth surface)	C_f (smooth surface)	Re_m (rough surface)	C_f (rough surface)	Increase of C_f (%)
40	2,790	0.00740	-	-	-
50	2,810	0.00739	-	-	-
60	3,110	0.00726	-	-	-
70	3,590	0.00704	-	-	-
80	3,320	0.00718	4,560	0.0126	76
90	3,650	0.00703	4,500	0.0125	78
100	3,500	0.00711	5,300	0.0112	58
110	4,170	0.00694	4,850	0.0111	60

Table 5.12: The skin friction coefficient for the HFR

x/H	Re_m (smooth surface)	C_f (smooth surface)	Re_m (rough surface)	C_f (rough surface)	Increase of C_f (%)
40	4,920	0.00661	-	-	-
50	6,520	0.00624	-	-	-
60	6,950	0.00620	-	-	-
70	6,640	0.00628	-	-	-
80	6,090	0.00643	-	-	-
90	6,910	0.00621	9,000	0.0109	75
100	7,380	0.00619	10,000	0.0109	75
110	7,690	0.00617	10,100	0.0106	72

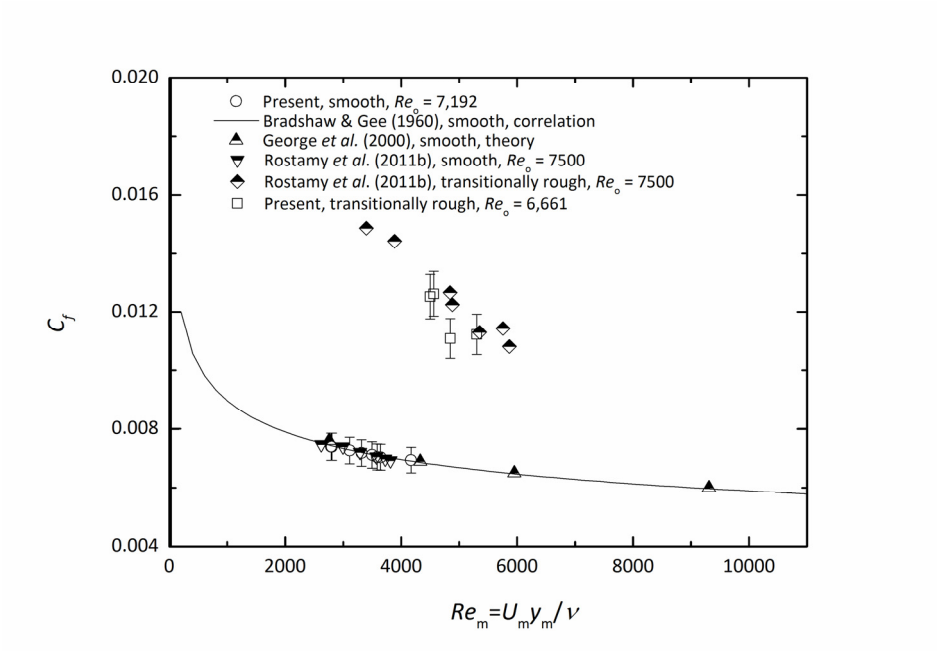

Figure 5.27: Skin friction coefficient for the plane turbulent wall jet for the LFR

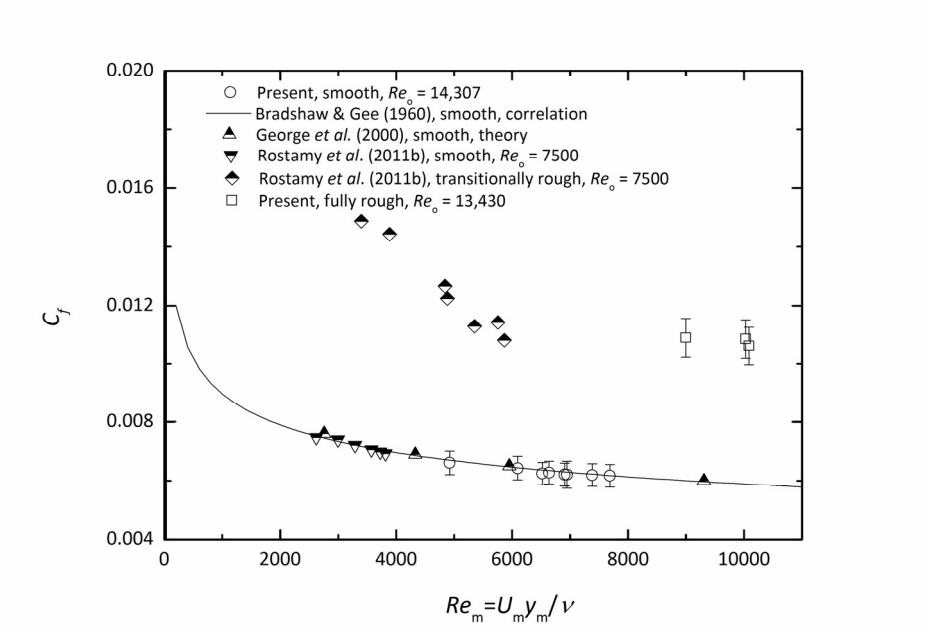

Figure 5.28: Skin friction coefficient for the plane turbulent wall jet for the HFR

5.3 Chapter Summary

This chapter presents an extensive analysis and discussion of the mean velocity field in the fully developed region. Focus is given to the effects of the slot Reynolds number Re_o and the surface roughness on the characteristic parameters of the plane wall jet. It is found that the change in Re_o has distinct effects on the smooth and rough surface cases. This is to be expected because for the smooth surface case, the increase in Re_o does not change the flow condition, but the increase in Re_o makes the wall jet on a rough surface transition from a transitionally rough flow to a fully rough flow. The effect of surface roughness is observed to be significant on the flow field in the inner layer and also penetrate into the outer layer, although the effect on the latter is minimal. The next chapter will investigate the hypothesis of incomplete similarity for the plane wall jet.

CHAPTER 6

INCOMPLETE SIMILARITY

6.1 Introduction

This chapter will use the results documented in the previous chapter to examine the incomplete similarity of the present wall jet on smooth and rough surfaces following the approach of Barenblatt *et al*. (2005), Rostamy *et al*. (2011c), and Tang *et al*. (2015). The scaling laws used in this chapter were introduced in Chapter 2 as Equations (2.10) and (2.11). As discussed by Barenblatt *et al*. (2005), these two scaling laws contrasted the effectiveness of the half-width for the outer and inner layer for scaling the entire velocity field across the wall jet. The effect of surface roughness on the self-similar profiles will also be discussed in detail. Note that the analysis in this chapter uses the data sets in the fully developed region, i.e. $40 \leq x/H \leq 110$, $80 \leq x/H \leq 110$ and $90 \leq x/H \leq 110$ for the smooth, transitionally rough and fully rough cases.

So far there is no definitive criterion for the "collapse" of velocity profiles that has been presented in the literature. In this chapter, the velocity profiles are claimed to "collapse" in a specific wall-normal range when no less than 90% of the scaled velocity data at various downstream locations (i.e. different values of x/H) overlap with each other. More specifically, this criterion is examined by determining if the polylines remain within the area specified by the uncertainty bars for the velocity data. A polyline is used in data plotting to visually connect the discrete data points in a single velocity profile. It should be noted that the polyline is not a result of curve fitting. When the polylines are confined to a band no greater than the uncertainty level at $x/H = 100$ for each flow case, the velocity data are considered to collapse. Every 5^{th} data point

in the outer layer and every data point in inner layer, together with every 25th uncertainty bar in the outer layer and every 2nd uncertainty bar in the inner layer are shown for better legibility.

6.2 Outer Scaling

Figure 6.1 presents the scaled mean velocity profile for the LFR case on the smooth surface. Figure 6.1(a) shows that the profiles collapse across most of the outer layer, i.e. from the location where $U/U_m \approx 1$ up to $A_o\left[y/\left(y_{1/2}\right)_{out}\right] \approx 0.2$. This is near the outer edge of the wall jet where self-similarity is expected to be diminished by the shear in the turbulence mixing region produced by the reverse flow. In contrast, Figure 6.1(b) shows that the profiles using outer scales gradually lose similarity from the location where $U/U_m \approx 1$ down to $A_o\left[y/\left(y_{1/2}\right)_{out}\right] \approx 0.01$ then clearly separate from each other closer to the wall. This indicates that the outer scales are able to collapse the outer layer profiles and even the upper 45% of the inner layer profiles, but fail to capture the similarity feature of the profiles in the remainder of the inner layer.

Figure 6.2 presents the LFR case on the rough surface. Figure 6.2(a) shows that the outer scales again collapse the profiles well across most of the outer layer, specifically from the location where $U/U_m \approx 1$ up to $A_o\left[y/\left(y_{1/2}\right)_{out}\right] \approx 0.2$. Figure 6.2(b) shows that the profiles using outer scales start to lose similarity from the location $A_o\left[y/\left(y_{1/2}\right)_{out}\right] \approx 0.015$ downwards to the wall. Overall, the extent of the collapse of the inner layer data increases to approximately 65%, which is a noticeable increase compared to the LFR case on the smooth surface as shown in Figure 6.1(b).

For the HFR case on the smooth surface, Figure 6.3(a) supports the validity of using the outer scales to collapse the data in the outer layer. For the inner layer profiles, Figure 6.3(b)

indicates that the profiles using outer scales begin to lose similarity from the location $A_o\left[y/\left(y_{1/2}\right)_{out}\right] \approx 0.017$ downwards to the wall. The extent of the collapsed data in the inner layer is approximately 40%, which is slightly less than for the LFR case on the smooth surface.

Figure 6.4 shows the HFR case on the rough surface. Figure 6.4(a) indicates that the outer scales successfully collapse the outer profiles for the fully rough case. For the inner layer, Figure 6.4(b) indicates that the profiles using outer scales begin to lose similarity from the location $A_o\left[y/\left(y_{1/2}\right)_{out}\right] \approx 0.014$ downwards. This implies that the extent of the collapsed data in the inner layer is approximately 75%, which is a significant increase compared to the HFR case on the smooth surface.

These analyses demonstrate that the outer scaling extends into the inner layer, i.e. part of the top region of the inner layer velocity profiles collapse even though the outer scales are used. This indicates that the top region of the inner layer in a plane wall jet is essentially part of the outer layer in a canonical zero-pressure-gradient turbulent boundary layer, which clarifies an ambiguity among previous wall jet studies. In addition, the analysis of the outer scaling in the inner layer illustrates that the velocity profiles in the inner layer generally tend to collapse better when the rough surface is present compared to the smooth surface. This implies that the surface roughness enhances the interaction and coupling between the inner and outer layers.

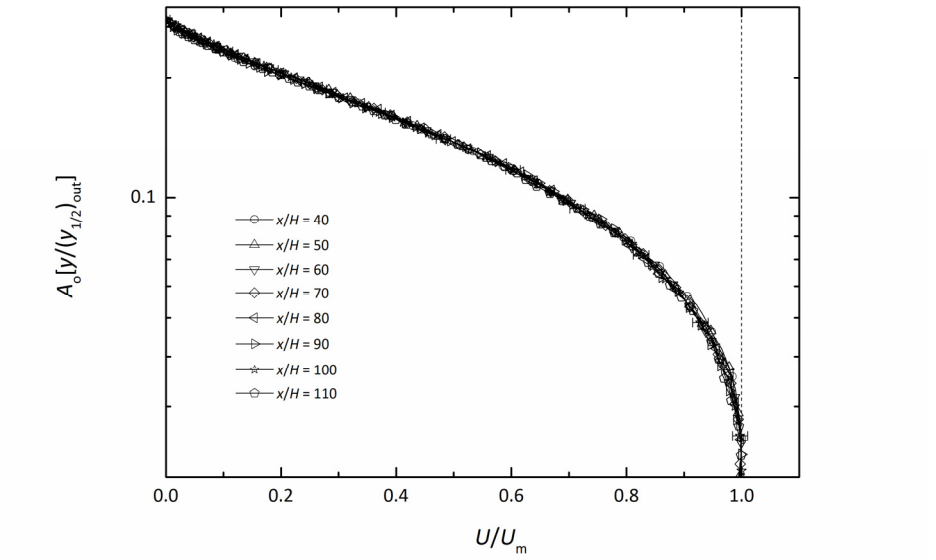

(a)

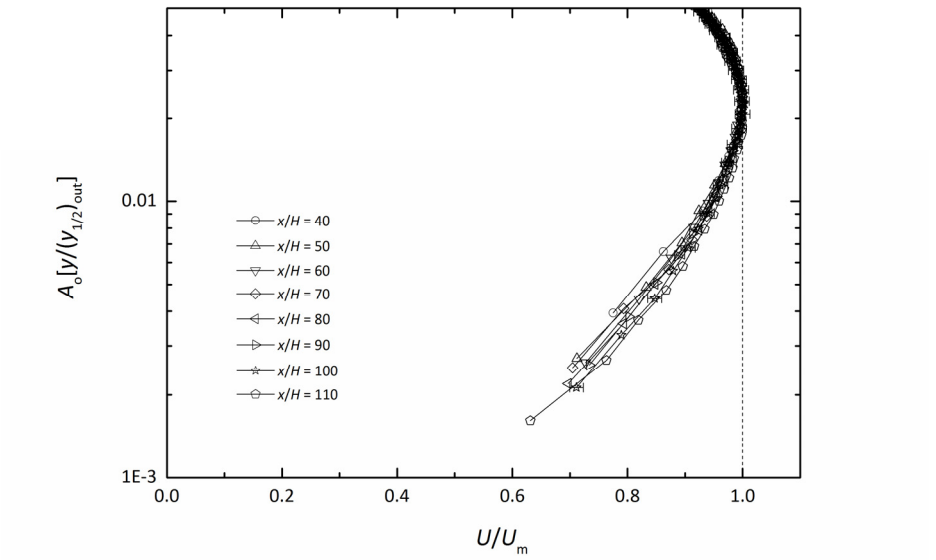

(b)

Figure 6.1: Scaling of the mean velocity profile using the outer scales for the LFR on a smooth surface in (a) the outer layer, and (b) the inner layer.

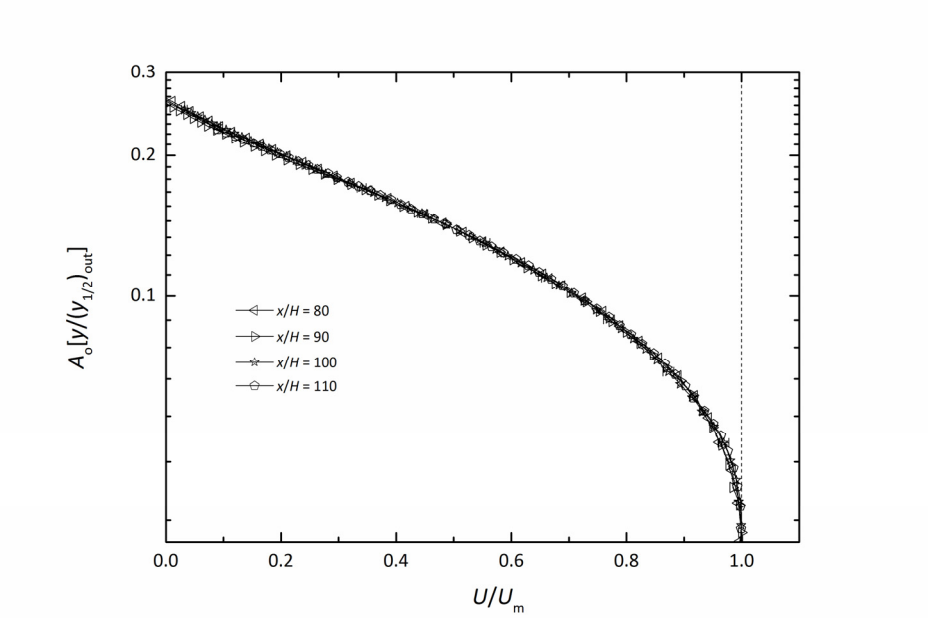

(a)

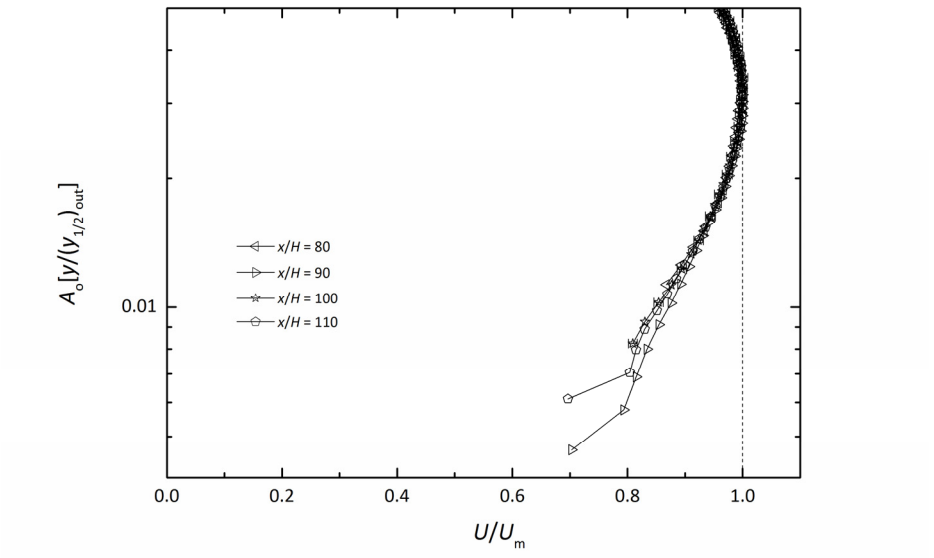

(b)

Figure 6.2: Scaling of the mean velocity profile using the outer scales for the LFR on a rough surface in (a) the outer layer, and (b) the inner layer.

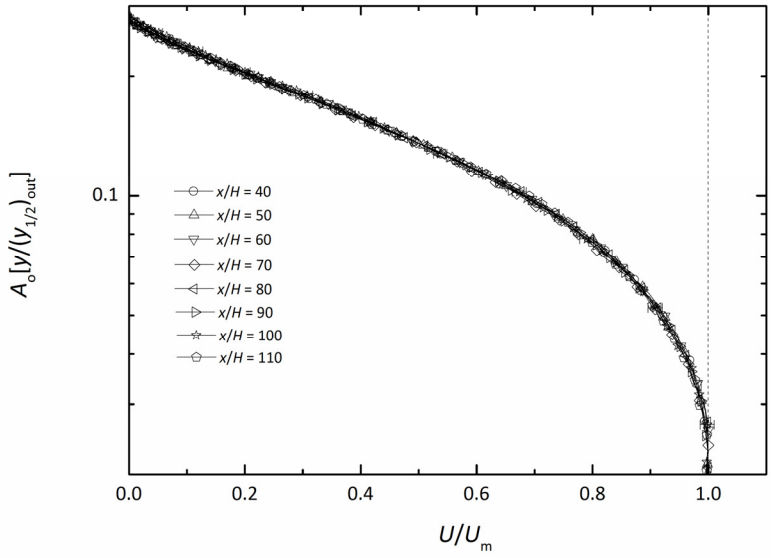

(a)

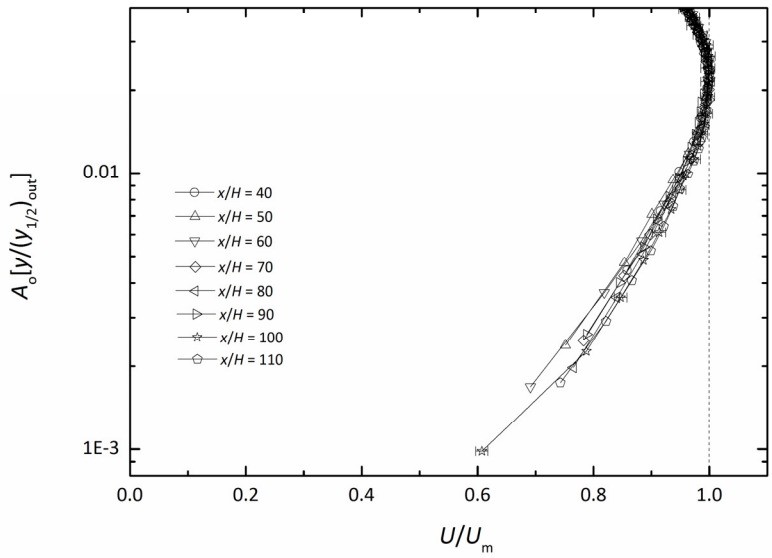

(b)

Figure 6.3: Scaling of the mean velocity profile using the outer scales for the HFR on a smooth surface in (a) the outer layer, and (b) the inner layer.

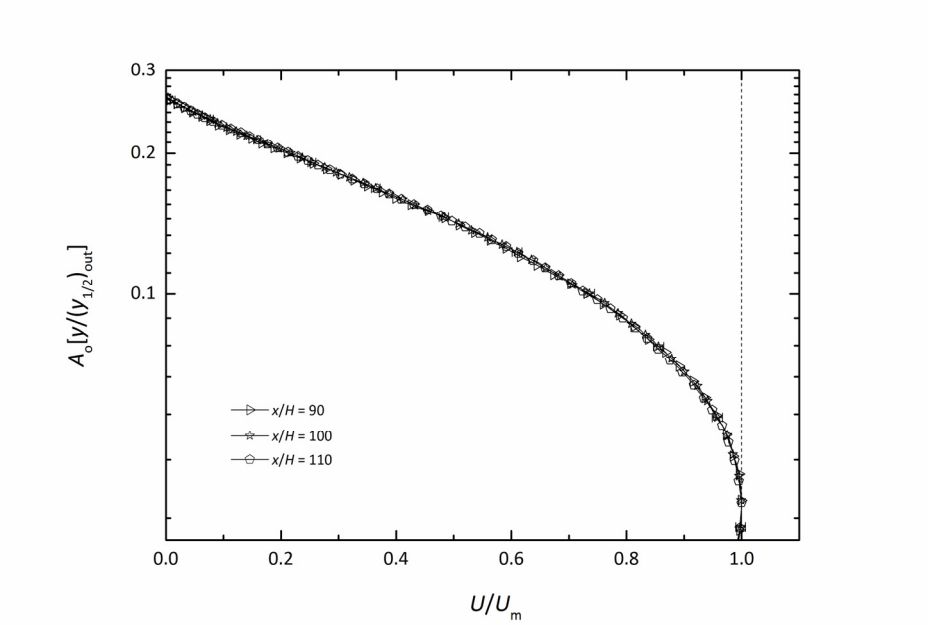

(a)

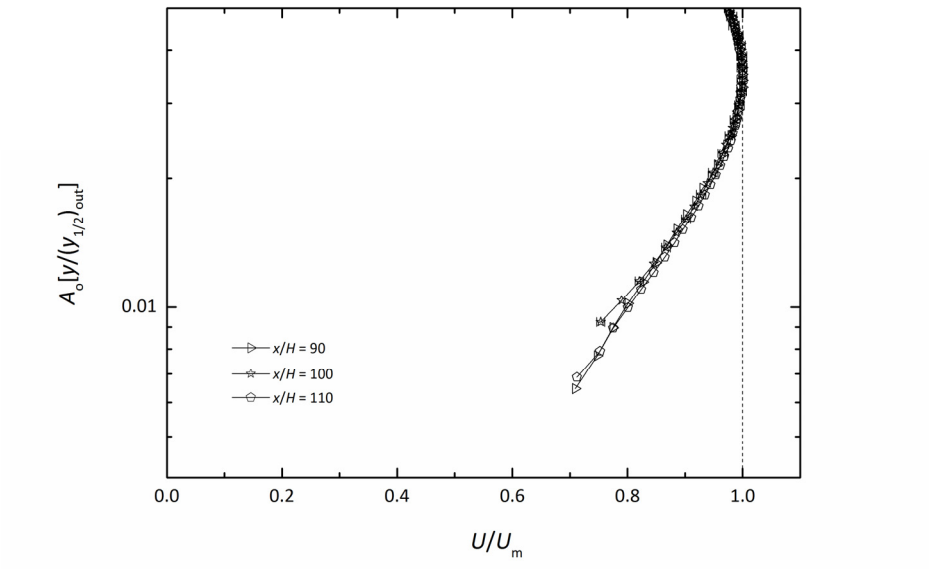

(b)

Figure 6.4: Scaling of the mean velocity profile using the outer scales for the HFR on a rough surface in (a) the outer layer, and (b) the inner layer.

6.3 Inner Scaling

Next the focus turns to the inner scales. Figure 6.5 presents the scaled mean velocity profiles for the LFR case on the smooth surface. Figure 6.5(a) clearly shows that the inner scales completely fail to collapse the outer profiles. In contrast, Figure 6.5(b) shows that with the exception of the profile for $x/H = 40$, the inner scales collapse the inner profiles from the location where $U/U_m \approx 1$ down to the wall. The anomaly with the profile for $x/H = 40$ indicates that the self-similar state represented by the inner scaling laws of Barenblatt *et al*. (2005) is not yet established at this location.

Figure 6.6 shows the LFR case on the rough surface. Figure 6.6(a) indicates that the inner scales fail to collapse the outer profiles, but with much reduced differences between the profiles compared to the LFR case on the smooth surface. This indicates that the inner scales, obtained based on the characteristic variables related to the streamwise development of the inner layer, are correlated with the outer profiles which may be most likely due to the effect of surface roughness, yet the exact mechanism is unclear. As for the inner layer, the inner scales collapse the inner profiles down to the location $A_i\left[y/(y_{1/2})_{in}\right] \approx 0.013$, which accounts for approximately 86% of the inner layer. Note that the profiles for $x/H = 90$ and $x/H = 110$ in the region of $A_i\left[y/(y_{1/2})_{in}\right] < 0.01$ show peculiar behavior, and the cause for these anomalies is not yet clear. Excluding this problematic portion of data, it is found that the region of collapse comprises more than 90% of the data in the inner layer.

Figure 6.7 shows the HFR case for the smooth surface. Similar to the observations for the LFR case on the smooth surface, Figure 6.7(a) indicates that the inner scales cannot collapse the outer profiles. For the inner layer profiles, Figure 6.7(b) indicates that the profiles using inner

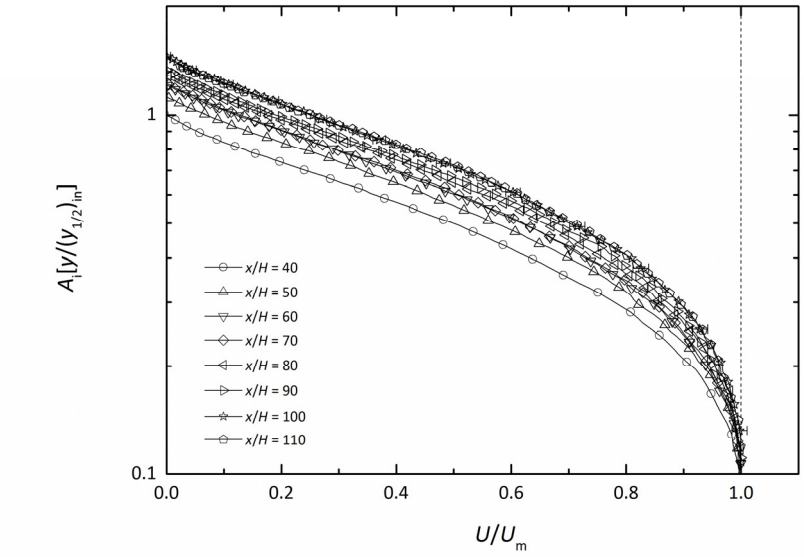

(a)

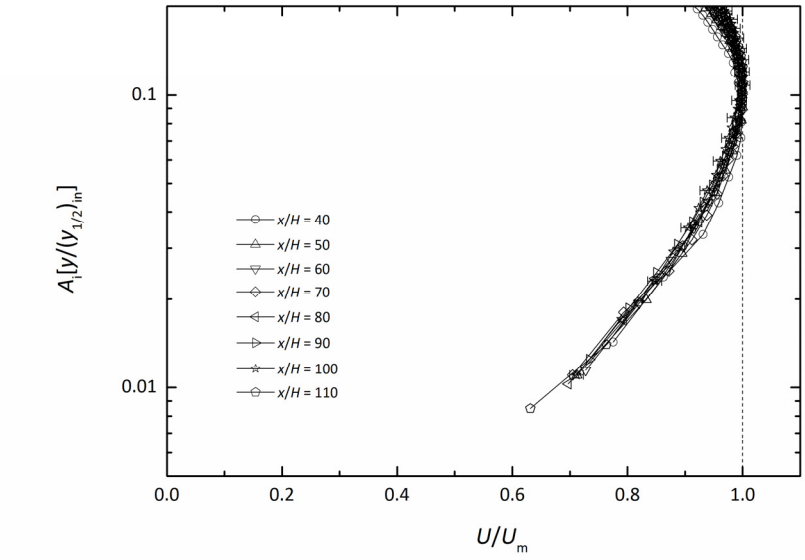

(b)

Figure 6.5: Scaling of the mean velocity profile using the inner scales for the LFR on a smooth surface in (a) the outer layer, and (b) the inner layer.

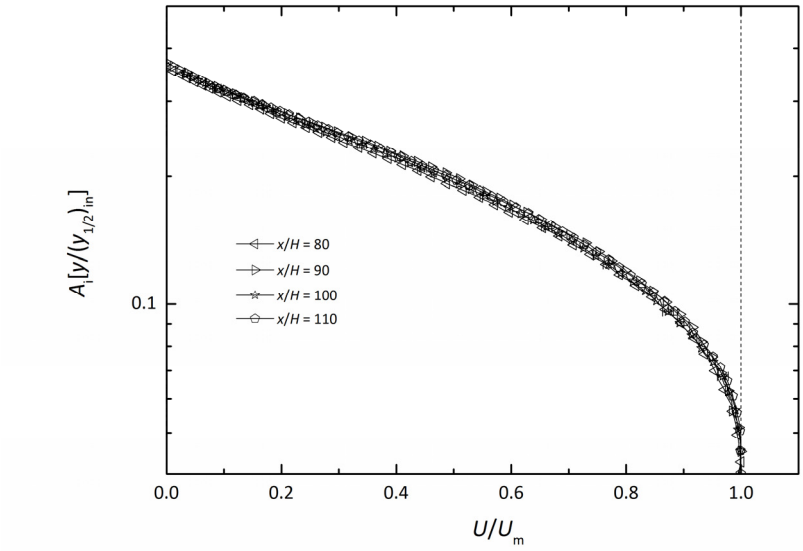

(a)

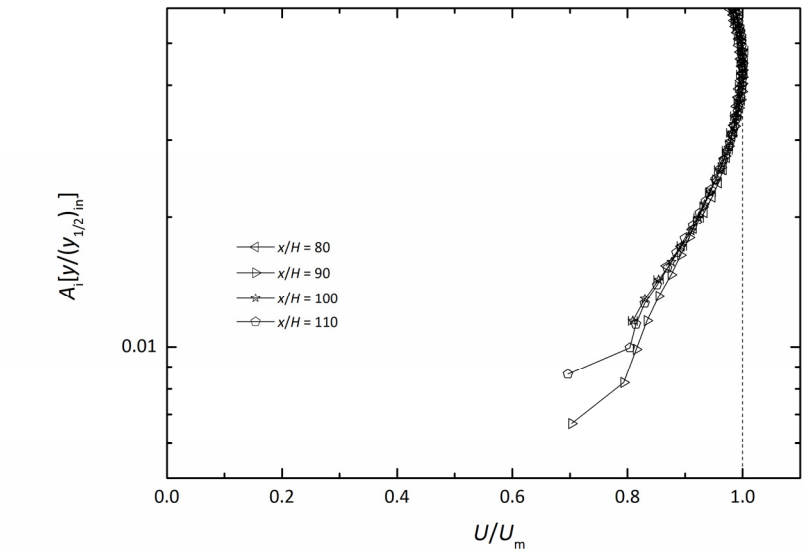

(b)

Figure 6.6: Scaling of the mean velocity profile using the inner scales for the LFR on a rough surface in (a) the outer layer, and (b) the inner layer.

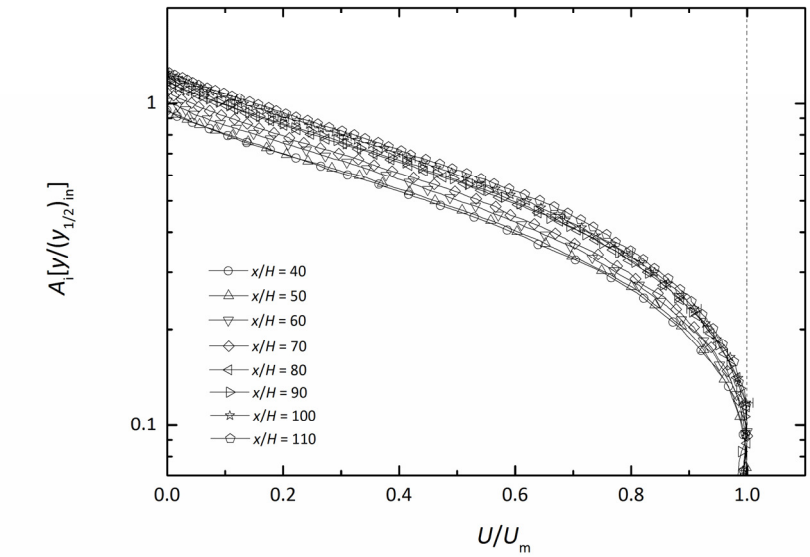

(a)

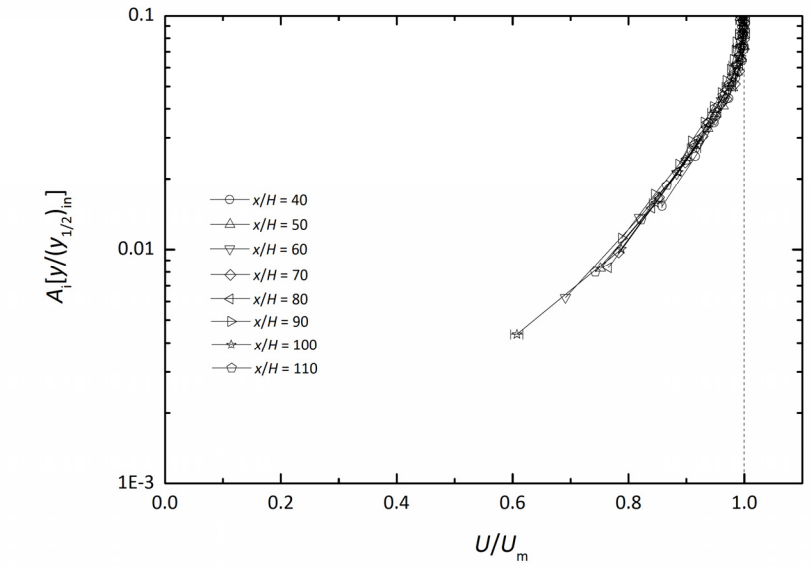

(b)

Figure 6.7: Scaling of the mean velocity profile using the inner scales for the HFR on a smooth surface in (a) the outer layer, and (b) the inner layer.

scales collapse throughout, but again with a slight deviation of the profile for x/H = 40, which indicates that the self-similar state represented by inner scaling laws is not yet established at the location $x = 40H$ for the HFR case on the smooth surface.

Figure 6.8 shows the HFR case on the rough surface. Figure 6.8(a) indicates that the inner scales do not collapse the outer profiles for the fully rough case, but with a slightly lower level of difference between profiles compared to the HFR case on the smooth surface. For the inner layer, Figure 6.8(b) indicates that the inner scales collapse the inner profiles down to the location $A_i\left[y/\left(y_{1/2}\right)_{in}\right] \approx 0.03$, so that approximately 95% of the data in the inner layer show a collapse of the velocity profiles.

The above analysis on the inner scaling in the outer layer illustrates that the velocity profiles in the outer layer generally tend to collapse better when the rough surface is present compared to the smooth surface cases. This further implies that the surface roughness enhances the coupling between the flow fields in the inner and outer layers.

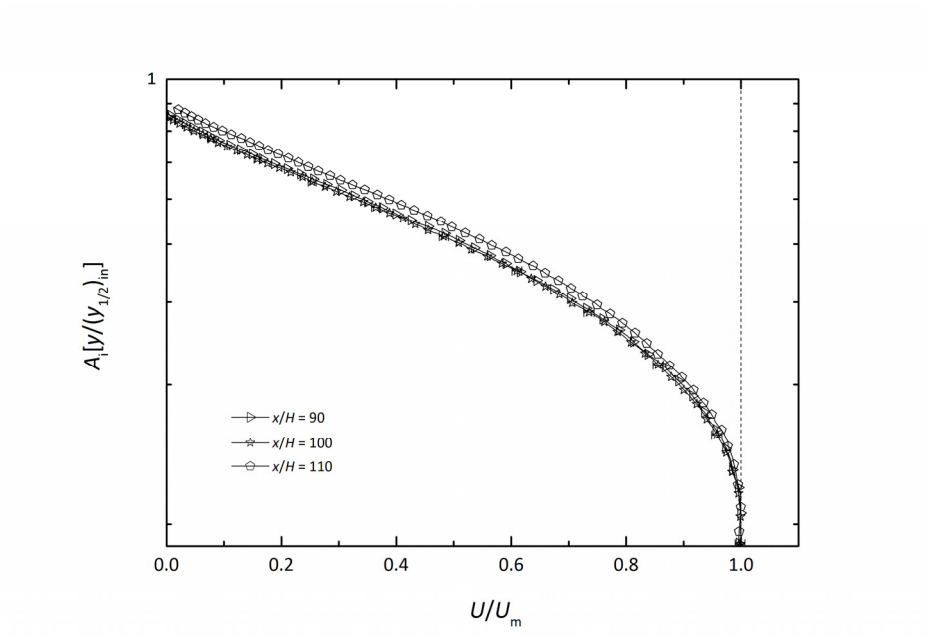

(a)

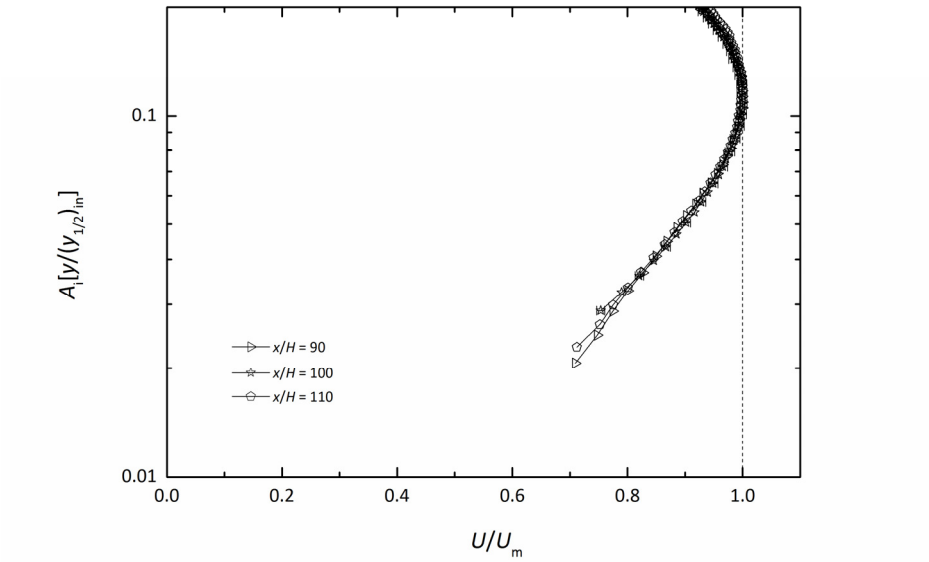

(b)

Figure 6.8: Scaling of the mean velocity profile using the inner scales for the HFR on a rough surface in (a) the outer layer, and (b) the inner layer.

6.4 Summary for the Outer and Inner Scaling

The above analyses of Figures 6.1 to 6.8 indicate that for all four flow cases considered in this study, when non-dimensionalized by the outer scales of Barenblatt *et al*. (2005), the mean streamwise velocity profiles in the outer layer collapse well onto a single self-similar profile, but deviate from each other in the inner layer. In contrast, when non-dimensionalized by the inner scales of Barenblatt *et al*. (2005), the mean streamwise velocity profiles in the inner layer collapse reasonably well onto a single self-similar profile, but deviate from each other in the outer layer. This indicates that, regardless of the surface roughness, the outer and inner layers of the plane wall jet each exhibit their own distinct self-similar profile based on the scaling laws of Barenblatt *et al*. (2005). These conclusions generally agree with the conclusions of Barenblatt *et*

al. (2005), Rostamy *et al*. (2011c), and Tang *et al*. (2015) in terms of scaling of the mean streamwise velocity for plane turbulent wall jets on smooth and transitionally rough surfaces. However, the present PIV data show an intrusion of the outer scaling into the inner layer with different levels of penetration for various flow conditions. More specifically, the outer scales can collapse as much as 40% - 45% of the inner layer data for the smooth surface cases, and this percentage rises to 65% for the transitionally rough case and even higher to 75% for the fully rough case. This may be indicative of the distinct mechanisms which determine the interaction between the outer and inner layers for wall jets on surfaces with different hydraulic roughness. A significant conclusion of this study is that the velocity profiles generally tend to collapse better when the rough surface is present compared to the smooth surface, which implies that the surface roughness strengthens the coupling between the inner and outer layers.

6.5 Conclusion on Incomplete Similarity

With the scaling laws of Barenblatt *et al*. (2005) verified, next the focus is turned to the values of the power law coefficients directly associated with these scaling laws to investigate the incomplete similarity of the wall jet. Table 6.1 summarizes the coefficients obtained by fitting the data to Equations (2.7) to (2.9), which have been extensively discussed in Chapter 5. The present power law coefficients show that $\gamma_o \neq 1$, $\gamma_i \neq 1$, and $\gamma_m \neq -0.5$ for all four flow cases considered in this study. This confirms the incomplete similarity of the plane turbulent wall jet in terms of the slot height H for the hydraulically smooth, transitionally rough and fully rough flow cases based on the discussion given in Section 2.2.

Table 6.1: Comparison of power law coefficients

Study	Surface	H (mm)	Re_o	γ_o	γ_i	γ_m
Barenblatt *et al*. (2005)	Smooth	9.6	9,600	0.93	0.68	-0.56
Rostamy *et al*. (2011c)	Smooth	6.0	7,500	0.78	0.50	-0.41
Tang *et al*. (2015)	Transitionally rough	6.0	7,500	0.82	0.40	-0.58
Present: the LFR for smooth surface	Smooth	6.0	7,190	0.91	0.55	-0.52
Present: the LFR for rough surface	Transitionally rough	6.0	6,660	0.94	0.86	-0.56
Present: the HFR for smooth surface	Smooth	6.0	14,300	0.88	0.56	-0.54
Present: the HFR for rough surface	Fully rough	6.0	13,400	0.91	0.65	-0.59

6.6 Chapter Summary

This chapter presents a detailed analysis of the present data using the scaling laws of Barenblatt *et al*. (2005) to assess the hypothesis of incomplete similarity for the plane wall jet considered in this study. The effectiveness of the outer and inner scaling laws for collapsing the mean streamwise velocity profiles generally agree with the conclusions of other studies. Two new observations relate to: 1) the penetration of the outer scaling into the top of the nominal inner layer of the plane wall jet; and 2) the effect of surface roughness to collapse the velocity profiles better than the smooth surface. The next chapter will summarize the main conclusions of this thesis and provide suggestions for future work.

CHAPTER 7

CONCLUSIONS AND FUTURE WORK

7.1 Summary

This study presents an experimental investigation of a plane turbulent wall jet on smooth, transitionally rough and fully rough surfaces based on a new set of PIV measurements. The slot Reynolds numbers for the LFR and HFR for the smooth surface were 7,190 and 14,300, respectively. The slot Reynolds numbers for the LFR and HFR for the rough surface were 6,660 and 13,400, respectively. For the rough surface, the equivalent sand grain roughness k_s^+ was determined to be in the range of $35 < k_s^+ < 47$ for the LFR case and in the range of $81 < k_s^+ < 88$ for the HFR case, which corresponds to the transitionally rough and fully rough flow condition, respectively. The inlet boundary conditions as well as the initial development of the plane wall jet were first examined. The inlet streamwise velocity profile was reasonably uniform with a low turbulence intensity level which compares favorably with previous studies. Next an extensive analysis and discussion of the mean velocity field in the fully developed region was presented to investigate the effects of the slot Reynolds number Re_o and the surface roughness on the characteristic parameters of the plane wall jet. Finally, a detailed analysis of the present data using the scaling laws of Barenblatt *et al*. (2005) was conducted to assess the hypothesis of incomplete similarity for the plane wall jet. The major conclusions of this study are listed in Section 7.3.

7.2 Contributions

To accomplish the present study, the water tank facility for a plane turbulent wall jet in the Department of Mechanical Engineering at University of Saskatchewan was revisited and upgraded. PIV was implemented for measurements with in-house PIV software written and provided by Professor James D. Bugg. The experimental results, mainly of the mean velocity field, were analyzed and compared to relevant literature.

The major contributions of this study are as follows:

1. The present study adds significantly to the existing state of knowledge of a plane turbulent wall jet on both the smooth and rough surface. A specific contribution is a new data set for the case of a fully rough surface.
2. Velocity measurements covering the entire streamwise extent, i.e. the inflow, developing and fully developed regions, of a hydraulically smooth, transitionally rough and fully rough plane wall jet have been obtained.
3. The effect of surface roughness and flow rate, i.e. slot Reynolds number Re_o, especially for the fully rough flow case, is extensively examined.
4. Incomplete similarity of a plane wall jet on the hydraulically smooth, transitionally rough and fully rough surface is confirmed.

7.3 Conclusions

1. The surface roughness decreases the streamwise mass flux across a unit wall-normal extent near the wall (y < 3.0 mm) at the inlet boundary due to the enhanced wall shear stress. It also reduces the downward-moving entrained flow above the slot due to the overall upward displacement of the jet caused by the rough surface. The enhanced wall

friction associated with the rough surface shortens the potential core region, which means the surface roughness does affect the initial development of the plane wall jet.

2. For a two-dimensional wall jet facility, a reverse flow is often encountered in the upper region above the jet to supply the entrainment required by the jet development. A reverse flow was observed in the present fully developed region, but did not affect the characteristics of the mean velocity field compared to other studies.

3. For the effect of surface roughness on the mean velocity profile in the fully developed region, the surface roughness causes the onset of the fully developed region to appear further downstream on the rough surface than on the smooth surface. For the LFR rough surface case, the roughness shift, i.e. ΔU^+, decreases monotonically with distance from the slot, which indicates that the effect of surface roughness on the mean velocity profile decreases. Such a systematic change is not observed for the HFR case. It is found that for the fully rough case, an improved agreement between the modified logarithmic law and the fitted data was obtained using a revised value of von Karman's constant, i.e. $\kappa = 0.38$ which is different from the conventional value of $\kappa = 0.41$ used for smooth or transitionally rough wall-bounded flows in most other studies. This suggests that the value of the log-law constant κ may depend on the surface roughness. However, the present data set is insufficient to allow a definitive conclusion on this topic.

4. In the fully developed region, for the LFR, the surface roughness enlarges the thicknesses of both the outer and inner layer, though such an effect is much more significant for the inner layer than for the outer layer. This is also observed for the HFR but with a much more noticeable effect of surface roughness. The surface roughness increases the spread rate of the inner layer significantly and penetrates into the outer layer, although the

impact is much less for the outer layer. The surface roughness accelerates the attenuation of U_m/U_o, which is expected considering the enhanced wall shear stress on the rough surface. It also decreases the magnitude of U_m/U_o compared to the smooth surface cases. The surface roughness increases the spread rate of y_m, especially for the HFR, and also significantly increases the magnitude of y_m. As for the spread rates, for the LFR, while in general the surface roughness tends to increase the streamwise growth rate of the inner and outer half-widths, the magnitude of this effect becomes stronger as the wall-normal distance to the surface decreases. However, such a pattern is not observed for the HFR and the reason is not clear. The present values of C_f for both smooth surface cases compare favorably with previous studies. The present results for the transitionally rough case generally compare well to the data of Rostamy *et al*. (2011b). For the HFR on the rough surface, a small deviation of less than 3% in the values of C_f is observed over the range of 9,000 $\leq Re_m \leq$ 10,100, which is evidence of a fully rough flow condition. A significant increase in the skin friction, as large as 58% - 78% for the LFR and 72% - 75% for the HFR, due to the surface roughness is observed.

5. For the effect of slot Reynolds number, Re_o, on the mean velocity profile in the fully developed region using outer scales, for both the smooth and rough surface cases, the independence of the nominally self-similar profile in the outer layer on the slot Reynolds number Re_o is observed. However, the surface roughness leads to a different self-similar profile than for the smooth surface case. The increase in Re_o decreases the size of both the outer and inner layers of the smooth surface wall jet, while such an effect is only observed for the outer layer of the rough surface wall jet. This is most likely because for the smooth surface case, the increase in Re_o does not change the flow condition, but for

the rough surface case, the increase in Re_o makes the wall jet transition from a transitionally rough flow to a fully rough flow. For the spread rates of the outer and inner half-widths, the differences in power law coefficients between the present data and other studies are supposedly due to the dependence on the slot Reynolds number Re_o, as suggested by Barenblatt *et al*. (2005). However, their assumed relation, $\gamma = 1 - C/\ln(Re_o)$ where C is a constant independent of Re_o for a certain type of wall-bounded flow, is not supported by the present results. For the present PIV data, the effect of slot Reynolds number on the spread rate of the outer half-widths is minimal. As for the inner half-width, for the smooth surface the effect of slot Reynolds number on the spread rate of the inner layer is still minimal as expected, but for the rough surface the effect is not negligible due to the fact that the wall jet transitions from a transitionally rough flow condition to a fully rough one with the increase in Re_o. For the present PIV data, the increase in Re_o accelerates the attenuation of U_m/U_o, although the magnitude of U_m/U_o increases with the increase in Re_o. The power law coefficients for the decay of y_m are dependent on Re_o. The increase of the slot Reynolds number slightly decreases the spread rate of y_m on the smooth surface but increases it on the rough surface. The skin friction coefficient C_f slightly decreases by 10% - 16% due to the increase in Re_o for the smooth surface case and by 3% - 13% for the rough surface case.

6. Incomplete similarity of the plane turbulent wall jet in terms of the slot height H is confirmed for all the flow conditions considered in this study: the hydraulically smooth, transitionally rough and fully rough flow cases. More specifically, for all four flow cases, the outer scaling collapses the outer layer velocity profiles and the inner scaling collapses the inner layer velocity profiles. The outer scaling is observed to extend into the inner

layer with varied extents for the different flow cases, smooth, transitionally rough and fully rough cases. This indicates that the top region of the inner layer in a plane wall jet is essentially part of the outer layer in a canonical zero-pressure-gradient turbulent boundary layer. It is also indicative of the distinct mechanisms which determine the interaction between the outer and inner layers for wall jets on surfaces with different hydraulic roughness. The velocity profiles generally tend to collapse better when the rough surface is present compared to the smooth surface, which implies that the surface roughness strengthens the coupling between the inner and outer layers.

7.4 Future Work

On the basis of the data set and the conclusions of this study, recommendations for future work are as follows:

1. Utilize the present PIV data for the fluctuating velocity field to study the Reynolds stresses in the initial developing and fully developed regions on the hydraulically smooth, transitionally rough and fully rough surface.
2. Use the spatial distribution of the velocity from the present data to explore the vortex structures in the wall jet. Also use the present data to apply the techniques of Dejoan and Leschziner (2005) involving the Reynolds Stress Transport Equation (RSTE), as well as Banyassady and Piomelli (2014) who used a Joint Probability-Density Function (JPDF), to study the coupling mechanism between the outer and inner layers of a plane wall jet on the hydraulically smooth, transitionally rough and fully rough surface.

3. Conduct highly resolved near-wall measurements to clarify the velocity profile close to the surface. This may also facilitate a better understanding of the appropriate value for log-law constant κ for a fully rough plane wall jet.
4. Study the slot Reynolds number dependence of the power law coefficients by conducting measurements for the velocity field in the fully developed region with a wider range of the inlet conditions, i.e. a more diverse range of inlet bulk velocities and slot heights.

LIST OF REFERENCES

Abrahamsson H, Johansson B and Lofdahl L. A turbulent plane two-dimensional wall-jet in a quiescent surrounding. *European Journal of Mechanics - B/Fluids*. 1994; 13: 533 - 556.

Banyassady R and Piomelli U. Turbu Interaction of inner and outer layers in plane and radial wall jets. *Journal of Turbulence*. 2015; Vol. 16, No. 5: 460 - 483.

Banyassady R and Piomelli U. Turbulent plane wall jets over smooth and rough surfaces. *Journal of Turbulence*. 2014; Vol. 15, No. 3: 186 - 207.

Barenblatt GI. *Scaling*. Cambridge: Cambridge University Press; 2003.

Barenblatt GI, Chorin AJ, Prostikishin VM. The turbulent wall jet: a triple-layered structure and incomplete similarity. *Journal of Applied Mathematics*. 2005; 102: 8850 - 8853.

Bergstrom DJ, Tang Z, Rostamy N, Bugg JD and Sumner D. Incomplete similarity in a plane turbulent wall jet on a rough surface. Abstract paper presented at:14th European Turbulence Conference; September, 1 - 4, 2013; Lyon, France.

Bradshaw P and Gee MT. Turbulent wall jet with and without an external stream. Aeronautics Research Council, Report and Memoranda No. 3252. 1960.

Brzek B, Bailon-Cuba J, Leonardi S and Castillo L. Theoretical evaluation of the Reynolds shear stress and flow parameters in transitionally rough turbulent boundary Layers. *Journal of Turbulence*. 2009; Vol. 10, No. 5: 1 - 28.

Colebrook CF. Turbulent Flow in Pipes, with Particular Reference to the Transition between the Smooth and Rough Pipe Laws. *Journal of the Institution of Civil Engineers*. 1939; 11: 133 - 156.

Colebrook CF and White CM. Experiments with fluid motion in roughened pipes. *Proceedings of The Royal Society London A*. 1937; 161: 367 - 381.

Coleman HW and Steele WG. *Experimentation and Uncertainty Analysis for Engineers: 2nd edition*. New York: Wiley-Interscience. 1999.

Dejoan A and Leschziner MA. Large eddy simulation of a plane turbulent wall jet. *Physics Of Fluids*. 2005; 17: 025102-1 - 025102-16.

Dunn M. An experimental study of a plane turbulent wall jet using particle image velocimetry. M.Sc. Thesis. Saskatoon, Canada: Department of Mechanical Engineering, University of Saskatchewan; 2010.

Eriksson JG, Karlsson RI and Persson J. An experimental study of a two-dimensional plane turbulent wall jet. *Experiments in Fluids*. 1998; 25: 50 - 60.

Flack KA and Schultz MP. Review of hydraulic roughness scales in the fully rough regime similarity. *Transactions of the ASME: Journal of Fluids Engineering*. 2010; 132: 041203-1 - 041203-10.

Flack KA, Schultz MP, and Connelly JS. Examination of a critical roughness height for outer layer similarity. *Physics of Fluids*. 2007; 19: 095104-1 - 095104-9.

George WK. The self-preservation of turbulent flows and its relation to initial conditions and coherent structures.. *Advances in Turbulence* (Edited by George WK and Arndt R). New York: Hemisphere. 1989. 1 - 41.

George WK, Abrahamsson H, Eriksson J, Karlsson RI, Lofdahl L, and Wosnik M. A similarity theory for the turbulent plane wall jet. *Journal of Fluid Mechanics*. 2000; 425: 367 - 411.

George WK. Asymptotic Effect of Initial and Upstream Conditions on Turbulence. *Transactions of the ASME: Journal of Fluids Engineering*; 2012; 134: 061203-1 - 061203-27.

Hall JW and Ewing D. The Rectangular Wall Jet - Part 1: The Effect of Varying Aspect Ratio. The 43rd AIAA Aerospace Sciences Meeting and Exhibit; 10 - 13 January, 2005; Reno, Nevada; Paper No. AIAA-2005-115.

Hammond GP. Complete velocity profile and optimum skin friction formulas for the plane wall-jet. *Transactions of the ASME: Journal of Fluids Engineering*; 1982; 104: 59 - 66.

Hogg AJ, Huppert HE and Dade WD.. Erosion by planar wall jets. *Journal of Fluid Mechanics*. 1997; 338: 317 - 340.

ISO 5167-1, *Measurement of fluid flow by means of pressure differential devices – Part 1: Orifice plates, nozzles and Venturi tubes inserted in circular cross-section conduits running full*. 1991. International Organization for Standardization, Switzerland.

Karlsson R, Eriksson J and Persson J. An experimental study of a two-dimensional plane turbulent wall jet. Technical Report VU-S93-B36. 1993; Alvkarleby Laboratory, Sweden.

Karlsson R, Eriksson J and Persson J. LDV measurements in a plane wall jet in a large enclosure. In *Proceedings of the 6th International Symposium: Laser Techniques and Application in Fluid Mechanics* (edited by Adrian R, Durao D, Durst F, Heitor M, Maeda M and Whitelaw J); July 20 - 23, 1992; Lisbon, Portugal; pp. 311 - 332.

Karlsson R, Eriksson J and Persson J. ERCOFTAC database: classic collection at University of Surrey; 1991. Available from: http://cfd.me.umist.ac.uk/eroftac/database/cases/case55/case_data.

Launder BE and Rodi W. Turbulent wall jet. *Progress in Aerospace Sciences*. 1981; 19: 81 - 128.

Launder BE and Rodi W. The turbulent wall jet – measurements and modeling. *Annual Review of Fluid Mechanics*. 1983; 15: 429 - 459.

Moody LF. Friction Factors for Pipe Flow. *Transactions of ASME*. 1944; 66: 671 - 684.

Naqavi I, Tyacke J and Tucker P. A numerical study of a plane wall jet with heat transfer. In Proceedings of the Eight International Symposium on Turbulence, Heat and Mass Transfer (THMT-8) (Edited by Hanjalic K, Miyauchi T, Borello D, Hadziabdic M and Venturini P); September 15-18, 2015; Sarajevo, Bosnia and Herzegovina; Paper No. E179.

Narasimha R, Yegna Narayan K and Parthasarathy S. Parametric analysis of turbulent wall jets in still air. *Aeronautical Journal*. 1973; 77: 355-359.

Nikuradse J. Strömungsgesetze in Rauhen Rohren. English version: laws of flow in rough pipes. *VDI Forschungsh*. 1933; 361; NACA Technical Memorandum No. 1292.

Osterlund JM, Johansson AV, Nagib HM and Hites MH. A note on the overlap region in turbulent boundary layers. *Physics of Fluids*. 2000; 12, Number 1: 1 - 4.

Prandtl and Schlichting. Das widerstandsgesetz rauher platten. English translation: The resistance law of rough plates. *Werft Reederer Hafen*. 1934; 15: 1 - 4.

Rajaratnam N. *Developments in Water Science - Volume 5 - Turbulent Jets*. Amsterdam: Elsevier Scientific Publishing Company; 1976.

Rajaratnam N. Plane turbulent wall jets on rough boundaries. *Water Power*. 1967; 19: 149 - 153.

Raju NVS. *Optimization Methods for Engineers*. New Delhi, India: PHI Learning Pvt. Ltd; 2014.

Raupach MR, Antonia RA, Rajagopalan S. Rough-wall turbulent boundary layers. *Applied Mechanics Reviews*. 1991; 44: 1 - 25.

Rostamy N, Bergstrom DJ, Sumner D and Bugg JD. Estimating the friction velocity in a turbulent plane wall jet over a transitionally rough surface. Proceedings of the 8th International Symposium on Turbulence and Shear Flow Phenomena (TSFP-8) (Edited by Johansson AV, Friedrich R, Smits AJ, Sung HJ, Tavoularis S, Bonnet JP); August 28 - 30, 2013; Poitiers, France. Paper No. P19.

Rostamy N, Bergstrom DJ, Sumner D and Bugg JD. The effect of surface roughness on the turbulence structure of a plane wall jet. *Physics of Fluids*. 2011a; 23: 085103:1 - 085103:10.

Rostamy N, Bergstrom DJ, Sumner D and Bugg JD. An experimental study of a turbulent wall jet on smooth and transitionally rough surfaces. *Transactions of the ASME: Journal of Fluids Engineering*. 2011b; 133: 111207:1 - 111207:8.

Rostamy N, Bergstrom DJ, Sumner D and Bugg JD. Incomplete similarity of a plane turbulent wall jet. Proceedings of the 7th International Symposium on Turbulence and Shear Flow Phenomena (TSFP-7) (Edited by Tavoularis S, Friedrich R, Johansson AV, Smits A,

Sung HJ, Marusic I); July 28 - 31, 2011c; Ottawa, Canada. Ottawa: University of Ottawa. Volume 2, Session 5C – Jets (6 pages).

Rostamy N, Bergstrom DJ, Sumner D and Bugg JD. An Experimental Investigation of the Skin Friction in a Plane Turbulent Wall Jet over Smooth and Rough Surfaces. Proceedings of the ASME 2010 3rd Joint US-European Fluids Engineering Summer Meeting (FEDSM2010); August 1 - 5, 2010; Montreal, Canada. Paper No. FEDSM-ICNMM2010-30519.

Seo J and Castillo L. Rough surface turbulent boundary layer: the composite profiles. 42nd AIAA Aerospace Sciences Meeting and Exhibit. January 5 - 8, 2004; Reno, NV, USA. AIAA Paper No. 2004-1287.

Shinneeb, AM. Confinement effects in shallow water jets. Ph.D. Thesis. Saskatoon, Canada: Department of Mechanical Engineering, University of Saskatchewan; 2006.

Shinneeb AM, Bugg JD and Balachandar R. Variable threshold outlier identification in PIV data. *Measurement Science & Technology*. 2004; 15: 1722 - 1732.

Smith BS. Wall jet boundary layer flows over smooth and rough surfaces. Ph.D. thesis. USA: Virginia Polytechnic Institute and State University; 2008.

Stewart RW and Townsend AA. Similarity and self-preservation in isotropic turbulence. *Philosophical Transactions of the Royal Society of London. Series A, Mathematical and Physical Sciences*. 1951; 243, No. 867: 359 - 386.

Tachie MF, Balachandar R and Bergstrom DJ. Roughness effects on turbulent plane wall jets in an open channel. *Experiments in Fluids*. 2004; 37: 281 - 292.

Tang Z, Rostamy N, Bergstrom DJ, Bugg JD and Sumner D. Incomplete similarity of a plane turbulent wall jet on smooth and transitionally rough surfaces. *Journal of Turbulence*. 2015; Vol. 16, No. 11: 1076 - 1090.

White FM. *Fluid Mechanics (Seventh Edition)*. New York: McGraw-Hill. 2011.

Wygnanski I, Katz Y, and Horev E. On the Applicability of Various Scaling Laws to the Turbulent Wall Jet. *Journal of Fluid Mechanics*. 1992; 234: 669 - 690.

APPENDIX

UNCERTAINTY ANALYSIS

The objective of this appendix is to the present the calculation to estimate uncertainties primarily for the mean streamwise velocity U and the friction velocity U_τ. These calculations can only use output information that is accessible to the in-house PIV software. A good general reference for the procedures followed here is Coleman & Steele (1999).

A.1 Uncertainty in the Mean Velocity

First recall the mean velocity is relevant to Reynolds decomposition of the instantaneous velocity, i.e.

$$\widetilde{U} = U + u, \tag{A.1}$$

where $\widetilde{U}$ is the instantaneous velocity and u is the fluctuating velocity. The relationship between the mean U and the instantaneous measurements is

$$U = \frac{1}{N}\sum_{i=1}^{N}\widetilde{U}_i, \tag{A.2}$$

where N is the ensemble size of measured $\widetilde{U}$.

Assuming the uncertainties in the N measurements of $\widetilde{U}$ are uncorrelated, and following Equation 2.13 in Coleman & Steele (1999), the absolute uncertainty in the mean velocity U is

$$U_U = \frac{U_{\widetilde{U}}}{\sqrt{N}}. \tag{A.3}$$

Using the $S_{\widetilde{U}}$ to denote the standard deviation in the sample of N measurements of $\widetilde{U}$, the uncertainty in $\widetilde{U}$ is $1.96 S_{\widetilde{U}}$ at the 95% confidence level. Hence Equation (A.3) can be rewritten to be

$$U_U = \frac{1.96 S_{\widetilde{U}}}{\sqrt{N}}. \tag{A.4}$$

This is a well-known result given in any general statistics reference (see, for example, Equation 2.14 in Coleman & Steele, 1999). The value of $S_{\widetilde{U}}$ equals the root-mean-square of the fluctuating velocity u which is one of the output parameters from the in-house PIV software.

A.2 Uncertainty in the Friction Velocity

The Monte Carlo simulation is used to estimate uncertainty in the friction velocity calculated from the profile fitting. The fundamental idea of this method is to apply random percentage of the above absolute uncertainty in the mean velocity to the measured mean velocity data, then use these simulated data to do the profile fitting to obtain a series of new U_τ results. The standard deviation of these new U_τ results multiplying 1.96 will be the uncertainty in the friction velocity at the 95% confidence level. The random percentage numbers are generated with Normal Distribution.

By using this method, the relative uncertainty in the friction velocity obtained in the present study is determined to be approximately 3.0%.

A.3 Uncertainty in Compound Variables

The following compound variables contain two or more variables in which the uncertainty can be determined using methods above. Uncertainties in these compound variables will be used in plotting figures in the main body of this thesis. In the following equations, U_m is the local maximum mean streamwise velocity, U_o is the inlet bulk velocity, C_f is the skin friction coefficient.

$$U_{\frac{U}{U_m}} = \sqrt{\left(U_U \frac{1}{U_m}\right)^2 + \left(U_{U_m} \frac{U}{(U_m)^2}\right)^2} \tag{A.5}$$

$$U_{\frac{U}{U_\tau}} = \sqrt{\left(U_U \frac{1}{U_\tau}\right)^2 + \left(U_{U_\tau} \frac{U}{(U_\tau)^2}\right)^2} \tag{A.6}$$

$$U_{\frac{U_m}{U_o}} = \sqrt{\left(U_{U_m} \frac{1}{U_o}\right)^2 + \left(U_{U_o} \frac{U_m}{(U_o)^2}\right)^2} \tag{A.7}$$

$$U_{\ln\left(\frac{U_m}{U_o}\right)} = \left| U_{\frac{U_m}{U_o}} \frac{1}{\left(\frac{U_m}{U_o}\right)} \right| \tag{A.8}$$

$$U_{C_f} = U_{\left[2\left(\frac{U_\tau}{U_m}\right)^2\right]} = \sqrt{\left(U_{U_\tau} \frac{4U_\tau}{U_m^{\,2}}\right)^2 + \left(U_{U_m} \frac{-4\left(U_\tau^{\,2}\right)}{U_m^{\,3}}\right)^2} \tag{A.9}$$